Understanding the first steps of the complement classical pathway: Structural studies on C1-antibody complexes

Deniz Ugurlar

Understanding the first steps of the complement classical pathway: Structural studies on C1-antibody complexes

Inzichten in de eerste stappen van de klassieke complement-route: Structuuronderzoek aan C1-antilichaamcomplexen

(met een samenvatting in het Nederlands)

Proefschrift

ter verkrijging van de graad van doctor aan de Universiteit Utrecht op gezag van de rector magnificus, prof. dr. H.R.B.M. Kummeling, ingevolge het besluit van het college voor promoties in het openbaar te verdedigen op woensdag 13 juni 2018 des middags te 12.45 uur

door

Deniz Ugurlar

geboren op 07 juni 1986
te Istanbul, Turkije

Promotor
Prof. dr. P. Gros

This thesis is dedicated to my aunt Fatma Ozkaya
who inspired me for answering questions

Bu tezi Fatos Teyzem'e ithaf ediyorum,
bana soru cozmeyi sevdirdigi icin

"Nothing in life is to be feared, it is only to be understood. Now is the time to
understand more, so that we may fear less."

Marie Curie

Table of Contents

Chapter 1

General introduction

We survive every day from infections due to the ability of our immune system to defend our body. The immune system acts as a bodyguard against foreign invaders such as bacteria, viruses, and other infectious agents in order to maintain the health of our body. The defense mechanism is crucial for all parts of our body including the brain, which has been mistaken in the past as "immune privileged" (*1*). **Different cell populations such as T and B lymphocytes, macrophages, antigen presenting cells and natural killer cells collaborate with molecules such as antibodies, complement proteins and cytokines in order to fight infection. If the foreign invader manages to overcome the initial barriers such as skin and mucus secretions, the innate immune system takes place by recognizing the foreign invader and providing an immediate immune response. Additional immune response is generated by the adaptive immune system, which, through an immunological memory, provides an efficient and strong response during a second encounter with the invader. A major player of the innate immunity is the complement system, which acts rapidly to prevent the infection and further links the innate immune system to the adaptive immune system for a long-term response. However, recent studies have shown that the functions of complement system go beyond the clearance of invaders. Other key roles of complement include clearance of cellular debris and apoptotic cells, tissue repair and organ development. Understanding this sophisticated machinery helps us solve the puzzles of a wide range of diseases and develop new therapies that enhance our chances of survival.**

Complement system

Complement is a major part of the innate immune system and consists of a set of soluble and membrane-bound proteins circulating in blood and tissue fluids. It is an ancient system found in early invertebrates 1.6 billion years ago (*2*). However, the current molecules in jawed vertebrates are rather modern - they appeared only around 600 million years ago (*3*). Complement was first discovered as a factor that helps or "complements" antibodies for bacterial lysis. Over the years, it has been shown to be involved in many other biological functions: the clearance of altered or apoptotic cells (*4*), regulation of the adaptive immune system (*5*), tissue maintenance (*6*), synaptic clearance (*7*) and cross-talk with other systems (e.g. toll-like receptors or the coagulation cascade) (*8*, *9*).

Inefficient or exaggerated activation of complement activity can be life threatening (*10–13*). Without an adequately functioning complement system, the body increases vulnerability to infections, infarctions and other diseases, including autoimmune disorders such as systemic lupus erythematosus (SLE). Individuals with deficiency of C1q have the most severe symptoms of SLE (*14, 15*). Other autoimmune diseases such as rheumatoid arthritis (*16*) and Guillain-Barre syndrome (*17*) are also caused by aberrant activation of the host immune system linked to complement activation. Due to its role in tissue homeostasis, complement is involved in periodontitis, where complement levels are elevated in the tissue around the teeth causing inflammation (*18*). In aged tissues, complement levels are also found elevated, suggesting a contribution to a variety of symptoms related to ageing. High C1q concentration in aged tissues activates canonical Wnt signaling pathway, which is known to play a key role in tissue development including stem cell self-renewal, degenerative diseases, and carcinogenesis (*19*). Another crucial role of complement is the protection of the central nervous system against infections, removal of toxic or aggregated proteins and synaptic pruning. Therefore, sustained or chronic complement activation plays an important role in neurodegenerative diseases such as Alzheimer's (*20*), dementia with Lewy bodies (*21*), Huntington's (*22*), prion diseases (*23*) and Schizophrenia (*24*). Considering such a broad involvement of the complement system in different physiological processes, complement research remains crucial for understanding the mechanisms underlying clearance and disease.

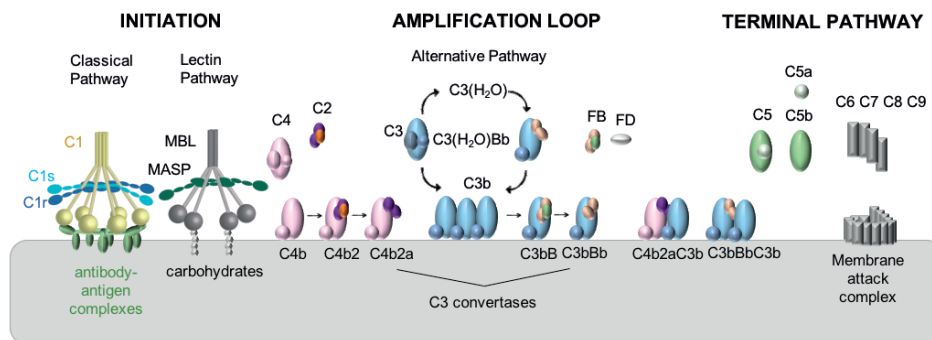**Figure 1. Schematic representation of the three stages of the complement system.**

Differentiating self from non-self is crucial for a healthy immune system. Pattern recognition molecules recognize certain patterns on the surface of cells and trigger complement by three different pathways: Classical Pathway (CP), Lectin Pathway (LP) and Alternative Pathway (AP) (Figure 1). CP is activated when C1,

the initiation complex, binds to danger patterns on cell surfaces such as antibody-antigen complexes, DNA (*25*), pentraxins (PTX-3, CRP) (*26*), or phosphatidylserine (*27*). The recognition molecules in the LP are MBL-MASP or ficolin-MASP complexes, which are activated through binding to sugars or N-acetyl groups on foreign cell surfaces (*28*). In the AP, the system is continuously activated by the spontaneous hydrolysis of an internal thioester in C3 inducing a constant low level of complement activation (reviewed by Merle *et al*, 2015a, 2015b) (*29, 30*). All of the complement pathways lead to the formation of C3 convertase, which activates C3, the central protein of the complement system. $C1r_2s_2$ proteases (CP) and MASP proteases (LP) cleave the soluble protein C4 into two fragments; the small fragment C4a and the larger fragment C4b (Figure 1). C4b binds covalently to the target surface through the thioester group and C2 binds to C4b on the cell surface. Subsequent cleavage of C2 into C2a and C2b results in the generation of the active C3 convertase C4b2a. In the AP, the C3 convertase is similarly formed by C3b and Factor B, which are homologs of C4b (C3b) and C2 (Factor B) of the CP. Spontaneous hydrolysis of C3 in fluid phase, $(C3H_2O)$, adopts a similar conformation as C3b. FB binds to surface-attached C3b or fluid-phase $C3H_2O$ and is specifically cleaved by the soluble, self-inactivated protease factor D (FD) which releases the Ba fragment and results in the C3bBb convertase. Therefore, C3 convertase in the AP (C3bBb) generates a positive feedback loop resulting in the amplification of C3b production and the deposition of many C3b molecules on target surfaces, leading to opsonization. C3b can associate with either C4b2a (CP) or C3bBb (AP) to form the C5 convertase that cleaves C5 into C5a and C5b and initiates the terminal complement cascade, ultimately resulting in the formation of the multimeric membrane attack complex (MAC), which creates physical pores in the cell membrane and causes lysis (*31*). Besides lysis through MAC pores, complement pathway has other effector mechanisms, such as inflammation through anaphylatoxins, C3a and C5a (*32*), phagocytotic uptake through opsonization by C3b (*33*) and interaction of its degradation products iC3b and C3dg with complement receptors (CRs) (*34*). Similarly, C1q binding to C1q receptors (gC1qR and cC1qR) also contributes to clearance by phagocytosis (*35*). Furthermore, iC3b and C3dg binding to CR2 on B cells regulates the adaptive immune response (*5*).

On healthy cells and in plasma, the system is regulated through a set of fluid-phase and surface-bound regulators. The recognition complexes of CP and LP are regulated by soluble C1 esterase inhibitor (C1-INH) which controls the spontaneous activation of C1r, C1s and MASPs (*36*). MAP19 and sMAP regulate MASP-MBL complexes by competing with MASPs for binding to MBLs (*37*). On

healthy cells, AP needs to be tightly regulated because the spontaneous hydrolysis of C3 to C3(H2O) leads to C3b attaching to healthy host cells. Membrane-bound CD35, CD46 and CD55 and soluble C4b-binding protein (C4BP) and factor H (FH) regulate C3 and C5 convertase formation by accelerating convertase decay and/or inducing degradation of C3b and C4b as cofactors for factor I (FI) (*38*, *39*). Lastly, formation of MAC is stopped by CD59, clusterin and vitronectin (*40*, *41*).

Classical pathway of complement

The initiation molecule of the classical pathway (CP), C1, is a 790 kDa Ca^{2+}-dependent complex assembled from the recognition protein C1q and a hetero-tetramer of two modular proteases, C1r and C1s ($C1r_2s_2$), which mediate proteolytic activity of the complex (*42*). The recognition molecule, C1q, is a 460 kDa protein which is composed of 18 polypeptide chains (6A, 6B and 6C) forming six hetero-trimeric globular heads and six collagen-like arms (*43*) (Figure 2). The six C-terminal globular heads, named as gC1q, recognize the ligands; whereas the collagen-like arms capture C1r and C1s proteases for proteolytic activity. In between Gly-X-Y sequence repeats, collagen-like arms have lysine residues (LysB61 and LysC58) that are essential for binding C1r and C1s, and a kink region that allows helices to bend and form divergence in stalks and segmental flexibility in the molecule (*44*). Six collagen arms merge into the 'stalk' fragment of an 18-chain bundle at the N terminal region connected by disulfide bonds between A-B and C-C chains, forming three non-covalent ABC-CBA triple helices over the collagen-like regions (*45*).
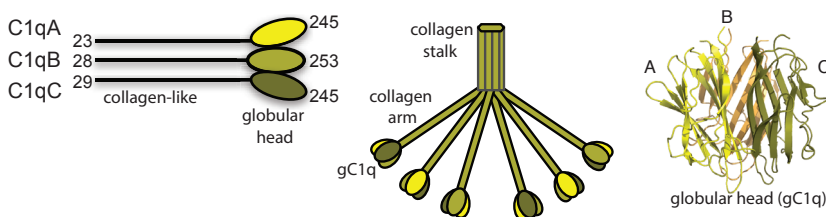

Figure 2. C1q domain composition from hetero-trimer chains A, B and C (left). Cartoon representation of C1 (middle) formed by six chain of C1q A, B and C and the crystal structure of gC1q (1PK6) (*46*)(right).

The C1r and C1s serine proteases are modular proteases that comprise, starting from the N-terminal end, a CUB module, an epidermal growth factor (EGF)-like

module, a second CUB module, two contiguous complement control protein (CCP) modules and a chymotrypsin-like SP domain (*37*) (Figure 3). This type of modular architecture is shared by MASPs, and homologs of C1r and C1s in the lectin pathway. The N-terminal CUB1-EGF-CUB2 region mediates the Ca^{2+}-dependent association between C1r and C1s and is also involved in the interaction between the tetramer and the collagen-like region of C1q; whereas the C-terminal CCP1–CCP2–SP catalytic domains are responsible for the autolytic activation of C1r and the subsequent proteolytic cleavage of C1s (*47*). C1r and C1s are present in zymogenic state until the globular C1q heads bind to the activator surface. The first enzymatic event upon C1q binding to the activator structure is the autoactivation of C1r involving the cleavage of the Arg446–Ile447 bond in the protease domain. Once C1r is activated, it cleaves the Arg437–Ile438 bond of C1s and activates the zymogen C1s. Activated C1s cleaves C4 and C2, which are the components of the classical pathway C3 convertase complex.
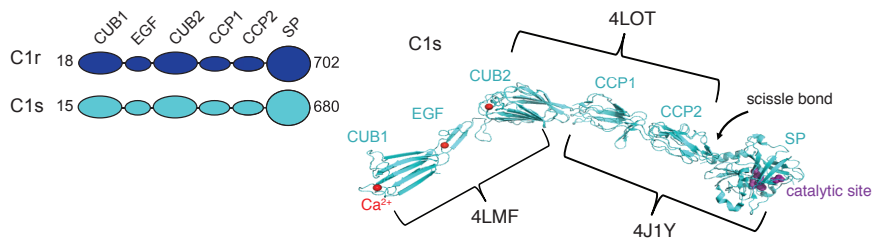

Figure 3. Domain compositions of C1r and C1s (left) and the structure of C1s modeled by using crystal structures of CUB1-EGF-CUB2 (4LOT)(*48*), CUB2-CCP1-CCP2 (4LMF)(*48*) and CCP1-CC2-SP (4J1Y)(*49*).

C1 ligands

C1q differs from its homo-trimeric homologs like collectins and ficolins in that it consists of a heterotrimer recognition subunit, C1q A, B and C chain. The divergent chains of the globular head of C1q provide binding a large spectrum of ligands. The structure of the hetero-trimeric globular head of C1q (*46*) and a considerable amount of gC1q mutagenesis data (*50–52*) revealed that the charged residues on gC1q hetero-trimer, especially in the B chain, are responsible for binding IgG, IgM and most of the other ligands. During the last two decades it became clear that, in addition to IgG and IgM, C1q also recognizes an amazing variety of structurally different (self and non-self)- target molecules. C1q provides further host defense by binding pentraxins PTX3 (*53*) and C-reactive

protein (CRP) (*26*) in complex with phosphocholine on bacterial cell membrane (*54*). Bacterial porins and lipopolysaccharides are also targeted by C1q (*55*). Patterns on apoptotic cells such as phoshphatidylserine (*56*), DNA, histones, and Annexins A2 and A5 (*57*) are recognized by C1q for phagocytotic uptake. Other ligands include serum amyloid P component (*26*), beta-amyloid fibrils (*58*), mitochondrial membranes(*59*), E-LDL, OmpK36, prion protein PrP, fucoidan, HTLV-1 gp21, HIV-1 gp41, decorin, biglycan, heparin, fibronectin and fibrin, reviewed by Kojouharova *et al*, 2010 (*60*). Although C1q recognition has been well defined, C1r-C1s involvement and complement activation triggered by some of the ligands have not been extensively studied yet. For example, the localization of C1q in synapses and its functional role as synaptic pruning have been proven (*7*); however, whether C1r and C1s proteolytic activation is involved in neurodegenerative diseases remains unknown.

Antibodies

Antibodies, or immunoglobulins (Igs), are the strongest activators of C1. Out of 5 different subunits of Igs (IgA, IgD, IgG, IgE, IgM), C1q only binds IgM and IgG (*61*). They recruit C1 and use complement activation as an effector mechanism for host protection. IgGs are composed of two fragments, Fab and Fc, which separate after papain proteolysis (Figure 4). Fab fragments recognize antigens with their N-terminal domains with "hypervariable" regions, or alternatively "complementarity determining regions" (CDRs). Fc fragments bind C1 and Fcγ receptors. When IgGs bind Fcγ receptors on target cells, they stimulate antibody-dependent cell mediated cytotoxicity(*62*). On the other hand, binding to C1 triggers the activation of C1r and C1s proteases and initiates the classical pathway of complement. The region between the Fc and the Fab fragments is called the "hinge region" because there is some flexibility to enable the antibody to bind to pairs of epitopes at various distance apart on an antigen. The major C1q binding site on IgG has been mapped to the C-terminal heavy constant domains 2 (CH2) of the Fc portion of the molecule(*63–67*).
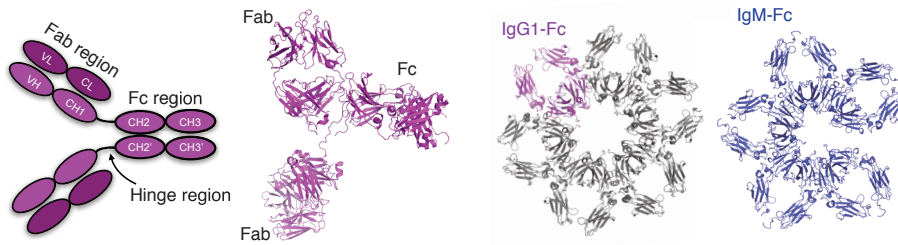
Figure 4. Cartoon representation of IgG1(left), crystal structure of IgG1-b12 (1HZH, 2nd left), oligomeric structures of IgG1-Fc (2nd right) and IgM-Fc (right).

C1 binding relies on the avidity of the Fc on the surface of the immune complex (*68*). It has been shown that C1q binds to Fcs only when multiple IgGs cluster on the cell surface (*51, 68–70*). Thus, the C1q subcomponent of C1 is a multivalent ligand that binds in a cooperative fashion to a cluster of antibody Fc regions, which are exposed on the surface of an immune complex. In recent cryo-electron tomography data, we demonstrated that multivalent C1 binds IgG hexamers that are bound to antigens on a cell surface (*71*). IgG hexamers are formed via non-covalent Fc-Fc interactions of neighboring IgG molecules. These hexamers provide an optimal platform for C1 binding and complement activation. In order to create a stable hexamer IgG platform, specific residues on Fc CH3 domains were mutated (RGY). The IgG1-RGY mutant has been shown to bind C1 and activate complement efficiently in fluid-phase. These variants have shown the strength of the avidity effect for C1q binding. Although pentameric and hexameric IgM occurs naturally in covalent forms in fluid-phase (*72*), their C1q binding sites become exposed only by conformational change upon antigen binding (*73–75*). It has also been shown that mouse IgM hexamers are able to interact with C1q and activate complement better than IgM pentamers (*76, 77*). These data suggest that C1 binding occurs most efficiently with antibody hexamers.

Structural insights into assembly of C1

In the past 30 years, extensive structural studies about C1 complex have been performed; however, neither the overall structure of C1, nor the molecular mechanism of its activation have been uncovered so far. The size (790 kDa), complexity and flexibility of C1 make the research very challenging and equally inspiring. In the 1980s, the first negative-electron microscopy studies and neutron scattering experiments showed that $C1r_2s_2$ has an elongated S-shaped structure

and C1q is a bunch of tulips (*78–80*). When $C1r_2s_2$ was cross-linked to C1q, its conformation changed from elongated to a more compact disk (*79*). Using limited proteolysis and coupling a bead at the C terminal part of the proteins, it was discovered that two C1s locate at the ends of the tetramer, two C1r molecules interact with each other in the middle of the tetramer with C-terminal domains and they interact with C1s with N-terminal domains (*81*, *82*). Later, fragments containing various domain combinations have been expressed and successfully crystallized. The zymogen form of C1r, CCP1-2-SP domains, has been crystallized and has shown how homo-dimers of C1r C-terminal domains sit in a head to tail arrangement in the middle of the elongated tetramer (*83*). The N-terminal CUB1-EGF-CUB2 structures of C1s and MASPs have also revealed head-to-tail homo-dimers through a highly-conserved interface involving interactions between the CUB1 module of one monomer and the EGF module of its counterpart (*48*, *84*, *85*). The homo-dimer interface represents the C1r-C1s hetero-dimer interface at their N terminal region. Crystal structures of C1s CUB2-CCP1 and CUB2-CCP1-CCP2 domains revealed the remaining pieces of the elongated tetramer (*86*).

The compact structure of C1 and how $C1r_2s_2$ hetero-tetramers is assembled in between the collagen arms has remained unknown (Figure 5). In 2009, Bally *et al.* and Philips *et al.* revealed similar models where two anti-parallel C1rs hetero-dimers lie alongside each other in a planar arrangement, held together by the interactions with C1q subunit (*87*, *88*). CUB1 and CUB2 domains of C1r, and CUB1 domains of C1s, simultaneously interact with the protein-binding motif on each C1q collagen arm, making in total 6 contact sites. Site directed mutagenesis experiments also imply that $C1r_2C1s_2$ tetramers present six separate binding sites to C1q that are located on both C1r CUB domains and C1s CUB1 domains (*44*, *87*). The homo-tetrameric arrangement present in the structure of C1s CUB1-EGF-CUB2 (4LMF) provided a model of $C1r_2s_2$ hetero-tetramer arrangement in C1q (*86*). Thus, the compact arrangement of the C1r and C1s N terminal domains inside C1q is in full agreement with earlier analysis of the C1 complex by electron microscopy and neutron scattering. However, how the elongated $C1r_2s_2$ tetramer model converts to the compact conformation when it binds to C1q arms, yielding $C1qr_2s_2$ or C1, has remained unknown.

Activation mechanism of C1

C1 is activated by either danger patterns on cell surfaces or by slow and spontaneous fluid-phase activation. It is crucial that the activation signal is specific to danger patterns; therefore, spontaneous fluid-phase activation of C1 is inhibited by C1-INH (*89*). C1 activation that is induced by the surface-bound activators suggests a structural triggering mechanism (*90*), where the activation signal is passed from C1q to C1r and C1s proteases for proteolytic cleavage. C1r first activates itself, and then C1s, which is responsible for the specific proteolytic activity of C1 toward its substrates C4 and C2. C1r catalytic domains adopt the conformation that allows the cleavage of Arg-Ile bond by the catalytic site of the neighboring monomer. According to the crystal structures of the catalytic domain of C1r in the zymogen and active form (*47*, *83*), C1r CCP1-CCP2-SP domains form a dimer in a head-to-tail arrangement in the complex of the zymogen form and subsequently change their conformation to an enzyme-product relation for autoactivation. Since there is no C1r-C1s hetero-dimer crystal structure, it is assumed to adopt similar conformations as suggested by C1r-C1r activation. However, how the triggering danger patterns change the conformations of C1r and C1s remains unclear.

Until now, several models have been proposed for the underlying mechanism of C1r and C1s activation (*87*, *91–93*)(Figure 5). Most of these models suggested an intramolecular activation mechanism where C1r and C1s CCP1-CCP2-SP domains are folded in between C1q arms and are activated upon binding to the surface. Distortion of any of the C1q stems upon binding of C1 to a target surface is expected to generate part of the mechanical stress necessary to trigger activation. The major assumption of all functional C1 models is the significant flexibility of the $C1r_2s_2$ tetramer and that of the whole complex. Crystal structures indicate that there is a flexible junction between the CCP2 and SP domains in the C1r molecule (*47*, *83*). This flexibility could help in orienting the SP domain towards the cleavable substrate; however, we still do not know whether it is enough to provide the overall flexibility necessary for C1 activation and whether such a large movement between C1q arms is at all possible, considering the limited space inside the C1q cone.
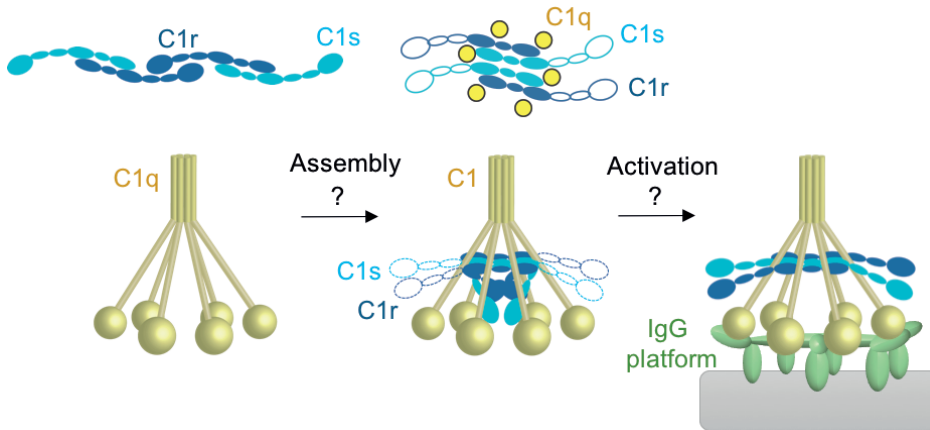
Figure 5. Assembly and activation models of C1. The question marks represent the research questions presented in this thesis.

Recent findings on MASP-MBL complexes suggest an intermolecular activation mechanism between MASPs (*94*). Similarly, the extended SAXS model of the C1 suggests a similar intermolecular activation for C1 molecules based on their SAXS structure that shows an extended conformation for C1r and C1s CCP1-CCP2-SP (*93*). Although MASPs are homologs of C1r and C1s in the lectin pathway, they form homo-dimers (MASP1-MASP1 and MASP2-MASP2), in contrast to C1r and C1s which form hetero-tetramers (*91*). Moreover, MASP2 requires only one activation step, i.e. MASP2 autoactivation, whereas C1 activation requires two steps: C1r and C1s activation. Therefore, C1r and C1s activation might include different activation mechanisms than MASPs, although similar extended conformations have been shown for both C1 and MBL-MASP complexes. Until now, structural and functional evidences have not been sufficient to understand the activation steps and prove any of the previously predicted models.

Scope of the thesis

This thesis covers the research which is aimed at understanding C1 assembly and activation. **Chapter 2** shows the cryo-electron microscopy structures of C1-IgG1$_6$ (both single particle and tomography). C1-antibody complex structure at mid-resolution provides a complete C1 structure from stalk to the globular domains bound to Fc regions. Moreover, the structures reveal information on the arrangement of C1r$_2$s$_2$ hetero-tetramer inside C1q cone and determine how C1q binds the Fc platforms. The identified C1q-Fc interaction site is further proven

by mutagenesis and complement-dependent-cytotoxicity analysis. **Chapter 3** describes the dynamic assembly of C1 through C1rs dimer exchange. In this chapter, structural insights into the assembly mechanism of C1 from an extended $C1r_2s_2$ hetero-tetramer and C1q are clarified using native-mass spectrometry. **Chapter 4** focuses on the structural heterogeneity of $C1\text{-}IgG1_6$ complex and reveals different binding modes of C1q to IgGs with the aid of single particle cryo-EM. **Chapter 5** summarizes all data chapters and discusses the implications of the results presented in this thesis.

Overall, this thesis connects the most important pieces of the C1 puzzle and presents new insights into the antibody mediated complement activation mechanism.

Chapter 1

REFERENCES

1. B. Beutler, Innate immunity: An overview. *Mol. Immunol.* **40**, 845–859 (2004).

2. M. Nonaka, A. Kimura, Genomic view of the evolution of the complement system. *Immunogenetics.* **58**, 701–713 (2006).

3. N. M. Thielens, F. Tedesco, S. S. Bohlson, C. Gaboriaud, A. J. Tenner, C1q: A fresh look upon an old molecule. *Mol. Immunol.* (2017).

4. L. a Trouw, a M. Blom, P. Gasque, Role of complement and complement regulators in the removal of apoptotic cells. *Mol. Immunol.* **45**, 1199–207 (2008).

5. M. C. Carroll, The complement system in regulation of adaptive immunity. *Nat. Immunol.* **5**, 981–6 (2004).

6. D. Ricklin, G. Hajishengallis, K. Yang, J. D. Lambris, Complement: a key system for immune surveillance and homeostasis. *Nat. Immunol.* **11**, 785–797 (2010).

7. B. Stevens *et al.*, The Classical Complement Cascade Mediates CNS Synapse Elimination. *Cell.* **131**, 1164–1178 (2007).

8. H. Hawlisch, J. Köhl, Complement and Toll-like receptors: Key regulators of adaptive immune responses. *Mol. Immunol.* **43** (2006), pp. 13–21.

9. U. Amara *et al.*, Interaction between the coagulation and complement system. *Adv Exp Med Biol.* **632**, 71–79 (2008).

10. D. Ricklin, E. S. Reis, J. D. Lambris, Complement in disease: a defence system turning offensive. *Nat. Rev. Nephrol.* **12**, 383–401 (2016).

11. K. R. Mayilyan, Complement genetics, deficiencies, and disease associations. *Protein Cell.* **3** (2012), pp. 487–496.

12. M. Botto *et al.*, Complement in human diseases: Lessons from complement deficiencies. *Mol. Immunol.* **46** (2009), pp. 2774–2783.

13. J. E. Figueroa, P. Densen, Infectious diseases associated with complement deficiencies. *Clin. Microbiol. Rev.* **4**, 359–395 (1991).

14. M. Chen, M. R. Daha, C. G. M. Kallenberg, The complement system in systemic autoimmune disease. *J. Autoimmun.* **34**, J276–J286 (2010).

15. M. J. Walport, K. A. Davies, M. Botto, C1q and systemic lupus erythematosus. *Immunobiology.* **199**, 265–285 (1998).

16. M. Okroj, D. Heinegård, R. Holmdahl, A. M. Blom, Rheumatoid arthritis and the complement system. *Ann. Med.* **39** (2007), pp. 517–530.

17. C. Hafer-Macko *et al.*, Acute motor axonal neuropathy: An antibody-mediated attack on axolemma. *Ann. Neurol.* **40**, 635–644 (1996).

18. G. Hajishengallis, J. D. Lambris, in *Advances in Experimental Medicine and Biology* (2013), vol. 734, pp. 197–206.

19. A. T. Naito *et al.*, Complement C1q activates canonical Wnt signaling and promotes aging-related phenotypes. *Cell.* **149**, 1298–1313 (2012).

20. S. Hong *et al.*, Complement and microglia mediate early synapse loss in Alzheimer mouse models. *Science.* **352**, 712–6 (2016).

21. D. M. Bonifati, U. Kishore, Role of complement in neurodegeneration and neuroinflammation. *Mol. Immunol.* **44**, 999–1010 (2007).

22. S. K. Singhrao, J. W. Neal, B. P. Morgan, P. Gasque, Increased complement biosynthesis by microglia and complement activation on neurons in Huntington's disease. *Exp. Neurol.* **159**, 362–376 (1999).

23. P. Erlich *et al.*, Complement protein C1q forms a complex with cytotoxic prion protein oligomers. *J. Biol. Chem.* **285**, 19267–19276 (2010).

24. A. Sekar *et al.*, Schizophrenia risk from complex variation of complement component 4. *Nature.* **530**, 177–183 (2016).

25. H. Païdassi *et al.*, The lectin-like activity of human C1q and its implication in DNA and apoptotic cell recognition. *FEBS Lett.* **582**, 3111–6 (2008).

26. T. W. Du Clos, C. Mold, Pentraxins (CRP, SAP) in the process of complement activation and clearance of apoptotic bodies through Fcγ receptors. *Curr. Opin. Organ Transplant.* **16**, 15–20 (2011).

27. L. Kouser *et al.*, Emerging and novel functions of complement protein C1q. *Front. Immunol.* **6** (2015).

28. V. Harmat *et al.*, The structure of MBL-associated serine protease-2 reveals that identical substrate specificities of C1s and MASP-2 are realized through different sets of enzyme-substrate interactions. *J. Mol. Biol.* **342**, 1533–46 (2004).

29. N. S. Merle, S. E. Church, V. Fremeaux-Bacchi, L. T. Roumenina, Complement system part I - molecular mechanisms of activation and regulation. *Front. Immunol.* **6**, 1–30 (2015).

30. N. S. Merle, R. Noe, L. Halbwachs-Mecarelli, V. Fremeaux-Bacchi, L. T. Roumenina, Complement system part II: Role in immunity. *Front. Immunol.* **6** (2015).

31. B. P. Morgan, The membrane attack complex as an inflammatory trigger. *Immunobiology.* **221** (2016), pp. 747–751.

32. P.-J. Haas, J. van Strijp, Anaphylatoxins: their role in bacterial infection and inflammation. *Immunol. Res.* **37**, 161–175 (2007).

33. J. Cook, M. Kazatchkine, The human C3b receptor. *Nouv. Rev. Fr. Hematol.* **25** (1983), pp. 297–301.

34. G. Bajic, L. Yatime, R. B. Sim, T. Vorup-Jensen, G. R. Andersen, Structural insight on the recognition of surface-bound opsonins by the integrin I domain of complement receptor 3. *Proc. Natl. Acad. Sci.* **110**, 16426–16431 (2013).

35. A. J. Tenner, C1q receptors: Regulating specific functions of phagocytic cells. *Immunobiology.* **199** (1998), pp. 250–264.

36. L. Beinrohr, J. Dobó, P. Závodszky, P. Gál, C1, MBL-MASPs and C1-inhibitor: novel approaches for targeting complement-mediated inflammation. *Trends Mol. Med.* **14**, 511–21 (2008).

37. P. Gál, J. Dobó, P. Závodszky, R. B. M. Sim, Early complement proteases: C1r, C1s and MASPs. A structural insight into activation and functions. *Mol. Immunol.* **46**, 2745–52 (2009).

38. F. Forneris *et al.*, Regulators of complement activity mediate inhibitory mechanisms through a common C3b-binding mode. *EMBO J.* **35**, 1133–1149 (2016).

39. X. Xue *et al.*, Regulator-dependent mechanisms of C3b processing by factor i allow differentiation of immune responses. *Nat. Struct. Mol. Biol.* **24**, 643–651 (2017).

40. K. T. Preissner, D. Seiffert, Role of vitronectin and its receptors in haemostasis and vascular remodeling. *Thromb. Res.* **89** (1998), pp. 1–21.

41. M. Schwarz *et al.*, Potential protective role of apoprotein J (clusterin) in atherogenesis: Binding to enzymatically modified low-density lipoprotein reduces fatty acid-mediated cytotoxicity. *Thromb. Haemost.* **100**, 110–118 (2008).

42. G. J. Arlaud *et al.*, Structural biology of C1: dissection of a complex molecular machinery. *Immunol. Rev.* **180**, 136–145 (2001).

43. K. B. Reid, R. R. Porter, Subunit composition and structure of subcomponent C1q of the first component of human complement. *Biochem. J.* **155**, 19–23 (1976).

44. I. Bally *et al.*, Expression of recombinant human complement C1q allows identification of the C1r/C1s-binding sites. *Proc. Natl. Acad. Sci. U. S. A.* **110**, 8650–5 (2013).

45. U. Kishore, K. B. Reid, C1q: structure, function, and receptors. *Immunopharmacology*. **49**, 159–70 (2000).

46. C. Gaboriaud *et al.*, The crystal structure of the globular head of complement protein C1q provides a basis for its versatile recognition properties. *J. Biol. Chem.* **278**, 46974–82 (2003).

47. J. Kardos *et al.*, Revisiting the mechanism of the autoactivation of the complement protease C1r in the C1 complex: structure of the active catalytic region of C1r. *Mol. Immunol.* **45**, 1752–60 (2008).

48. V. U. Girija, A. R. Gingras, J. E. Marshall, R. Panchal, A. Sheikh, Structural basis of the C1q/C1s interaction and its central role in assembly of the C1 complex of complement activation. *Proc. Natl. Acad. Sci.* **110**, 13916–20 (2013).

49. A. J. Perry *et al.*, A molecular switch governs the interaction between the human complement protease C1s and its substrate, complement C4. *J. Biol. Chem.* **288**, 15821–15829 (2013).

50. U. Kishore, K. B. Reid, Modular organization of proteins containing C1q-like globular domain. *Immunopharmacology*. **42**, 15–21 (1999).

51. U. Kishore *et al.*, Structural and functional anatomy of the globular domain of complement protein C1q. *Immunol. Lett.* **95**, 113–28 (2004).

52. A. S. Zlatarova *et al.*, Existence of different but overlapping IgG- and IgM-binding sites on the globular domain of human C1q. *Biochemistry*. **45**, 9979–9988 (2006).

53. L. T. Roumenina *et al.*, Interaction of C1q with IgG1, C-reactive protein and pentraxin 3: mutational studies using recombinant globular head modules of human C1q A, B, and C chains. *Biochemistry*. **45**, 4093–4104 (2006).

54. A. J. Szalai, A. Agrawal, T. J. Greenhough, J. E. Volanakis, in *Clinical Chemistry and Laboratory Medicine* (1999), vol. 37, pp. 265–270.

55. A. Zohair, S. Chesne, R. H. Wade, M. G. Colomb, Interaction between complement subcomponent C1q and bacterial lipopolysaccharides. *Biochem. J.* **257**, 865–873 (1989).

56. H. Païdassi *et al.*, C1q binds phosphatidylserine and likely acts as a multiligand-bridging molecule in apoptotic cell recognition. *J. Immunol.* **180**, 2329–2338 (2008).

57. M. Martin, J. Leffler, A. M. Blom, Annexin A2 and A5 serve as new ligands for C1q on apoptotic cells. *J. Biol. Chem.* **287**, 33733–33744 (2012).

58. P. Tacnet-Delorme, S. Chevallier, G. J. Arlaud, B-Amyloid Fibrils Activate the C1 Complex of Complement Under Physiological Conditions: Evidence for a Binding Site for A on the C1q Globular Regions. *J. Immunol.* (2001).

59. M. C. Peitsch, J. Tschopp, a Kress, H. Isliker, Antibody-independent activation of the complement system by mitochondria is mediated by cardiolipin. *Biochem. J.* **249**, 495–500 (1988).

60. M. Kojouharova, K. Reid, M. Gadjeva, New insights into the molecular mechanisms of classical complement activation. *Mol. Immunol.* **47**, 2154–60 (2010).

61. J. Charles A Janeway, P. Travers, M. Walport, M. J. Shlomchik, The distribution and functions of immunoglobulin isotypes. *Immunobiol. Immune Syst. Heal. Dis.*, 1–9 (2001).

62. S. M. Canfield, S. L. Morrison, The binding affinity of human IgG for its high affinity Fc receptor is determined by multiple amino acids in the CH2 domain and is modulated by the hinge region. *J. Exp. Med.* **173** (1991).

63. E. E. Idusogie *et al.*, Mapping of the C1q binding site on rituxan, a chimeric antibody with a human IgG1 Fc. *J. Immunol.* **164**, 4178–84 (2000).

64. E. E. Idusogie *et al.*, Engineered antibodies with increased activity to recruit complement. *J. Immunol.* **166**, 2571–2575 (2001).

65.   J. E. Thommesen, T. E. Michaelsen, G. Å. Loset, I. Sandlie, O. H. Brekke, Lysine 322 in the human IgG3 CH2 domain is crucial for antibody dependent complement activation. *Mol. Immunol.* **37**, 995–1004 (2001).

66.   G. L. Moore, H. Chen, S. Karki, G. A. Lazar, Engineered Fc variant antibodies with enhanced ability to recruit complement and mediate effector functions. *MAbs.* **2**, 181–189 (2010).

67.   S. Schneider, M. Zacharias, Atomic resolution model of the antibody Fc interaction with the complement C1q component. *Mol. Immunol.* **51**, 66–72 (2012).

68.   D. R. Burton, Immunoglobulin G: Functional sites. *Mol. Immunol.* **22**, 161–206 (1985).

69.   T. Borsos, H. J. Rapp, Hemolysin titration based on fixation of the activated first component of complement: evidence that one molecule of hemolysin suffices to sensitize an erythrocyte. *J. Immunol.* **95**, 559–566 (1965).

70.   N. C. Hughes-Jones, B. Gardner, Reaction between the isolated globular sub-units of the complement component Clq and IgG-complexes. *Mol. Immunol.* **16**, 697–701 (1979).

71.   C. A. Diebolder *et al.*, Complement is activated by IgG hexamers assembled at the cell surface. *Science.* **343**, 1260–3 (2014).

72.   A. Cattaneo, M. S. Neuberger, Polymeric immunoglobulin M is secreted by transfectants of non-lymphoid cells in the absence of immunoglobulin J chain. *EMBO J.* **6**, 2753–8 (1987).

73.   D. M. Czajkowsky, Z. Shao, The human IgM pentamer is a mushroom-shaped molecule with a flexural bias. *Proc. Natl. Acad. Sci. U. S. A.* **106**, 14960–5 (2009).

74.   A. Feinstein, N. Richardson, M. I. Taussig, Immunoglobulin flexibility in complement activation. *Immunol. Today.* **7** (1986), pp. 169–174.

75.   D. R. Burton, Is IgM-like dislocation a common feature of antibody function? *Immunol. Today.* **7**, 165–167 (1986).

76.   E. J. Wiersma, C. Collins, S. Fazel, M. J. Shulman, Structural and functional analysis of J chain-deficient IgM. *J. Immunol.* **160**, 5979–89 (1998).

77.   A. Bhandoola *et al.*, Differential activation of human and guinea pig complement by pentameric and hexameric IgM. *Eur. J. Immunol.* **32**, 1802–1810 (2002).

78.   J. Tschopp, W. Villiger, H. Fuchs, E. Kilchherr, J. Engel, Assembly of subcomponents C1r and C1s of first component of complement: electron microscopic and ultracentrifugal studies. *Proc. Natl. Acad. Sci. U. S. A.* **77**, 7014–7018 (1980).

79.   C. J. Strang, R. C. Siegel, M. L. Phillips, P. H. Poon, V. N. Schumaker, Ultrastructure of the first component of human complement: electron microscopy of the crosslinked complex. *Proc. Natl. Acad. Sci. U. S. A.* **79**, 586–90 (1982).

80.   P. H. Poon, V. N. Schumaker, M. L. Phillips, C. J. Strang, Conformation and restricted segmental flexibility of C1, the first component of human complement. *J. Mol. Biol.* **168**, 563–577 (1983).

81.   V. Weiss, C. Fauser, J. Engel, Functional model of subcomponent C1 of human complement. *J. Mol. Biol.* **189**, 573–581 (1986).

82.   C. L. Villiers, G. J. Arlaud, M. G. Colomb, Domain structure and associated functions of subcomponents C1r and C1s of the first component of human complement. *Proc. Natl. Acad. Sci. U. S. A.* **82**, 4477–4481 (1985).

83.   M. Budayova-Spano *et al.*, Monomeric structures of the zymogen and active catalytic domain of complement protease c1r: further insights into the c1 activation mechanism. *Struct. London Engl. 1993.* **10**, 1509–1519 (2002).

84.   A. R. Gingras *et al.*, Structural basis of mannan-binding lectin recognition by its associated serine protease MASP-1: implications for complement activation. *Structure.* **19**, 1635–43 (2011).

85. H. Feinberg *et al.*, Crystal structure of the CUB1-EGF-CUB2 region of mannose-binding protein associated serine protease-2. *EMBO J.* **22**, 2348–59 (2003).

86. U. V. Girija *et al.*, Structural basis of the C1q/C1s interaction and its central role in assembly of the C1 complex of complement activation. *Proc. Natl. Acad. Sci.*, 201311113 (2013).

87. I. Bally *et al.*, Identification of the C1q-binding Sites of Human C1r and C1s: a refined three-dimensional model of the C1 complex of complement. *J. Biol. Chem.* **284**, 19340–8 (2009).

88. A. E. Phillips *et al.*, Analogous interactions in initiating complexes of the classical and lectin pathways of complement. *J. Immunol.* **182**, 7708–17 (2009).

89. R. J. Ziccardi, A new role for C1-inhibitor in homeostasis: Control of Activation of the first component of human complement. **128**, 2–5 (1982).

90. R. J. Ziccardi, The Role of immune complexes in the activation of the first component of human complement, **132** (1984).

91. A. E. Phillips *et al.*, Analogous interactions in initiating complexes of the classical and lectin pathways of complement. *J. Immunol.* **182**, 7708–17 (2009).

92. R. Wallis, D. A. Mitchell, R. Schmid, W. W. Schwaeble, H. Anthony, UKPMC Funders Group Paths reunited : initiation of the classical and lectin pathways of complement activation. *Russell J. Bertrand Russell Arch.* **215**, 1–11 (2010).

93. S. A. Mortensen *et al.*, Structure and activation of C1, the complex initiating the classical pathway of the complement cascade. *Proc. Natl. Acad. Sci.* **114**, 986–991 (2017).

94. S. E. Degn *et al.*, Complement activation by ligand-driven juxtaposition of discrete pattern recognition complexes. *Proc. Natl. Acad. Sci.* **111**, 13445–13450 (2014).

Chapter 2

Structures of C1-IgG1 provide insights into how danger pattern recognition activates complement

Deniz Ugurlar[1], Stuart C. Howes[2], Bart-Jan de Kreuk[3], Roman I. Koning[2,4], Rob N. de Jong[3], Frank J. Beurskens[3], Janine Schuurman[3], Abraham J. Koster[2,4], Thomas H. Sharp[2], Paul W.H.I. Parren[5], Piet Gros[1]

[1]*Crystal and Structural Chemistry, Bijvoet Center for Biomolecular Research, Department of Chemistry, Faculty of Science, Utrecht University, Padualaan 8, 3584 CH Utrecht, The Netherlands.*
[2]*Section Electron Microscopy, Department of Molecular Cell Biology, Leiden University Medical Center, Einthovenweg 20, 2300 RC Leiden, The Netherlands.*
[3]*Genmab, Yalelaan 60, 3584 CM Utrecht, The Netherlands.*
[4]*NeCEN, Gorlaeus Laboratories, Leiden University, 2333 CC Leiden, The Netherlands*
[5]*Department of Immunohematology and Blood Transfusion, Leiden University Medical Center, Albinusdreef 2, 2333 ZA Leiden, the Netherlands*

ABSTRACT

Danger patterns on microbes or damaged host cells bind and activate C1, inducing innate immune responses and clearance through the complement cascade. How these patterns trigger complement initiation remains elusive. Here, we present cryo-electron microscopy analyses of C1 bound to monoclonal antibodies in which we observed heterogeneous structures of single and clustered C1-immunoglobulin G1 (IgG1) hexamer complexes. Distinct C1q binding sites are observed on the two Fc-CH2 domains of each IgG molecule. These are consistent with known interactions and also reveal additional interactions, which are supported by functional IgG1-mutant analysis. Upon antibody binding, the C1q arms condense, inducing rearrangements of the $C1r_2s_2$ proteases and tilting C1q's cone-shaped stalk. The data suggest that C1r may activate C1s within single, strained C1 complexes or between neighboring C1 complexes on surfaces.

One Sentence Summary: Cryo-EM structures of C1 bound to antibodies suggest mechanisms for how danger patterns on cell membranes trigger an immune response.

The complement system is part of our innate immune system. The classical complement pathway is triggered by activation of the C1 initiation complex upon binding to cell surfaces. C1, or $C1qr_2s_2$, consists of four proteases, C1r and C1s, that associate with C1q, which contains antibody-binding sites. The homologous serine proteases C1r and C1s each consist of six domains (fig. S1A). C1q comprises 18 polypeptide chains; three chains of C1q A, B and C trimerize to form six collagen-like triple helices connected to six globular (trimeric) ligand-recognition (gC1q) modules (fig. S1B) (*1*). Binding of C1 through its gC1q modules to mediators of inflammation, such as immunoglobulin G (IgG) or IgM antibodies (fig. S1, C and D), on cell surfaces activates the associated proteases and initiates the proteolytic cascade of complement (*2–4*). Previously, we demonstrated that IgG molecules, bound to their cognate antigens on liposomes or cell membranes, oligomerize through interactions between their Fc regions and form a hexameric, high avidity, C1-binding structure reminiscent of multimeric IgM antibodies (fig. S1D) (*5*). Mutagenesis studies (*6–8*) showed that amino-acid residues in IgG1 that are important for direct C1 binding are situated in the CH2 domains near the Fab-Fc hinge at the periphery of these Fc-platforms (fig. S1C). In C1q, globular head residues of predominantly C1q B mediate IgG binding (*4*, *9*, *10*). However, the molecular sequence of events leading to C1 activation by IgG hexamers remains poorly understood (*11*). We used IgG monoclonal antibodies (mAbs) oligomerized through antigen-binding on liposomes or preformed antibody-complexes in solution and applied tomography and single-particle cryo-electron microscopy (cryo-EM) to resolve the mechanisms of C1 binding and activation.

Liposomes carrying di-nitrophenyl (DNP) haptens were incubated with an anti-DNP chimeric IgG1 mAb and C1 to allow extensive formation of surface-bound C1-IgG1 complexes (Fig. 1A). Tomograms showed marked structural variations in C1 binding to antibodies on these liposomes (Fig. 1A and fig S2A and B). Alignment and classification of single membrane-bound C1-IgG1 complexes (Fig. 1B) yielded a reconstruction at ~25-Å resolution (fig. S2, C and D). Focused alignment and classification on the Fc-C1 complex (excluding the membrane and Fab domains; (fig. S2, B and E) revealed six densities corresponding to gC1q domains binding an Fc-platform formed by six IgG1 molecules, a rhomboidal platform accounting for bound $C1r_2s_2$ proteases and a protruding C1q-collagen stalk on top (Fig. 1C), which is consistent with a previous reconstruction obtained with a goat polyclonal antibody to DNP at ~65-Å resolution (*5*). Analysis of sub-volumes of C1-IgG1 complexes revealed persistent density for neighboring C1 complexes (Fig. 1D and fig. S2E), as previously observed by using normal human serum (*12*). Distances between nearest neighbors varied from ~11 to 40 nm center-to-center, with a peak at 23 nm (fig. S2F), reflecting a variation of arrangements of neighboring complexes.

The C1 complexes are not evenly distributed across the surfaces of the liposomes, suggesting that there is preference for the complexes to associate, rather than occupy all available liposome surface (Fig. 1A and fig. S2A).
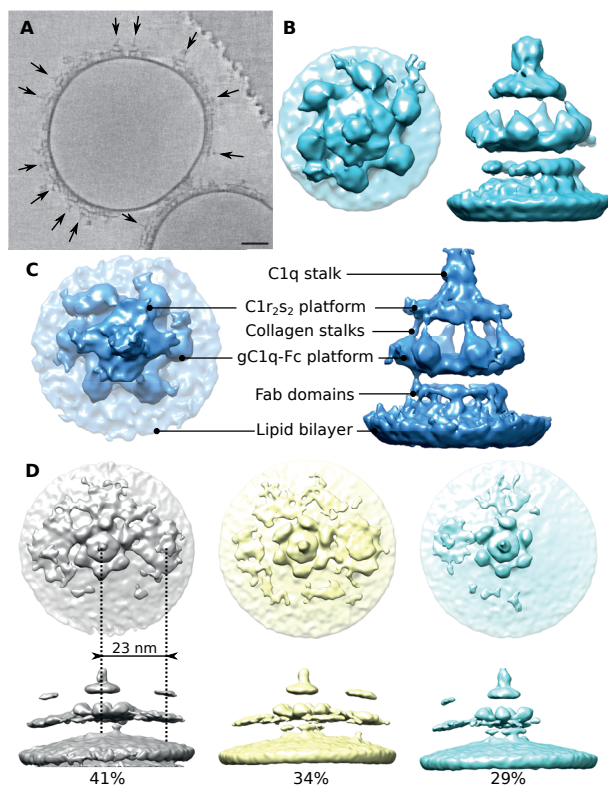

Figure 1. C1-mAb complexes observed on liposomes with tomography.

A) A 10 nm-thick slice through a dual-axis tomogram showing C1 complexes (arrows) bound to surface-associated antibody complexes. Scale bar, 20 nm. B) Reconstruction of a single C1-IgG1 complex shown from the top (left) and side (right) at 25 Å resolution. C) Focused alignment and classification of the complexes, excluding the membrane and Fab regions (masks used in focused reconstructions are provided in fig. S2E) revealed density from the $C1r_2s_2$ platform extending out either side of the C1q stalk. D) Neighboring C1-mAb complexes from larger sub-volumes showing a common spacing of 23 nm between complexes, as measured from centers of IgG1 platforms. All volumes were filtered to 25 nm resolution, and masked, and disconnected densities with volumes less than 5 nm^3 were removed for clarity.

Soluble C1-IgG1$_6$ complexes of 1.7 MDa were obtained (fig. S3A and B) by incubating C1, with catalytically inactive proteases C1r (Ser^{654}Ala) and C1s (Ser^{632}Ala), with a human IgG1 mAb containing three mutations that drive the formation of IgG hexamers in solution (IgG1 Glu^{345}Arg, Glu^{430}Gly and Ser^{440}Tyr) (*5*, *13*, *14*). Classification

and averaging of single-particle densities yielded separate classes with four, five, or six gC1q domains in contact with the Fc platforms (Fig. 2, A and B, and fig. S4C). One class containing ~79,000 particles with six gC1q domains bound to the Fc platform yielded a map at 10-Å resolution (fig. S4D), resulting in an overall structure 32 nm high and 25 nm wide that is consistent with densities observed in tomography (fig. S5). The reconstruction reveals densities for all C1q collagen-like triple helices and gC1q modules, C1r and C1s proteases and IgG1-Fc regions (Fig. 2, C and D).
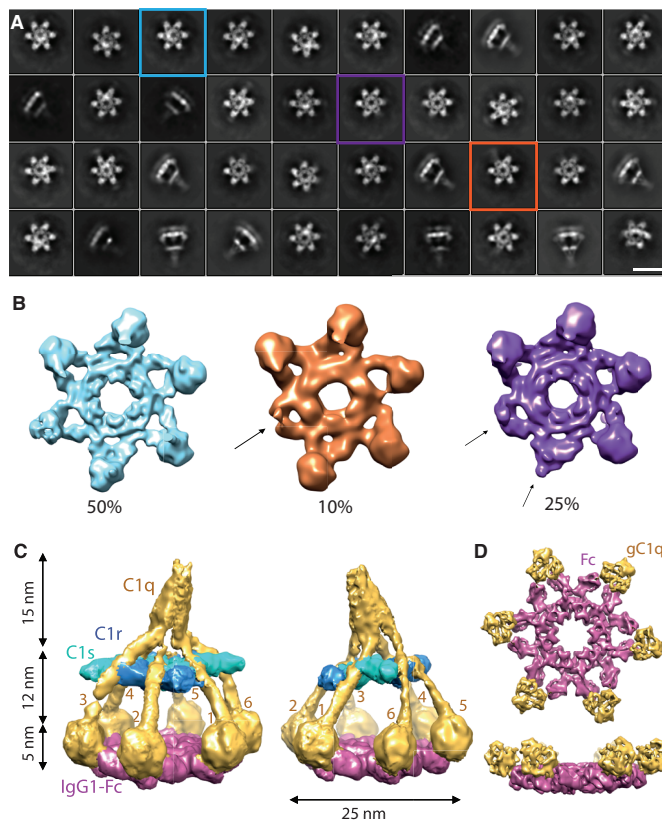

Figure 2. Soluble C1-IgG1$_6$ complexes display heterogeneous structures.

A) Representative two-dimensional (2D) class averages. Colored boxes indicate three classes corresponding to main 3D classes, as shown below. Scale bar, 25 nm. B) Main 3D classes after focused 3D classification and 3D refinement, showing the "bottom platform" segment of the reconstructions indicating heterogeneities (highlighted by arrows). Percentage of particles in each class are indicated. Particle colors correspond to the color of the boxes in (A). C) 3D reconstructions after post-processing of the major class, showing two side views (left and middle). Densities have been colored to indicate density for C1q (yellow; with collagen arms and gC1q units numbered 1 through 6), C1r and C1s (blue and magenta, respectively) and IgG1-Fc regions (pink). D) Top and side views of the bottom platform after six-fold averaging (right top and bottom, respectively).

31

Imposing six-fold symmetry on the IgG1 platform bound to gC1q yielded a density map at 7.3-Å resolution (Fig. 3A and fig. S4D). Crystal structures of Fc CH2 and CH3 domains (pdb-code 1HZH) (*15*) and gC1q (1PK6) (*16*) were modeled in this density map (Fig. 3A). In the resulting model, each gC1q domain contacts peripheral areas on both CH2 and CH2' domains of an IgG-Fc dimeric segment, burying ~540 Å^2 of surface area (fig. S6A). The Fc segments adopt an open conformation, characterized by a long distance of 31 Å between Pro329 and Pro329' of the CH2 domains (fig. S6B). This contrasts with observations of closed conformations in many crystal structures of Fc domains with Pro329-Pro329' distances of ~12 to 19 Å, but resembles that of full-length IgG1-b12 (1HZH) (*15*) and deglycosylated Fc fragments of human IgG4 (4D2N) (*17*), both of which exhibit a six-fold (crystal) packing of their Fc portions, which have Pro329-Pro329' distances of 24 and 29 Å, respectively. Densities are present for N-linked glycans at Asn297 and Asn297' (Fig. 3A). However, no direct contact is observed between the glycans and gC1q, supporting the idea that glycosylation affects C1 binding through IgG hexamerization (*13*). Fitting of hetero-trimeric gC1q to the density yielded similar correlation coefficients for three possible A-B-C domain orientations, with a marginally higher score for chains B and C facing the antibodies, which is consistent with mutation data that has identified chains B and C harboring the antibody-binding sites (*9*).

The Fc-gC1q structure identified distinct C1q-binding sites on the two Fc-CH2 domains of an IgG1. The observed binding sites are corroborated with extensive mutagenesis, which shows that both previously established amino acid contacts and contacts newly identified in our structure modulate complement activation (Fig. 3, B and C, fig. S6C)(*6–8*, *18*). Mutations were introduced in the CD20 mAb IgG1-7D8 and the impact on complement-dependent cytotoxicity (CDC) of CD20-expressing Raji cells was assessed (Fig. 3C and table S1). The first binding site is formed by loop FG (residues 325 to 331) of Fc CH2, which is known to be involved in binding both C1q and Fcγ receptors (*18–20*). Critical residues Pro329-Ala330-Pro331 (*3*, *6*, *18*) form the tip of the FG loop, with Pro329 making contact with hydrophobic C1q-B residue Phe178 (Fig. 3B). IgG1 CH2 residue Lys322 (*21*) provides additional charged interactions with C1q-C residue Asp195 (Fig. 3B). Mutation of Ala327 into a positively charged lysine decreased CDC, whereas the mutation Ala327Gly enhanced CDC (Fig. 3C). Consistent with previous observations, variant Lys326Ala/Glu333Ala stimulated CDC (*6*). The secondary binding site consists of loop BC (residues 266 to 272) and loop DE (residues 294 to 300) of CH2', which form a negatively charged patch that interacts with C1q-B residues Arg114 and Arg129 (Fig. 3B) (*4*, *22*). Introducing a positive charge at residues Glu269, Glu294 or Tyr300 abolished CDC (Fig. 3C). By contrast, the mutation Tyr300Asp enhanced CDC (Fig. 3C). Mutations Asn297Gln and Ser298Lys decreased CDC, likely because of

the absence of glycosylation. Furthermore, Fab-Fc hinge region residues Glu233, Leu234, Leu235, Gly236 and Gly237, contributed to C1q binding and CDC (fig. S6C). Alanine substitutions of these residues decreased CDC, whereas Gly236Asp enhanced CDC, suggesting a possible charge interaction with C1q-B Arg150. The Fab regions themselves are positioned flexibly below the Fc platform, as is apparent in the tomography reconstructions (Fig. 1, B and C, and fig. S5), and appear not to contribute directly to C1 binding and activation.
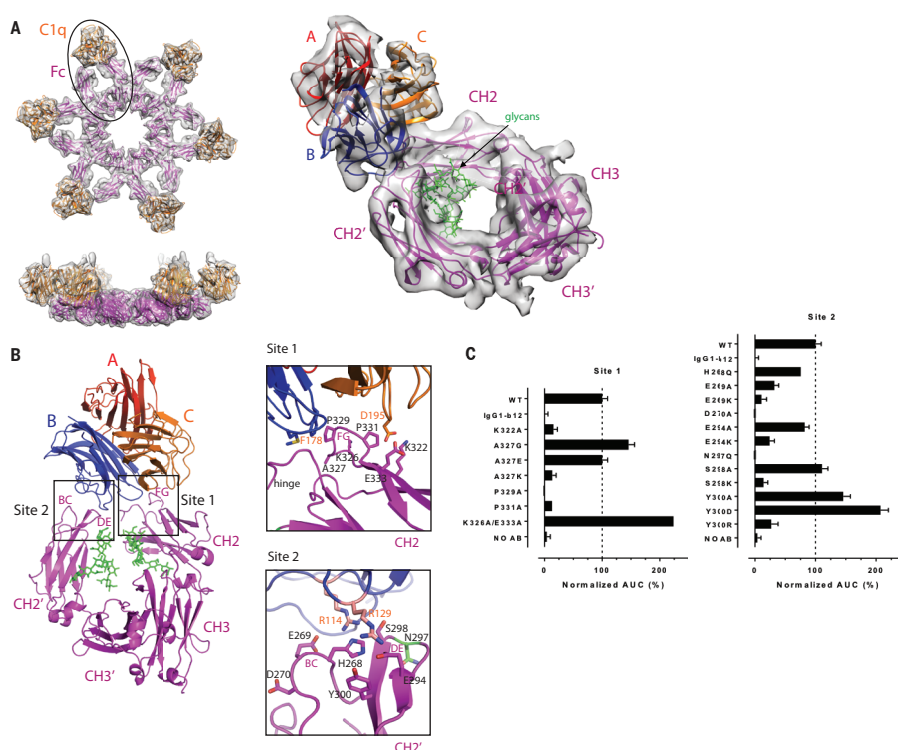
Figure 3. Fc-gC1q interactions in C1-IgG1$_6$.

A) Structural models of Fc regions (magenta) and gC1q headpieces (orange) fitted into the density, top and side view of the Fc-gC1q hexamer (left) and zoom in of a gC1q trimeric with C1q-A, B and C domains (red, blue, and orange, respectively) and an Fc dimer with CH2-CH3 and CH2'-CH3' (right), with Fc glycans shown in green. B) (Left)gC1q-Fc interaction site 1 and site 2 are shown indicated by boxes, with interacting loops FG (site 1), and BC and DE (site 2) labelled. (Right) Zoom in of interaction sites 1 and 2, with key interacting residues shown in stick representation and labelled. (C) Complement dependent cytotoxicity assays of Raji cells opsonized with wild-type (WT) and mutated CD20 mAb IgG1-7D8 (n=3) exposed to C1q-deficient serum to which a titration of 1 ng/mL to 60 μg/mL C1q was added. Cell lysis was assessed with flow cytometry by using propidium iodide staining. Bars show the average area under the curve (AUC) for this dose response normalized against the AUC obtained with the unmutated WT IgG1-7D8 set to 100% NO AB: control reactions without IgG1 added.

We fitted structural models of C1q, C1r, and C1s into the density reconstruction of C1-IgG1$_6$ (Fig. 4 and fig. S7). On top of the C1 structure, the six C1q-A, -B, and C collagen-like triple helices form a stalk that adopts a continuous, hollow cone-shaped structure, which is tilted by 15° from the vertical axis. Six triple helices emerge from the stalk, extend downwards (with an irregular small right-handed supercoil) and connect to the gC1q modules that bind the IgG1-Fc hexamer platform. In particular, the collagen-like helices 3 and 6 display a marked bending (Fig. 4A). Density positioned in between the collagen-like helices is consistent with previously proposed binding of N-terminal domains of C1r$_2$C1s$_2$ between the C1q arms, with arms 2, 3, 5 and 6 contacting C1r and arms 1 and 4 contacting C1s molecules (Fig. 4B) (23–25). Using crystal structures of C1r and C1s (25–28), and their homologs MASP1 and MASP2 (29, 30), domains CUB1-EGF-CUB2-CCP1 of both C1r and C1s (fig. S1A) were modeled into the densities (fig. S7). No density is observed for the CCP2-SP domains of either C1r or C1s in the 10-Å resolution single-particle reconstruction, indicating flexible arrangements for these parts. However, density obtained for CCP1 domains allows completion of the model with the superposition of CCP1-CCP2-SP crystal structures onto CCP1 of C1r and C1s (Fig. 4C and fig. S1A). This results in a model in which C1r CCP1 orients CCP2-SP to curve around the C1q collagen-like helix towards C1s and in which C1s CCP1-CCP2-SP sticks outwards, consistent with their proteo-lytic functions in the complement cascade (Fig. 4C and fig. S7D).

The observed arrangement of the C1r and C1s hetero-tetramer differs from predictions based on a tetrameric C1s arrangement (25, 31) The CUB2 domains of C1r and C1s are rotated and the C1r-C1s dimers are shifted along each other, shortening the contact sites of C1q-collagen helices 2 and 5 from 14 (31) to 11 nm in C1-IgG1$_6$ (fig. S7, A to C). The arrangement of the C1q arms, induced upon binding the Fc hexamer, is also indicative of a compaction. The gC1q domains in unbound C1 are spread apart up to 30 to 35 nm (31). Bending of the collagen-like helices of arms 3 and 6, which embrace C1r$_2$s$_2$ in the longest dimension, and incomplete binding of the gC1q heads (on arms 5 and 6) to Fc platforms support the notion of a surface-induced conformational change.

The affinity of gC1q modules for single IgG antibody molecules is very low. For IgG antibody molecules to form a recognition pattern therefore requires their clustering or aggregation, allowing the formation of a multivalent complex with C1. IgM molecules are already multivalent, but require their occluded C1 binding sites to be revealed upon interacting with surface antigen. Here we show that the multivalent binding of C1 to IgG hexamers results in compaction of C1q arms, which rearranges the N-terminal (CUB1-EGF-CUB2) platform of the C1r$_2$s$_2$ proteases and may allow the catalytic SP domain of the C1r CCP1-CCP2-SP arm
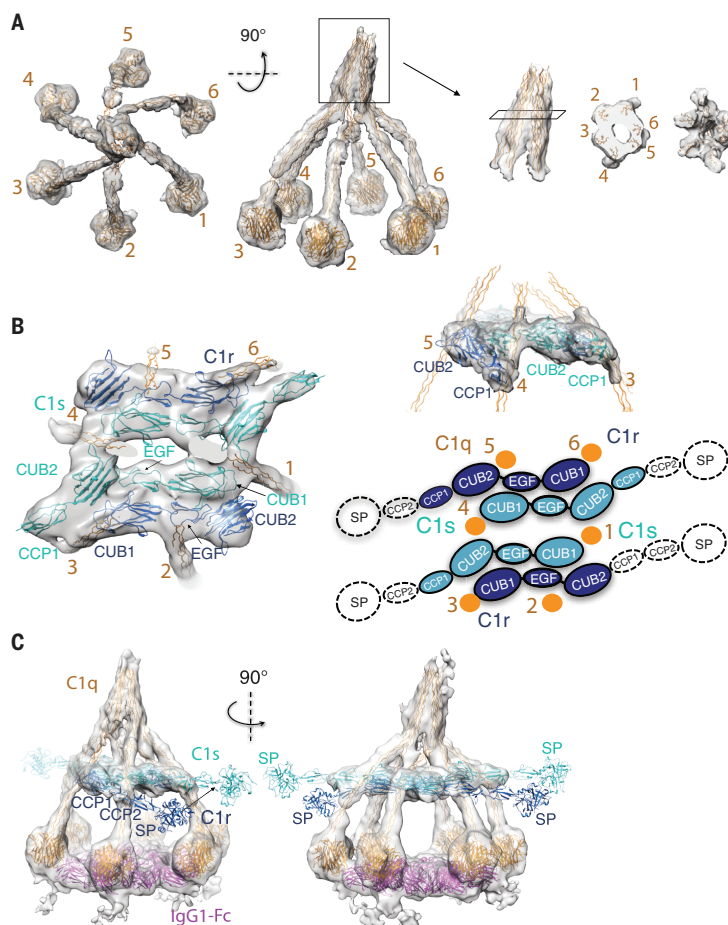
Figure 4. Structural model of C1 fitted into C1-IgG1$_6$ density.

A) Model for C1q-A, B and C hexamer indicating collagen-like segments forming a N-terminal stalk region, six collagen-like triple helices and C-terminal trimeric gC1q modules. Shown are top and side views (left and middle) of C1q and side, sliced-through top and bottom view (third column left to right) of the C1q stalk region. Numbering of each C1q arm is as in Fig. 2. B) Model for C1r and C1s hetero-tetramer showing C1r CUB1-EGF-CUB2 (blue) and C1s CUB1-EGF-CUB2-CCP1 domains (cyan). Shown are (left) top view and (top right) side view at lower contour level, with the latter revealing density for the CCP1 domain of C1r. An illustration of the domain arrangement is shown for clarity (bottom right). C) Overall C1-IgG1$_6$ models in density. CCP2-SP domains lacking density have been added by using orientations derived from crystal structures.

to reach the scissile loop in C1s CCP1-CCP2-SP. Alternatively, the extended conformations of the CCP1-CCP2-SP domains may allow inter-complex proteolysis induced by neighboring complexes. This is consistent with the C1-antibody com-

plexes that form on crowded surfaces, as observed in tomograms of IgG mAb hexamers bound to liposomes. Intercomplex activation has been proposed for MBL-MASP2$_2$ complexes of the lectin-binding complement pathway, in which MASP1 proteases present in separate MBL-MASP1$_2$ complexes mediate activation (*31*, *32*). Direct binding of C1 to ubiquitous and fluid ligands in a membrane, such as phosphatidylserines on apoptotic cells, would likely not induce compaction of the C1q arms and activation may depend on intercomplex proteolysis of surface-bound C1 complexes. Our data suggest that danger pattern recognition by C1 may lead to proteolysis and activation within an isolated complex through a conformational change as suggested by an observed bending of C1q arms and the arrangement of proteases. Close interactions observed between separate C1-IgG complexes however suggest that proteolysis may also result from intercomplex activation.

REFERENCES

1. G. J. Arlaud *et al.*, Structural biology of C1: dissection of a complex molecular machinery. *Immunol. Rev.* **180**, 136–145 (2001).

2. N. C. Hughes-Jones, B. Gardner, Reaction between the isolated globular sub-units of the complement component Clq and IgG-complexes. *Mol. Immunol.* **16**, 697–701 (1979).

3. D. R. Burton *et al.*, The Clq receptor site on immunoglobulin G. *Nature.* **288**, 338–344 (1980).

4. L. T. Roumenina *et al.*, Interaction of C1q with IgG1, C-reactive protein and pentraxin 3: mutational studies using recombinant globular head modules of human C1q A, B, and C chains. *Biochemistry.* **45**, 4093–4104 (2006).

5. C. A. Diebolder *et al.*, Complement is activated by IgG hexamers assembled at the cell surface. *Science.* **343**, 1260–3 (2014).

6. E. E. Idusogie *et al.*, Engineered antibodies with increased activity to recruit complement. *J. Immunol.* **166**, 2571–2575 (2001).

7. A. R. Duncan, G. Winter, The binding site for C1q on IgG. *Nature.* **332**, 738–740 (1988).

8. G. L. Moore, H. Chen, S. Karki, G. A. Lazar, Engineered Fc variant antibodies with enhanced ability to recruit complement and mediate effector functions. *MAbs.* **2**, 181–189 (2010).

9. M. S. Kojouharova *et al.*, Mutational analyses of the recombinant globular regions of human C1q A, B, and C chains suggest an essential role for arginine and histidine residues in the C1q-IgG interaction. *J. Immunol.* **172**, 4351–4358 (2004).

10. U. Kishore *et al.*, Structural and functional anatomy of the globular domain of complement protein C1q. *Immunol. Lett.* **95**, 113–28 (2004).

11. C. Gaboriaud, W. L. Ling, N. M. Thielens, I. Bally, V. Rossi, Deciphering the fine details of C1 assembly and activation mechanisms: "Mission impossible"? *Front. Immunol.* **5**, 565 (2014).

12. T. H. Sharp, F. G. A. Faas, A. J. Koster, P. Gros, Imaging complement by phase-plate cryo-electron tomography from initiation to pore formation. *J. Struct. Biol.* **197**, 155–162 (2016).

13. G. Wang *et al.*, Molecular basis of assembly and activation of complement component C1 in complex with immunoglobulin G1 and antigen. *Mol. Cell.* **63**, 135–145 (2016).

14. R. N. de Jong *et al.*, A novel platform for the potentiation of therapeutic antibodies based on antigen-dependent formation of IgG hexamers at the cell surface. *PLoS Biol.* **14** (2016), doi:10.1371/journal.pbio.1002344.

15. E. O. Saphire *et al.*, Crystal structure of a neutralizing human IGG against HIV-1: a template for vaccine design. *Science.* **293**, 1155–1159 (2001).

16. C. Gaboriaud *et al.*, The crystal structure of the globular head of complement protein C1q provides a basis for its versatile recognition properties. *J. Biol. Chem.* **278**, 46974–82 (2003).

17. A. M. Davies, R. Jefferis, B. J. Sutton, Crystal structure of deglycosylated human IgG4-Fc. *Mol. Immunol.* **62**, 46–53 (2014).

18. E. E. Idusogie *et al.*, Mapping of the C1q binding site on rituxan, a chimeric antibody with a human IgG1 Fc. *J. Immunol.* **164**, 4178–84 (2000).

19. M. H. Tao, R. I. Smith, S. L. Morrison, Structural features of human immunoglobulin G that determine isotype-specific differences in complement activation. *J. Exp. Med.* **178**, 661–667 (1993).

20. S. M. Canfield, S. L. Morrison, The binding affinity of human IgG for its high affinity Fc receptor is determined by multiple amino acids in the CH2 domain and is modulated by the hinge region. *J. Exp. Med.* **173** (1991).

21. T. E. Michaelsen *et al.*, A mutant human IgG molecule with only one C1q binding site can activate complement and induce lysis of target cells. *Eur. J. Immunol.* **36**, 129–138 (2006).

22. M. S. Kojouharova, I. G. Tsacheva, M. I. Tchorbadjieva, K. B. M. Reid, U. Kishore, Localization of ligand-binding sites on human C1q globular head region using recombinant globular head fragments and single-chain antibodies. *Biochim. Biophys. Acta.* **1652**, 64–74 (2003).

23. I. Bally *et al.*, Identification of the C1q-binding Sites of Human C1r and C1s: a refined three-dimensional model of the C1 complex of complement. *J. Biol. Chem.* **284**, 19340–8 (2009).

24. A. E. Phillips *et al.*, Analogous interactions in initiating complexes of the classical and lectin pathways of complement. *J. Immunol.* **182**, 7708–17 (2009).

25. V. U. Girija, A. R. Gingras, J. E. Marshall, R. Panchal, A. Sheikh, Structural basis of the C1q/C1s interaction and its central role in assembly of the C1 complex of complement activation. *Proc. Natl. Acad. Sci.* **110**, 13916–20 (2013).

26. M. Budayova-Spano *et al.*, Monomeric structures of the zymogen and active catalytic domain of complement protease c1r: further insights into the c1 activation mechanism. *Struct. London Engl. 1993.* **10**, 1509–1519 (2002).

27. M. Budayova-Spano *et al.*, The crystal structure of the zymogen catalytic domain of complement protease C1r reveals that a disruptive mechanical stress is required to trigger activation of the C1 complex. *Eur. Mol. Biol. Organ. J.* **21**, 231–239 (2002).

28. A. J. Perry *et al.*, A molecular switch governs the interaction between the human complement protease C1s and its substrate, complement C4. *J. Biol. Chem.* **288**, 15821–15829 (2013).

29. A. R. Gingras *et al.*, Structural basis of mannan-binding lectin recognition by its associated serine protease MASP-1: implications for complement activation. *Structure.* **19**, 1635–43 (2011).

30. H. Feinberg *et al.*, Crystal structure of the CUB1-EGF-CUB2 region of mannose-binding protein associated serine protease-2. *EMBO J.* **22**, 2348–59 (2003).

31. S. A. Mortensen *et al.*, Structure and activation of C1, the complex initiating the classical pathway of the complement cascade. *Proc. Natl. Acad. Sci.* **114**, 986–991 (2017).

32. S. E. Degn *et al.*, Complement activation by ligand-driven juxtaposition of discrete pattern recognition complexes. *Proc. Natl. Acad. Sci.* **111**, 13445–13450 (2014).

Acknowledgements

Author contributions

Chapter 2

Supplementary materials

Materials and methods

Expression and Purification of the Proteins

Plasma-purified human C1q was purchased from Complement Technology, Inc. (Tyler, TX, USA). IgG1-RGY variant (E345R, E430G, and S440Y), IgG1-b12 and IgG1-7D8 were described previously (*5, 15, 33*). IgG1-DNP consisted of the murine variable domain of antibody G2a2 fused to a human IgG1 constant domain (*34*). IgG1-DNP and IgG1-7D8 antibody variants were created by gene synthesis of codon optimized open reading frames (Geneart Thermo Scientific, Regensburg, Germany), subcloned into pcDNA3.3-derived expression vectors. All antibodies were expressed, purified and characterized as described (*14*). C1q-depleted serum was obtained from Quidel (San Diego, CA).

C1r (S654A) and C1s (S632A) mutants were generated using the Quikchange mutagenesis kit (Agilent Genomics, Santa Clara, CA) on TOPO clones inserted in pCR8 vectors (Thermo Fisher Scientific, Waltham, MA). All C1r and C1s constructs were sub-cloned into mammalian expression vectors carrying either a hexa-histidine tag or StrepII3-tag provided by U-Protein Express BV (U-PE), Utrecht, The Netherlands. C1r and C1s constructs were co-expressed in N-acetylglucosaminyltransferase I (GnTI)-deficient human embryonic kidney 293 cells that stably express Epstein-Bar virus nuclear antigen EBNA1 (HEK293-ES supplied by U-Protein Express BV). The supernatant was harvested on the 5th day of the expression, concentrated and dia-filtrated using a Quixstand system (GE Healthcare, Chicago, IL). $C1r_2s_2$ was purified by Ni-NTA affinity chromatography (GE Healthcare) followed by a size-exclusion chromatography step on a Super-dex 200 column (GE Healthcare). $C1-IgG1_6$ complexes were prepared by mixing $C1r_2s_2$, C1q and IgG1-RGY in 4:1:6 molar ratio. The complex was purified by gel filtration column BioSep 4000 15 ml column.

Cell culture

Raji cells (human Burkitt's lymphoma) were obtained from the American Type Culture Collection (ATCC no. CLL-86; Rockville, MD) and cultured according to the supplied instructions. Cells were routinely tested for mycoplasma contamination.

Tomography sample preparation and data collection

Liposomes were prepared from dried films of cholesterol, DMPC, DMPG and cap-DNP-PE (all sourced from Avanti Polar Lipids, Alabaster, AL) at a molar ratio of 100:90:10:1, respectively. Films were hydrated in buffer (50 mM HEPES, pH 8.0, 145 mM NaCl, and 3 mM $CaCl_2$) at 37°C for 4 hours and extruded through 200 nm pore filters at 45°C. Liposomes, IgG1-DNP, and plasma-purified human C1 complex (Complement Technology Inc., Tyler, TX) were mixed on ice at final concentrations of 1.3 mg/ml, 0.025 mg/ml and 0.017 mg/ml, respectively, then brought to room temperature and allowed to equilibrate for approximately 30 minutes. Gold fiducials coated in bovine serum albumin (Aurion, Wageningen, The Netherlands) were added to the samples immediately before 3 μl of the mixture was applied to freshly glow-discharged Quantifoil R2/1 300 mesh holey carbon grids in the chamber of a Leica EM-GP plunge-freezer (Leica, Germany) set at 96% humidity and 21°C. Grids were blotted for 1 sec and plunged into liquid ethane.

Tomograms were collected at NeCEN (Leiden, The Netherlands) on a Titan Krios (Thermo Fisher Scientific) operating at 300 kV equipped with a phase plate (Thermo Fisher Scientific) heated to 225°C. Zero-energy-loss images were acquired using the software program FEI Tomography 4 (Thermo Fisher Scientific), using a GIF-Quantum LS energy filter (Gatan, Pleasanton, CA) with a slit width of 20 eV. A K2 Summit direct electron detector (Gatan) was used in counting mode at a nominal magnification of 53,000× for a pixel size of 2.69 Å at the sample. Tomographic tilt series were collected from ±50° in 2° increments with a dose rate of 0.9 electrons per Å^2 per sec for a total dose of 60 electrons per Å^2 per tilt axis (dual-axis tomograms received a total dose 120 electrons per Å^2). Exposures of 0.9 seconds were dose-fractionated into 6 movie frames per tilt angle. Before each tilt series, the Volta phase plate was advanced and conditioned for 5 minutes to generate an approximate phase shift of 90°. The phase plate was also conditioned for an additional 5 s between every fifth tilt image. Defocus values were set to -0.3 μm after tilting and before each image acquisition, which is sufficient to maintain negative phase contrast up to ~19 Å (*35*).

Tomography reconstruction and sub-volume averaging

Raw frames were aligned using MotionCorr (*36*) and tomograms were reconstructed using IMOD (*37*) after binning the aligned frames by 2 (final pixel size of 5.38 Å). Single- and dual-axis tomograms were processed using the same workflow for the reconstruction of each axis. Axes for dual-axis tomograms were combined using IMOD. The surfaces of liposomes were manually segmented from simultaneous iterative reconstruction technique (SIRT) reconstructions us-

ing Dynamo (*38*) and equally spaced boxes across the surface were extracted from weighted back-projection reconstructions for further processing. Dynamo tracks the orientation for each particle, and thereby allows for Fourier-space masks to be constructed for each sub-volume to account for missing information caused by selected tilt geometries (*38*). An initial model was generated by manually aligning 107 sub-volumes from the dual-axis tomograms and low pass filtered to 6 nm (Fig. S2C). White noise was added using EMAN2 (*39*) to five copies of the filtered initial model, which were then used for the classification and alignment of all the dual-axis sub-volumes. The best average from the dual-axis alignments was again low pass filtered to 6 nm and four noisy copies used for the classification and alignment of the single-axis sub-volumes. Initial rounds of classification for bare or decorated membrane surfaces were performed using data further binned by 2 (binned by 4 from the raw images) and low pass filtered, using the membrane orientation as a constraint on the alignment parameters (±30° maximum deviation in the sub-volume's inclination from the starting orientation and full freedom to rotate in the azimuthal direction). If the aligned sub-volumes were not separated by at least 10 nm in the original tomogram, the sub-volume with the lower correlation score was discarded from further processing. From classes that were not bare membrane, sub-volumes containing C1 complexes (often mixed with antibody-alone sub-volumes) were manually selected and the correct orientation verified from individual sub-volume projections. These coordinates were used to re-extract the sub-volumes from weighted-back projection tomograms. The sub-volumes were then subjected to a global orientation search again using binned and low-pass filtered data for the initial rounds and refined following gold-standard procedures. Sub-volumes that did not align correctly were again manually discarded by inspecting projections of the sub-volumes after the orientation determined by the alignment procedure was applied. The C1-mAb complex shape and the membrane provide obvious features to verify the alignment. The final stack of verified C1-mAb sub-volumes was then subjected to further classification using the ellipsoidal mask shown in Fig. S2E to generate the classes shown in Fig. S2C. A box size of 128 pixels cubed was used for the initial alignment and classification steps of the dual-tilt tomograms. For the focussed alignment and classification shown in Fig. 1C, particles were aligned using the cylindrical mask shown in Fig. S2E and a box size of 84 pixels. A box size of 168 was used to investigate the neighboring C1-mAb complexes using a biased ellipsoid mask that fitted three mAb-C1 complexes in a line (Fig. S2E). The nearest neighbor distances were determined by computing the distance between aligned sub-volumes within each tomogram. The x-, y- and z-shifts were added to the original coordinates of the sub-volume to calculate the C1 complex centre. The center-to-center distance for

all particles was calculated and the minimum pairwise value was taken as the nearest neighbour distance shown in Fig. S2F. The final number of sub-volumes was 564 dual-axis and 3,190 single-axis. The final number of particles that contributed to the average shown in Fig. 1B is 1,660.

Sample preparation and data collection for single-particle cryo-EM

A volume of 3 μl of purified C1-IgG1$_6$ at a concentration of 0.2 mg/ml was applied to freshly glow discharged R1.2/1.3 holey carbon grids (Quantifoil). The grids were blotted for 1 s at 99% humidity in a Vitrobot plunge-freezer (Thermo Fisher Scientific). Cryo-EM images were collected at EM-square (Utrecht, The Netherlands) on a Talos Arctica (Thermo Fisher Scientific) operating at 200 kV equipped with a Falcon II direct detector (Thermo Fisher Scientific) operating in movie mode. Images were recorded manually at a nominal magnification of 42,000× yielding a pixel size at the specimen of 2.27 Å. Using the EPU software (Thermo Fisher Scientific), 3,493 micrographs were recorded. Movies were collected for 3 s with a total of 52 frames with a calibrated dose rate of 10.4 e$^-$/ Å^2 per second, a total dose of ~31 e$^-$/Å^2, and at defocus values between -1.8 and -3 μm. An example micrograph is shown in Fig. S4A.

Single Particle Analysis

Movie stacks were aligned using MotionCorr (*36*). CTF parameters were defined using Ctffind4 (*40*). A total of ~282,150 particles were picked using particle-picking software from Relion using 2D class averages of 2500 manually picked particles (*41*); see Fig. S4C for a schematic representation of the workflow. The particles were aligned and classified iteratively by 2D classification according to their 2D projection views using the software package Relion (*42*). ~168,341 particles were selected from classes with top projections of 6 gC1q domains bound to Fc platform and side views with visible collagen arms for *ab initio* 3D reconstruction in Cryosparc (*43*). Second set of 65,768 particles were selected from classes with top projections of 4 or 5 gC1q domains bound to Fc platform and the remaining side views. From the first particle set (left column in Fig.S4C), an unbiased 3D reconstruction without reference and mask yielded a class with ~79,120 particles which was selected as an initial model. The map was low-pass filtered and used as a reference for 3D classification on the gC1q-Fc platform. A soft mask in Relion around gC1q-Fc platform was generated by extending 3 pixels and softening the edge by further 10 pixels. Focused classification using this mask yielded five classes with a resolution up to 15 Å. 3D refinement of a selection of 126,372 particles in Relion resulted in a 14 Å map. Two masks were generated using this map around the full C1-IgG6 complex (extended by 3 pixels

and softening by 10 pixels) and around gC1q-Fc platform (extended by 2 pixels and softening by 20 pixels). The initial selected class of 79,120 particles was used for 3D refinement in Cryosparc (homogenous refinement option) with the 14 Å map used as a reference and the mask around full C1-IgG1$_6$ complex. After 3D refinement in Cryosparc and postprocessing in Relion, the resolution was 10 Å. 3D refinement applying C6 symmetry with the mask around gC1q-Fc platform and subsequent post-processing resulted in 7.3 Å map. The resolutions were estimated by Fourier shell correlation between two half maps (each calculated independently) as a function of resolution and using the gold-standard FSC = 0.143 criterion. For classification and refinement, a box size of 224 pixels was used. Particle-polishing procedure implemented in Relion software did not improve the resolution (data not shown). The second set of particles (right column in Fig.S4C) were used for 3D classsification using a mask around gC1q-Fc platform. 44,121 particles showing 4 gC1q domains abound to Fc platform was reconstructed by 3D refinement and postprocessing. 12,781 particles showing 5 gC1q domains bound to Fc platform was reconstructed by 3D refinement and postprocessing.

Modeling C1 structure into density map

Crystal structures were fitted into densities using the "Fit in Map" routine from Chimera (*44*) Fc CH2, CH3, CH2' and CH3' domains were taken from the IgG1 b12 structure (pdb-code 1HZH) (*15*) and fitted independently into the density map obtained at 7.3-Å resolution. gC1q globular heads (1PK6) (*16*) were fitted in the same map in three orientations for the C1q-A, B and C domains and the orientation with the highest correlation coefficient (0.95) calculated by Chimera was selected. The serine proteases C1r and C1s were fit into the map using previously modelled arrangements of C1r$_2$s$_2$ bound to C1q (*23–25*) see Fig. S7A. The hetero-dimer C1rs started from the C1s homo-dimer structure of CUB1-EGF-CUB2 (4LMF) (*25*). One C1s copy was modified into C1r CUB1-EGF-CUB2 using homology modeling (SWISSMODEL) (*45*) to generate the initial C1rs model. C1r and C1s CUB1 interactions with collagen (i.e. with C1q arm 3 and 1 resp.) were modeled using the orientations found in the crystal structure of C1s CUB1-EGF-CUB2 bound to a collagen peptide (4LOR) (*25*). C1r CUB2 interaction with collagen of C1q arm 2 was modeled using the crystal structure of MASP CUB2 bound to collagen peptide (3POB) (*29*). This model of the C1rs hetero-dimer, C1r CUB1-EGF-CUB2 and C1s CUB1-EGF-CUB2, was placed into the density map obtained at 10-Å resolution and adjusted to fit the density (Fig. S7A). Available densities for C1r and C1s CCP1 domains were modeled using the C1s CUB2-CCP1 structure (4LOS) (*25*). The model of C1rs CUB1-EGF-CUB2-CCP1 hetero-dimer was duplicated and rotated by 180° to model the other

half of the density and minor adjustments were made to fit the density. Finally, we predicted the positions for the CCP2-SP domains of C1r and C1s, for which no densities were observed in the map. Starting from the positions and orientations of CUB-CCP1 domains, the model was extended using CCP1-CCP2-SP from the structure of zymogen C1r (1GPZ and 1MD7) (*26*, *27*) and zymogen C1s (4J1Y) (*28*), and aligning them according to the arrangement observed in the structure of the C1s CUB2-CCP1-CCP2 fragment (4LOT) (*25*). The cross-correlation coefficient of C1-IgG1$_6$ model and the final map was 0.78 and gC1q-Fc and the bottom platform was 0.65 according to the scoring assessment tool of TEMPy (*46*).

Complement-dependent cytotoxicity assay

Raji cells were washed twice with PBS and subsequently re-suspended in RPMI 1640 medium (containing 0.1% BSA and Pen/Strep). Cells were added to a 96-well plate (1E+05 cells/well) followed by addition of mAbs at a concentration of 10 µg/mL and then incubated for 15 minutes (RT). Subsequently, a concentration series of 1 ng/mL to 60 ug/mL C1q protein (Quidel, A400) was added, and C1q-deficient serum (Quidel, A509) was added to a final concentration of 20% as a source of complement. After incubation for 45 minutes at 37°C, cells were immediately placed on ice. After centrifugation, supernatant was discarded and cells were re-suspended in BSA-PBS containing 1 µg/mL PI. The fraction of PI (+) cells (100% * (PI(+) cells/total cells) was determined using an iQue Screener flow cytometer (Intellicyt, Albuquerque, NM). The area under the curve (AUC) of three experimental replicates was calculated using a log transformed concentration axis with GraphPad Prism 7.02 and normalized relative to cell lysis measured for wild type IgG1-7D8 (WT) set at 100% and the nonbinding control IgG1-b12 set at 0%. AUC values were collected for IgG1-7D8 antibody variants in two independent series of three experimental replicates. Mean AUC (normalized per series) and standard deviation (SD) were determined and are presented in figures 3 and S6. One-way ANOVA of mean AUC was followed by Dunnett's Multiple Comparison Posthoc Test using GraphPad Prism 7.02. A p value <0.05 indicates that CDC obtained with the mutant is different from that obtained with WT 7D8. Data is summarized in supplementary table S1. Without C1q added, background cell lysis by 10 µg/mL IgG1-b12 or IgG1-7D8 was similar.
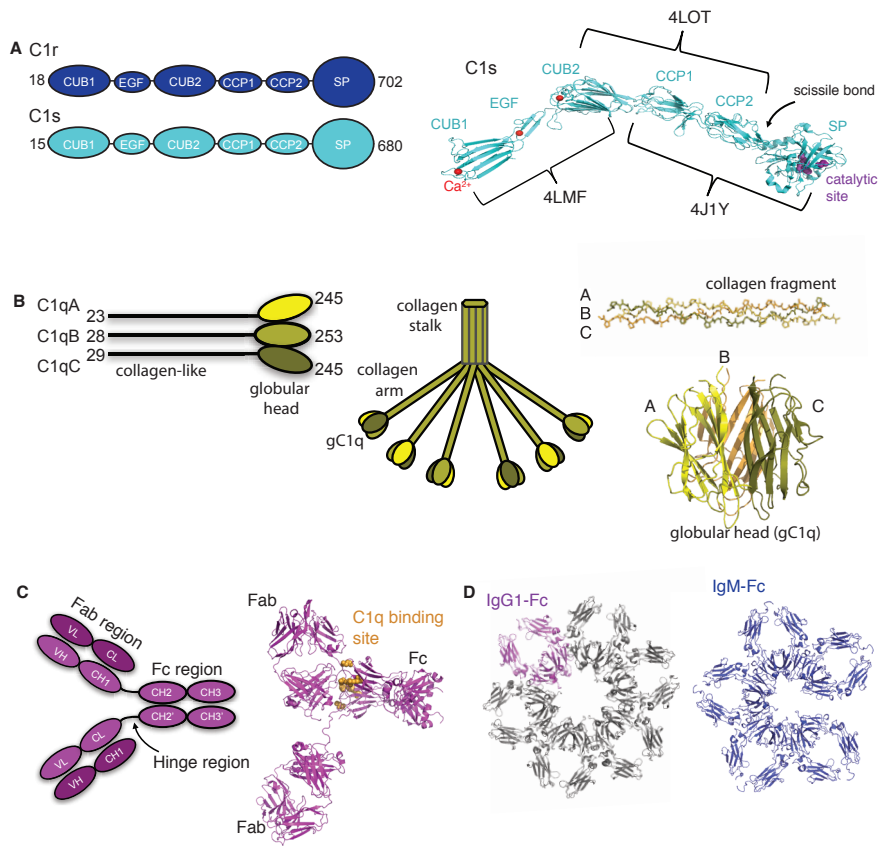
Supplementary Fig. S1. Domain compositions and prior structural information.

A) Domain compositions of C1r and C1s, indicating the first 'Complement C1r/C1s, Uegf, Bmp1' (CUB1), epidermal growth factor-like (EGF), second CUB (CUB2), first complement-control-protein (CCP1), second CCP (CCP2), and serine-protease (SP) domains; and, composite structural model of C1s built up from overlapping crystal structures (with pdb-codes 4LMF, 4LOT and 4JIY, as indicated (*25, 28*)). Generation of a composite model for C1r yields a highly similar domain arrangement as that for C1s (not shown). Indicated are the three calcium-binding sites (by red calcium ion), scissile bond (arrow) and catalytic site (purple). B) Composition of C1q, showing the hetero-trimer chains A, B and C, which form a collagen-like region and trimeric globular head (left). Six chain of C1q A, B and C form the overall C1q assembly (middle). A collagen triple helix model, (colored and labeled with as a hetero-trimer, mimicking the situation in C1q) and the crystal structure of gC1q (1PK6) (*16*). C) Composition of an IgG molecule, showing light chain and variable constant domains (VL and CL, resp.) and heavy chain variable, constant-1, 2 and 3 domains (VH, CH1, CH2 and CH3, resp.), antigen-binding fragment (Fab), Fc and hinge region. Shown are a cartoon (left) and crystal structure 1HZH (*15*). Residues involved in C1q binding are schematically shown by yellow dots. D) Six-fold arrangements of IgG1 Fc domains as observed in the crystal packing contacts in pdb 1HZH. The hexamer is shown in black with the Fc domain of a single IgG molecules highlighted in red (left). Model of the Fc arrangement in a single pentameric IgM molecule (right) (*47*)
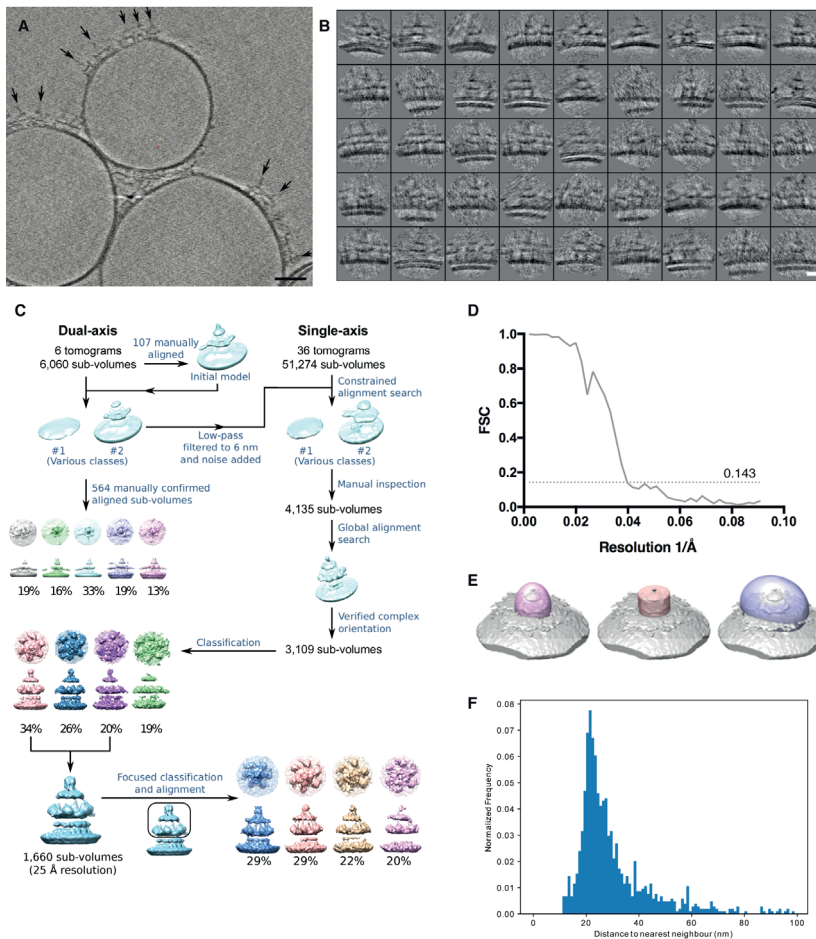
Supplementary Fig. S2. Cryo-EM tomography of C1 bound to IgG1 on liposomal surfaces and image analysis workflow.

A) A 10.8 nm-thick slice through a single-tilt tomogram of liposomes decorated with a chimeric anti-DNP IgG1 monoclonal antibody and C1 complexes. The scale bar indicates 20 nm. B) Raw images of IgG1-C1 complexes from single-tilt tomograms after coarse alignment. The scale bar indicates 10 nm. C) Sub-volume alignment and classification workflow. A subset of 107 sub-volumes from dual-axis tomograms were manually aligned to generate an initial model. The initial model was used to align and classify the dual-axis sub-volumes. The resulting average from the dual-axis data was used to process the single-axis sub-volumes. Due to the extensive flexibility, all assignments into the decorated class and final orientation of the aligned sub-volume were manually verified. Multi-reference refinement using five classes (dual-tilt) and four classes (single-tilt) revealed classes showing flexibility of the structure and consistent presence of six IgG1-Fc and gC1q domain-containing densities. The percentage of sub-volumes assigned to each class is shown below the image. From the single-axis sub-volumes, two of these classes were nearly identical and contained the majority of particles (54% total), which were subjected to a final alignment round, which yielded the density map shown in Fig. 1B.

Supplementary Fig. S2. Cryo-EM tomography of C1 bound to IgG1 on liposomal surfaces and image analysis workflow. *(continued)*

Focussed alignment and classification on the Fc domains and C1 complex yielded the reconstruction shown in Fig. 1C. (**D**) Fourier shell correlation (FSC) curve for the complete IgG1-C1 complex showing $FSC_{0.143} = 25$ Å. (**E**) Masks used during sub-volume alignment and classification of complete mAb-C1 complexes (left), focussed refinement of the Fc-C1 complex (middle), and to investigate neighboring mAb-C1 complexes (right). (F) Histogram showing the calculated distances between nearest neighbour mAb-C1-IgG1 complexes.
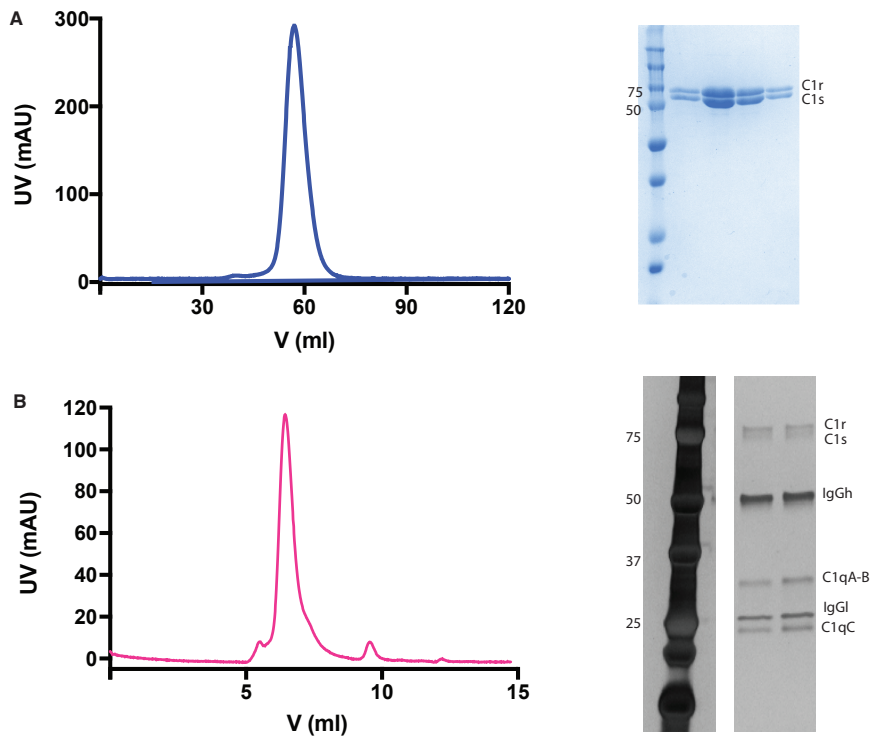
Supplementary Fig. S3. Sample preparation for single-particle cryo-EM.

A) Gel-filtration profile of $C1r_2s_2$ purified with a Superose 6 16/60 column. A Coomassie-stained reducing SDS-PAGE gel is shown on the right. B) Gel-filtration profile of $C1\text{-}IgG1_6$ purified with a BioSep 4000 column. Silver-stained reducing SDS-PAGE gel shows C1r, C1s, IgG1 heavy chain (IgGh) and light chain(IgGl), C1q-A, B and C chains on the right.
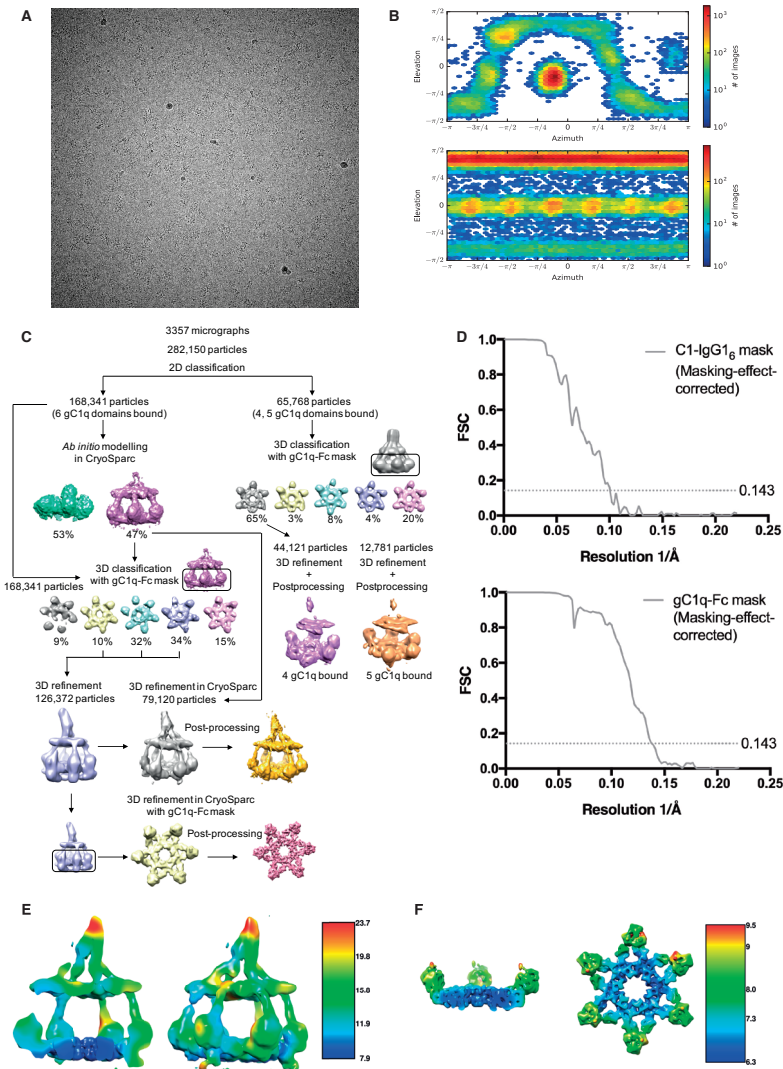
Supplementary Fig. S4. Cryo-EM single particle analysis of C1-IgG1$_6$ and single particle analysis workflow.

A) Representative micrograph of with a pixel size of 2.27 Å and a defocus value of -2.2 μm. B) Direction distribution plots of particles for non-symmetric C1-IgG1$_6$ map and C6-symmetry imposed gC1q-Fc map. C) Single particle reconstruction workflow. 2D classification, 3D classification, 3D refinement and postprocessing jobs were performed by Relion 2.0 except the jobs stated as "in Cryo Sparc". The mask applied around the gC1q-Fc region is shown as black box. The percentages of the particles for classification jobs are stated below the densities. D) Fourier-shell correlation curve of C1-IgG1$_6$ map (top) and C6-symmetry imposed gC1q-Fc map (bottom) E) Single-particle reconstruction of C1-IgG1$_6$ colored by local resolution expressed in Å F) C6-symmetry imposed single-particle reconstruction of gC1q units bound to Fc-platform colored by local resolution.
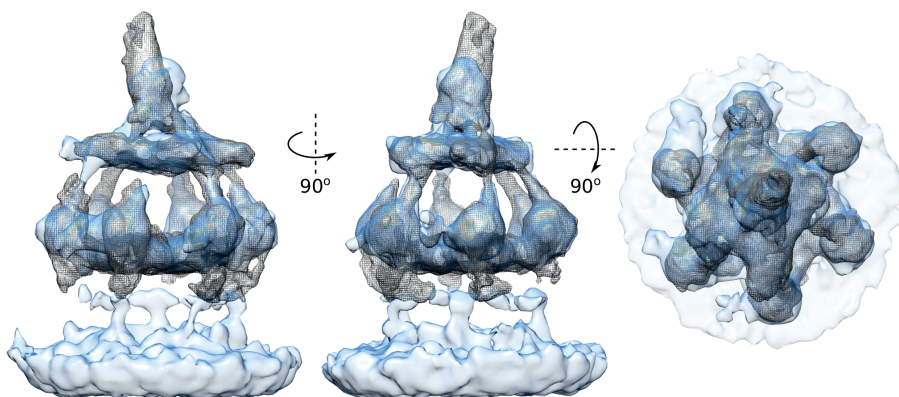
Supplementary Fig. S5. Comparing cryo-EM tomography and single-particle reconstructions.

Reconstructions derived from tomograms (blue surface; from Fig. 1C) and single-particle analysis (grey mesh; from Fig. 2C) aligned to show similarities in density from the side (left and middle) and top (right).
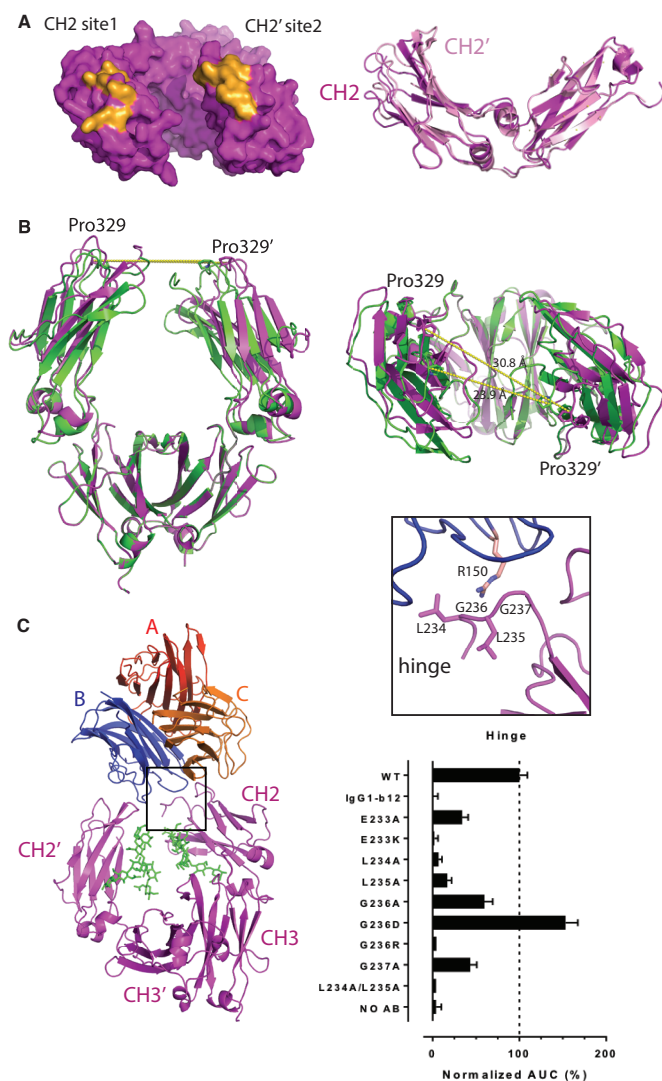
Supplementary Fig. S6. Identification of residues participating in gC1q-Fc interactions.

A) Surface-area representation of Fc (magenta) with binding sites on CH2 and CH2' as footprint of gC1q (orange) (left). Alignment of CH2 and CH2' in cartoon representation (right) B) Fc (magenta) with a distance of 31 Å between Pro329-Pro329' and Fc arrangement as observed in the IgG1- b12 crystal structure (1HZH) exhibiting Pro329-Pro329' distance 23.8 Å (green). C) The Fab-Fc hinge region contributes to C1q binding. IgG Fc domain in magenta, glycans in green, C1q-A, B and C domains in red, blue, and orange respectively. Right panel: Complement dependent cytotoxicity assays of Raji cells opsonized with wild-type (WT) and mutated CD20 mAb IgG1-7D8 (n=3) exposed to C1q-deficient serum to which a titration of 1 ng/mL to 60 μg/mL C1q was added. Cell lysis was assessed by flow cytometry using propidium iodide staining. Bars show the average area under the curve (AUC) for this dose response normalized against the AUC obtained with the unmutated WT IgG1-7D8 set to 100%.
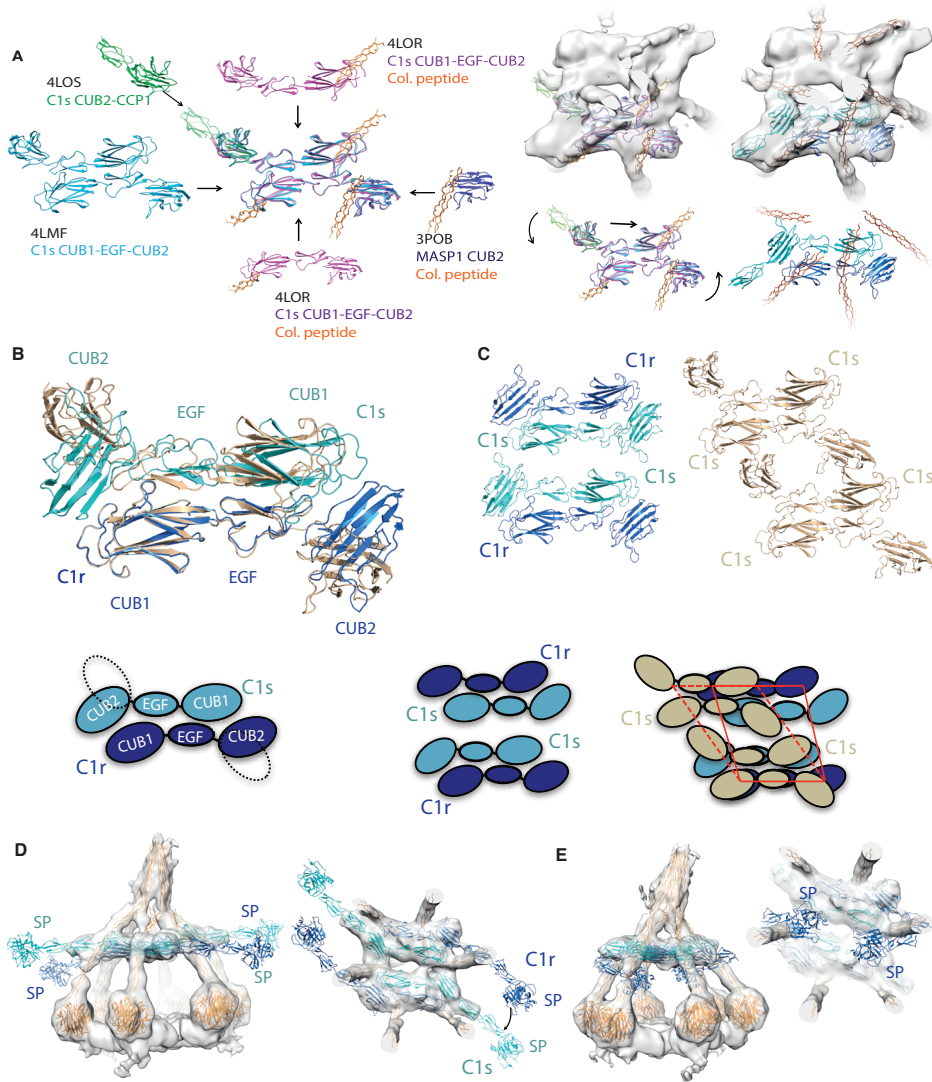
Supplementary Fig. S7. C1r and C1s arrangements.

A) Crystal structures used for fitting of C1r and C1s into the density. Initial positioning of each structure is shown on the left. The manual changes applied for fitting are shown by arrows. Final models (inside and outside the density) are shown on the right. *B*) Superposition of the N-terminal CUB1-EGF-CUB2 domains of C1r (blue) and C1s (cyan) in C1-IgG1$_6$ onto the C1s CUB1-EGF-CUB2 arrangement (beige) observed in crystal structure 4LMF (*25*), indicating different orientations of CUB2 domains. C) Comparison of C1s-C1s arrangements in C1-IgG1$_6$ and the tetrameric packing of C1s observed in crystal structure 4LMF. Cartoon representations of the N-terminal CUB1-EGF-CUB2 arrangement for the C1r-C1s hetero-dimer in C1-IgG1$_6$ (left), with dashed line indicating the orientation of CUB2 domains in 4LMF, arrangement of the CUB1-EGF-CUB2 of C1r-C1s-C1s-C1r in

C1-IgG1$_6$ (middle) and superposition of C1s CUB1-EGF-CUB2 stacking observed in 4LMF (right). Parallelograms in red solid and dashed lines indicate the effect of shifting the central C1s molecules by ca. 20 Å sideways. D) Hypothetical model obtained by extending CCP2-SP outwards in side (left) and bottom view (right). This arrangement, that is consistent with the observed density, supports the catalytic SP domain C1r to reach and cleave the scissile bond of the adjacent C1s. E) Modeling C1r CCP2-SP oriented inwards for putative auto-activation in side view (left) and bottom view (right), indicating that the observed density of C1-IgG1$_6$ is not consistent with an intra-complex auto-activation of C1r by the opposing C1r. Generation of a C1r-C1r enzyme-substrate arrangement within a single C1 would require domain rearrangements incongruent with the observed density. Moreover, no density is observed in between the N-terminal protease platform and Fc platform in our data (both from tomography and single-particle analysis).

Chapter 2

Supplementary Table S1

Experimental series 1

Antibody	Location	Mean AUC (%) (1)	SD (%) (2)	N (3)	One way ANOVA, Dunnett's multiple comparisons test		
WT IgG1-7D8	Control	100.0	9.2	3	**Mean difference**	**95% CI of difference**	**Adjusted p value (4)**
IgG1 b12	Control	0.0	5.9	3			
E233A	Hinge	34.0	6.8	3	66	40.7 to 91.3	<0.0001
E233K	Hinge	1.8	4.3	3	98.2	72.9 to 123	<0.0001
L234A	Hinge	6.8	4.0	3	93.2	67.9 to 119	<0.0001
L235A	Hinge	16.9	5.0	3	83.1	57.8 to 108	<0.0001
G236A	Hinge	59.7	9.5	3	40.3	15 to 65.6	<0.0001
G236D	Hinge	153.1	14.2	3	-53.1	-78.4 to -27.8	<0.0001
G236R	Hinge	4.2	3.4	3	95.8	70.5 to 121	<0.0001
G237A	Hinge	43.4	7.4	3	56.6	31.3 to 81.9	<0.0001
E269A	Site 2	32.0	7.2	3	68	42.7 to 93.3	<0.0001
E269K	Site 2	10.7	8.5	3	89.3	64 to 115	<0.0001
E294A	Site 2	82.0	7.3	3	18	-7.25 to 43.3	0.3575
E294K	Site 2	24.1	7.9	3	75.9	50.6 to 101	<0.0001
S298A	Site 2	110.6	9.7	3	-10.6	-35.9 to 14.7	0.9629
S298K	Site 2	14.1	7.0	3	85.9	60.6 to 111	<0.0001
Y300A	Site 2	145.6	11.8	3	-45.6	-70.9 to -20.4	<0.0001
Y300D	Site 2	207.2	13.0	3	-107	-133 to -81.9	<0.0001
Y300R	Site 2	26.8	11.3	3	73.2	48 to 98.5	<0.0001
K322A	Site 1	15.4	6.9	3	84.6	59.3 to 110	<0.0001
A327G	Site 1	145.6	10.6	3	-45.6	-70.9 to -20.4	<0.0001
A327E	Site 1	100.0	9.5	3	0	-25.3 to 25.3	0.9999
A327K	Site 1	13.3	6.8	3	86.7	61.4 to 112	<0.0001
No Ab	Control	3.8	6.1	3	96.2	70.9 to 121	<0.0001

Supplementary Table S1

Experimental series 2

Antibody	Location	Mean AUC (%) (1)	SD (%) (2)	N (3)	One way ANOVA, Dunnett's multiple comparisons test		
WT IgG1-7D8	Control	100.0	10.6	6	**Mean difference**	**95% CI of difference**	**Adjusted p value (4)**
IgG1 b12	Control	0.0	4.2	6			
H268Q	Site 2	75.4	7.3	3	24.6	6.39 to 42.7	0.0031
D270A	Site 2	-0.7	3.0	3	101	82.5 to 119	<0.0001
N297Q	Site 2	-0.4	2.6	3	100	82.2 to 119	<0.0001
K322A	Site 1	-0.4	2.7	3	100	82.2 to 119	<0.0001
P329A	Site 1	-2.0	2.9	3	102	83.9 to 120	<0.0001
P331A	Site 1	12.9	6.7	3	87.1	68.9 to 105	<0.0001
L234A/L235A	Hinge	3.8	4.8	3	96.2	78 to 114	<0.0001
K326A/E333A	Site 1	223.7	11.6	3	-124	-142 to -105	<0.0001
No Ab	Control	-0.7	3.8	3	101	82.6 to 119	<0.0001

Area under the curve (AUC) values for CDC of Raji cells normalized relative to the WT IgG1-7D8, which was set at 100% lysis. CDC data were collected in in two independent series of three experiments, and were normalized per series (top panel, bottom panel). Mean area under the curve (AUC) (1), standard deviation (SD) (2), number of replicates (N) (3), and multiplicity adjusted p-value of statistical analysis (4) are shown. One-way ANOVA was followed by Dunnett's Multiple Comparison Posthoc Test using GraphPad Prism 7.02. A p-value <0.05 indicates that the CDC induced by a mutant was different from that determined for wild-type IgG1-7D8.

Chapter 2

Suplementary References

33.   J. L. Teeling *et al.*, Characterization of new human CD20 monoclonal antibodies with potent cytolytic activity against non-Hodgkin lymphomas. *Blood.* **104**, 1793–1800 (2004).

34.   K. D. White, M. B. Frank, S. Foundling, F. J. Waxman, Effect of immunoglobulin variable region structure on C3b and C4b deposition. *Mol. Immunol.* **33**, 759–768 (1996).

35.   X. Fan *et al.*, Near-Atomic Resolution Structure Determination in Over-Focus with Volta Phase Plate by Cs-corrected Cryo-EM. *bioRxiv.* **25**, 1623–1630.e3 (2017).

36.   X. Li *et al.*, Electron counting and beam-induced motion correction enable near-atomic-resolution single-particle cryo-EM. *Nat. Methods.* **10**, 584–90 (2013).

37.   D. N. Mastronarde, S. R. Held, Automated tilt series alignment and tomographic reconstruction in IMOD. *J. Struct. Biol.* **197**, 102–113 (2017).

38.   D. Castaño-Díez, M. Kudryashev, H. Stahlberg, Dynamo Catalogue: Geometrical tools and data management for particle picking in subtomogram averaging of cryo-electron tomograms. *J. Struct. Biol.* **197**, 135–144 (2017).

39.   G. Tang *et al.*, EMAN2: An extensible image processing suite for electron microscopy. *J. Struct. Biol.* **157**, 38–46 (2007).

40.   A. Rohou, N. Grigorieff, CTFFIND4: Fast and accurate defocus estimation from electron micrographs. *J. Struct. Biol.* **192**, 216–221 (2015).

41.   S. H. W. Scheres, Semi-automated selection of cryo-EM particles in RELION-1.3. *J. Struct. Biol.* **189**, 114–22 (2015).

42.   S. H. W. Scheres, RELION: Implementation of a Bayesian approach to cryo-EM structure determination. *J. Struct. Biol.* **180**, 519–530 (2012).

43.   A. Punjani, J. L. Rubinstein, D. J. Fleet, M. A. Brubaker, cryoSPARC: algorithms for rapid unsupervised cryo-EM structure determination. *Nat. Methods.* **14**, 290–296 (2017).

44.   E. F. Pettersen *et al.*, UCSF Chimera—A Visualization System for Exploratory Research and Analysis. *J Comput Chem.* **25**, 1605–1612 (2004).

45.   J. Kopp, T. Schwede, The SWISS-MODEL Repository of annotated three-dimensional protein structure homology models. *Nucleic Acids Res.* **32**, D230-4 (2004).

46.   I. Farabella *et al.*, TEMPy: A Python library for assessment of three-dimensional electron microscopy density fits. *J. Appl. Crystallogr.* **48**, 1314–1323 (2015).

47.   S. J. Perkins, A. S. Nealis, B. J. Sutton, A. Feinstein, Solution structure of human and mouse immunoglobulin M by synchrotron X-ray scattering and molecular graphics modelling. A possible mechanism for complement activation. *J. Mol. Biol.* **221**, 1345–1366 (1991).

Chapter 3

C1 is assembled through C1rs hetero-dimers

Deniz Ugurlar[1]; Guanbo Wang[2], Rob N. de Jong[3], Frank J. Beurskens[3], Paul W.H.I. Parren[4], Albert J.R. Heck[2], Piet Gros[1]

[1] *Crystal and Structural Chemistry, Bijvoet Center for Biomolecular Research, Department of Chemistry, Faculty of Science, Utrecht University, Padualaan 8, 3584 CH Utrecht, The Netherlands*

[2] *Biomolecular Mass Spectrometry and Proteomics, Bijvoet Center for Biomolecular Research and Utrecht Institute for Pharmaceutical Sciences, Utrecht University, Padualaan 8, 3584 CH Utrecht, The Netherlands*

[3] *Genmab, Yalelaan 60, 3584 CM Utrecht, The Netherlands*

[4] *Department of Immunohematology and Blood Transfusion, Leiden University Medical Center, Albinusdreef 2, 2333 ZA Leiden, the Netherlands*

ABSTRACT

Complement-component C1 initiates cell clearance by recognizing danger patterns on cells that activate its associated proteases and trigger the complement cascade. The mechanism of assembly of proteases $C1r_2s_2$ and C1q into C1 and activation of C1r and C1s upon C1q binding to danger patterns are critical, but have remained unclear. Here, we show by native mass spectrometry and pull-down assays that $C1r_2s_2$ is a dynamic complex through spontaneous association and dissociation of C1rs hetero-dimers assembles with C1q into C1 ($C1qr_2s_2$). Binding of C1 to antibody complexes reduces the dissociation rate of C1rs hetero-dimers from C1. The dynamic $C1r_2s_2$ hetero-tetramer indicates that C1 assembly would not require major protease rearrangements. Instead, our data favors an assembly model, which distinguishes activating surfaces from fluid phase by reducing dissociation rates of the complexes, which is accompanied by complement activation on surfaces.

INTRODUCTION

Mammalian complement proteins form an immune protection system against invading microorganisms and altered host cells in blood and interstitial fluids (for reviews see e.g. Walport, 2001; Ricklin *et al*, 2016; Melis *et al*, 2015). The first complement component C1 recognizes a variety of danger patterns. It binds, among others, advanced apoptotic cells (*4*), beta-amyloid fibrils and various molecular motifs on Gram-negative bacteria and viruses (*5*). Moreover, C1 binds targets mediated by antibodies, C-reactive proteins or pentraxin PTX3 forming complexes on surfaces (McGrath *et al*, 2006). When bound to its target, the associated proteases C1r and C1s become activated and initiate the classical pathway of complement activation that labels target cells for clearance by phagocytic cells or lysis by pore formation. Deficiency of C1 activation leads to auto-immune diseases like systemic lupus erythematosus (*7*) and recurrent bacterial infections (*8*), whereas deficiency of C1 inhibitor (C1-INH), a member of the serine protease inhibitor (serpin) family, causes hereditary angioedema (*9*). C1 has also been shown to play a role in synaptic pruning, which links to neurodegenerative diseases such as schizophrenia (*10*), Alzheimer's disease (*11*), or virus-induced spatial memory impairment (*12*). Understanding of the underlying mechanisms of C1 assembly and activation will aid drug development against C1-associated diseases.

C1, or $C1qr_2s_2$, is a multi-molecular complex of ca. 790-kDa molecular weight consisting of a hetero-tetramer of two serine proteases C1r and C1s and a hexamer of trimeric recognition molecules C1q (Schumaker *et al*, 1987); see Table 1. C1r and C1s are homologous proteases that each consist of six domains, a 'complement C1r/C1s, Uegf, Bmp1' (CUB) domain, an epidermal-growth-factor-like (EGF) domain, a second CUB domain, two 'complement-control protein' (CCP) domains and at the C-terminus a serine protease (SP) domain (reviewed by Forneris *et al*, 2012), see Figure 1A. Like homologous trypsin and chymotrypsin proteases, the pro-enzymes C1r and C1s are activated by peptide cleavage; i.e. of Arg^{463}-Ile^{464} in C1r and Arg^{437}-Ile^{438} in C1s, located between the CCP2 and SP domains. Activated C1s cleaves C4 and C2, starting the subsequent steps of the complement cascade. C1-INH regulates surface-induced activation by promoting dissociation of the C1 complex and releasing C1r and C1s from C1 (*15*).

Free $C1r_2s_2$ exhibits a ~50-nm elongated structure, in which the proteases are arranged as C1s-C1r-C1r-C1s (*16–18*); see Figure 1A. In the center, an anti-parallel "head-to-tail" arrangement of CCP1-CCP2-SP domains is thought to keep C1r dimers inactive in free $C1r_2s_2$ (*19*). C1r and C1s interact *via* their

N-terminal CUB1-EGF-CUB2 domains in a Ca^{2+}-dependent manner forming C1rs anti-parallel hetero-dimers (*20*). A possible model for CUB1-EGF-CUB2 interactions in the C1rs hetero-dimer (*21*) is derived from the crystal structure of C1s CUB1-EGF-CUB2 dimers in the presence of Ca^{2+} (*21*). Finally, the C1s CCP1-CCP2-SP domains are exposed at either end of the $C1r_2s_2$ tetramer (Fig. 1A)(*22*). Association of $C1r_2s_2$ and C1q into C1 yields a more compact structure of ~20 nm (*16–18*). Binding studies revealed two Ca^{2+}-dependent binding sites for collagen on C1r and one on C1s (*23*). The data suggest an anti-parallel stacked arrangement of the four N-terminal CUB1-EGF-CUB2 domains of two C1r-C1s hetero-dimers in between the six collagen arms in the C1 complex (*23*, *24*); see Figure 1A. Crystal contacts in the structure of C1s CUB-EGF-CUB domains possibly reflect the hetero-tetrameric arrangement in C1 (*21*). A recent cryo-EM reconstruction of $C1\text{-}IgG1_6$ confirmed the stacked arrangement of $C1r_2s_2$ in between collagen arms (*25*), therefore suggesting a large conformational change from free elongated $C1r_2s_2$ to C1q-bound stacked $C1r_2s_2$.

Here, we sought to improve the understanding of the molecular mechanisms and dynamics of C1 assembly from $C1r_2s_2$ tetramers and C1q. We hypothesized that two C1r-C1s hetero-dimers associate with C1q by sliding alongside each other forming the antiparallel stacked arrangement as proposed for $C1r_2s_2$ in fully as-sembled C1. We tested our hypothesis by native mass spectrometry (MS) (*26*, *27*) and supporting pull-down assays. Next, we studied how C1 binding to danger signals affects complex dynamics, using soluble hexameric antibody platforms as a model (*28*, *29*). Our data provide insight into C1 assembly and, moreover, reveal that C1 is a dynamic complex in which C1rs dimers dissociate and associate until C1 binds its danger patterns when the dissociation rate is significantly reduced and complement activation on target surfaces is initiated.

RESULTS

Recombinant C1r-C1s hetero-tetramer and dimer complexes form C1

To study complex assembly, we produced human C1r and C1s as wild-type full-length proteins, SP domain-deletion C1s constructs (denoted as $C1s^{\Delta S}$), CCP2-SP domain deletion C1r constructs ($C1r^{\Delta CS}$) and inactive variants ($C1r^{\dagger}$ and $C1s^{\dagger}$, resp.) by mutating the catalytic serine into an alanine (C1r S654A and C1s S632A). C1r and C1s constructs were co-expressed in HEK293-ES cells and purified in the presence of calcium (see Experimental Procedures for details).

Expression of wild-type C1r and C1s yielded active $C1r_2s_2$ complexes that could not be purified to homogeneity, due to high propensity for aggregation. Co-expression of $C1r^\dagger$ and $C1s^\dagger$ yielded stable zymogen-like hetero-tetrameric $C1r^\dagger_2s^\dagger_2$ complexes (Fig. 1B and Supplementary Fig. 1). In addition, two shortened C1r-C1s variants were co-expressed and purified: $C1r^\dagger$ together with $C1s^{\Delta S}$ and $C1r^{\Delta CS}$ with $C1s^{\Delta S}$. Size-exclusion chromatography (SEC) with online multiple-angle light scattering (MALS) of the three products $C1r^\dagger$-$C1s^\dagger$, $C1r^\dagger$-$C1s^{\Delta S}$, and $C1r^{\Delta CS}$-$C1s^{\Delta S}$ yielded molecular weights of approximately 318, 247 and 88 kDa, respectively (Fig. 1B and Table 1). Using native MS, we observed molecular weights for these species of 326, 265 and 93 kDa, consistent with the theoretical masses of the hetero-tetramers $C1r^\dagger_2s^\dagger_2$ and $C1r^\dagger_2s^{\Delta S}_2$ and the hetero-dimer $C1r^{\Delta CS}s^{\Delta S}$, respectively (Table 1). Negative-stain EM of $C1r^\dagger_2s^\dagger_2$ samples revealed a flexible S-shaped elongated form, which was similar to $C1r_2s_2$ tetramers derived from human serum, as previously shown by Tschopp *et al.* (1980), see Figure 1C. EM micrographs of $C1r^\dagger_2s^{\Delta S}_2$ showed particles lacking the nodules on either end. $C1r^{\Delta CS}s^{\Delta S}$, however, yielded short particles of ~20-nm length that were consistent with the formation of C1rs hetero-dimers, in agreement with the absence of the C1r-C1r dimerization site due to the lack of C1r CCP2-SP domains. Overall, these data are consistent with the extended C1s-C1r-C1r-C1s model of $C1r_2s_2$ (Schumaker *et al*, 1987). In addition, we observed another ~50-nm long form that occurred when samples of $C1r^\dagger_2s^\dagger_2$ for negative-stain EM were either prepared by diluting a concentrated solution of ~3 mg/ml or appeared after incubation of the sample of ~0.2 mg/ml at 4°C for more than 3 hours after gel filtration (Fig. 1D). Although the length of this form is equal to that of the previously reported C1s-C1r-C1r-C1s tetramers (*16*), this alternative form of particles contained two globular shapes at either end suggesting a stacked dimer complex of tetramers (Fig. 1D). Native MS confirmed the presence of hetero-octamers $C1r_4s_4$ in concentrated samples (Fig. 1E). We did not observe this octamer in SEC or in SEC-SAXS studies, possibly due to weak interactions between the stacked tetramers. These data are similar to the negative stain EM images of free $C1r_2s_2$ shown by Mortensen et al. (2017), where they did not have an explanation for such a cross-shape model that contradicted their SAXS results and previous literature (*33*). Our data indicate that the alternative elongated form observed in negative-stain-EM is explained by a stacked dimer of $C1r_2s_2$ tetramers, yielding $C1r_4s_4$.
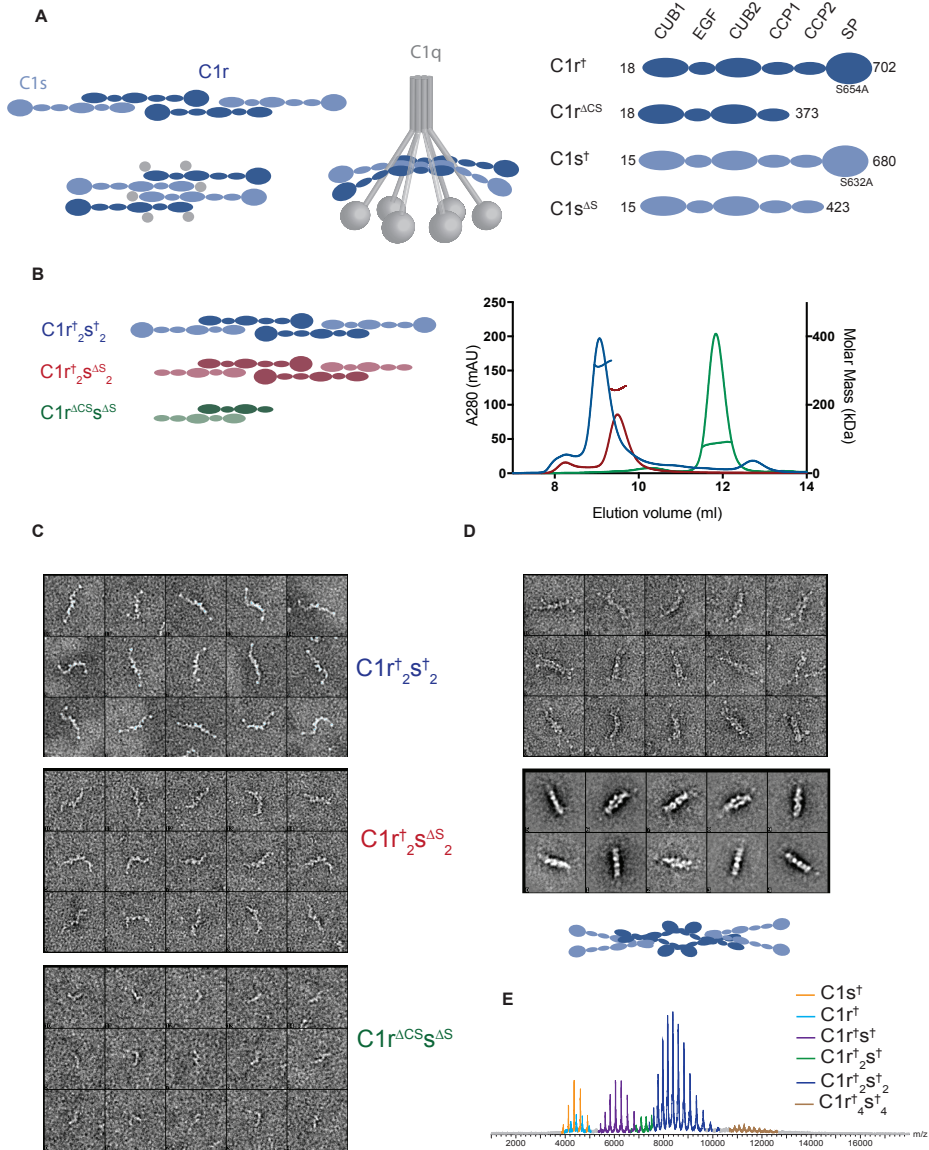
Figure 1. Analysis of C1r and C1s constructs.

A) Cartoon representation of anti-parallel linear arrangement and stack arrangement of C1r and C1s in C1. Schematic representation of domain organization of $C1r^\dagger$, $C1r^{\Delta CS}$, $C1s^\dagger$ and $C1s^{\Delta S}$ constructs. B) Cartoon representation of linear arrangements of $C1r^\dagger_2s^\dagger_2$, $C1r^\dagger_2s^{\Delta S}_2$ and $C1r^{\Delta CS}s^{\Delta S}$. Overlay of SEC-MALS profile of co-expressed $C1r^\dagger$-$C1s^\dagger$, $C1r^\dagger$-$C1s^{\Delta S}$, $C1r^{\Delta CS}$-$C1s^{\Delta S}$ constructs (blue, red and green respectively). C) Negative-stain EM images of (from top to bottom) $C1r^\dagger_2s^\dagger_2$, $C1r^\dagger_2s^{\Delta S}_2$ and $C1r^{\Delta CS}s^{\Delta S}$. D) Negative-stain EM images of $C1r^\dagger_4s^\dagger_4$ (top) and 2D class averages (bottom). E) Broad-range mass spectra of $C1r^\dagger$-$C1s^\dagger$ complex.

C1rs dimers assemble with C1q to form C1

We mixed C1q with the three complexes, either $C1r^{\dagger}_2 s^{\dagger}_2$, $C1r^{\dagger}_2 s^{\Delta S}_2$ tetramers or $C1r^{\Delta CS} s^{\Delta S}$ dimers, to form C1. Complexes were analyzed by native MS both in their free state and bound to IgG1 antibodies carrying three mutations (E345R, E430G and S440Y, denoted RGY), which induce hexamerization of antibodies in solution yielding soluble complement-activating C1-binding platforms (*28, 29*). Since some of these assemblies exceed a molecular weight of 1.5 MDa, a dedicated Q-ToF mass analyzer was applied, modified to be able to mass resolve and analyze high-molecular-weight assemblies (*34, 35*). The spectra in Figure 2A show that all three C1rs variants formed C1 and C1-IgG$_6$ complexes with masses corresponding to C1 containing hetero-tetramers of the C1r and C1s variants, i.e. $C1qr^{\dagger}_2 s^{\dagger}_2$ and $C1qr^{\dagger}_2 s^{\Delta S}_2$ and $C1qr^{\Delta CS}_2 s^{\Delta S}_2$. Thus, $C1r^{\Delta CS} s^{\Delta S}$ dimers, similar to $C1r^{\dagger}_2 s^{\dagger}_2$ and $C1r^{\dagger}_2 s^{\Delta S}_2$ tetramers, form tetrameric protease complexes within C1. In addition, native MS also captured intermediates of the fully as-sembled complexes C1r$_2$s$_2$ and C1. Figure 1E shows that the spectra of $C1r^{\dagger}_2 s^{\dagger}_2$ include, besides dimers ($C1r^{\dagger} s^{\dagger}$), small fractions of monomers ($C1r^{\dagger}$ or $C1s^{\dagger}$) and trimers ($C1r^{\dagger}_2 s^{\dagger}$). Figure 2B shows spectra of C1, which indicated the presence of incomplete C1q molecules, i.e. C1q tetramers and dimers (denoted as C1q$_{2/3}$ and C1q$_{1/3}$, resp.), similar to the data shown previously (*29*). However, the C1 spectra indicated only hetero-dimers and hetero-tetramers of proteases such as C1qrs, C1q$_{2/3}$rs, and C1q$_{2/3}$r$_2$s$_2$, but not trimers or monomers in contrast to data obtained for C1r$_2$s$_2$. When we titrated $C1r^{\dagger}_2 s^{\dagger}_2$ hetero-tetramers to C1q and IgG1$_6$, we observed intermediate species of $C1qr^{\dagger} s^{\dagger}$-IgG1$_6$, which disappeared as C1rs dimers filled up the complexes and formed $C1qr^{\dagger}_2 s^{\dagger}_2$-IgG1$_6$ (Fig. 2C). Also in these latter data, no monomers or trimers of proteases were observed in the C1-IgG1$_6$ complex. Thus, our native MS data suggest that C1 is assembled through C1rs hetero-dimers, because i) complete complexes are assembled from C1q and $C1r^{\Delta CS} s^{\Delta S}$ dimers and ii) only C1rs dimers and C1r$_2$s$_2$ tetramers are bound to hexameric C1q in C1 and C1-IgG1$_6$.
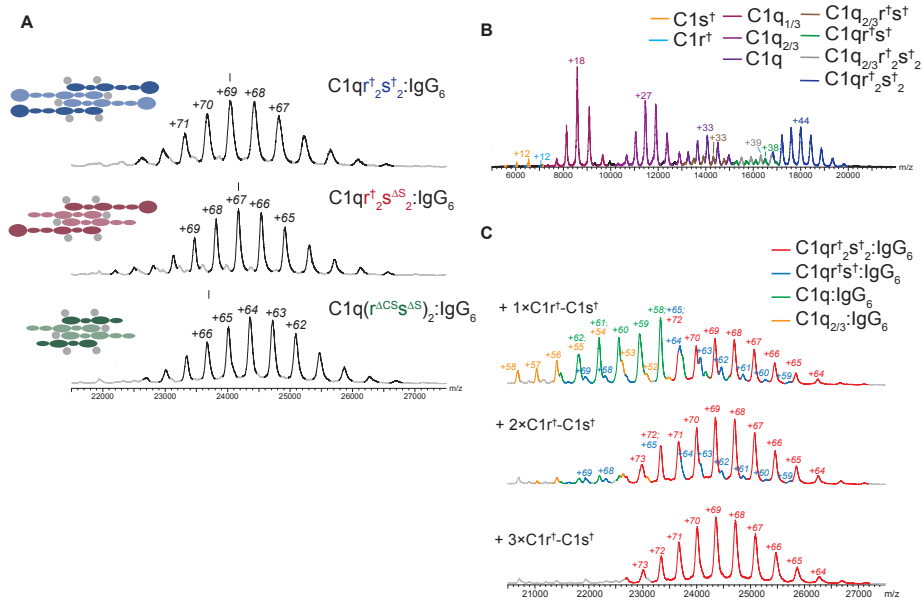
Figure 2. Dimer-exchange analysis of free tetramers in solution.

A) Native MS profiles of $C1r^{\dagger}_2s^{\dagger}_2$, $C1r^{\dagger}_2s^{\Delta S}_2$ and $C1r^{\Delta CS}s^{\Delta S}$ in complex with C1q and IgG_6 (from top to bottom). B) Broad-range mass spectra of $C1r^{\dagger}$-$C1s^{\dagger}$-C1q complex. C) Native MS of $C1qr^{\dagger}_2s^{\dagger}_2$-$IgG_6$ complex with titrating 1x, 2x or 3x $C1r^{\dagger}$-$C1s^{\dagger}$ (from top to bottom) into the complex until there is no free $C1r^{\dagger}$-$C1s^{\dagger}$ is observed in the spectra.

C1rs dimers exchange spontaneously in C1r$_2$s$_2$ and C1

Native MS spectra shown in Figure 3A reveal that mixing of $C1r^{\dagger}_2s^{\dagger}_2$ and $C1r^{\dagger}_2s^{\Delta S}_2$ hetero-tetramers at room temperature (RT; ~21°C) for 10 min resulted in a hybrid tetramer species $C1r^{\dagger}_2C1s^{\dagger}C1s^{\Delta S}$, besides the two starting complexes. Furthermore, in the broad-range spectra, peaks are present corresponding to $C1r^{\dagger}s^{\dagger}$ and $C1r^{\dagger}s^{\Delta S}$ dimers and lower abundant monomers ($C1r^{\dagger}$, $C1s^{\dagger}$, and $C1s^{\Delta S}$), trimers ($C1r^{\dagger}_2s^{\Delta S}$ and $C1r^{\dagger}_2s^{\dagger}$) and even some octamers ($C1r^{\dagger}_4s^{\dagger}_4$) (Supplementary Fig. 2 and Table 1). Following the reconstitution of different C1 complexes using $C1r^{\dagger}_2s^{\Delta S}_2$, $C1r^{\dagger}_2s^{\dagger}_2$, and $C1r^{\Delta CS}s^{\Delta S}$ respectively, we mixed the preformed C1 complexes at RT and monitored their exchange behavior by native MS. Similar to C1rs-dimer exchange between $C1r_2s_2$ complexes, we observed a hybrid version containing both C1s and $C1s^{\Delta S}$ constructs, i.e. $C1qr^{\dagger}_2s^{\Delta S}s^{\dagger}$ after mixing $C1qr^{\dagger}_2s^{\Delta S}_2$ and $C1qr^{\dagger}_2s^{\dagger}_2$ (Fig. 3B and Table 1). The relative abundance of this hybrid species remained stable since the first data point (obtained 3 min after mixing). Mixing $C1qr^{\dagger}_2s^{\Delta S}_2$ and $C1qr^{\Delta CS}_2s^{\Delta S}_2$ that differ in the C1r constructs similarly yielded a hybrid species comprising

different C1r constructs, i.e. $C1qr^{\dagger}r^{\Delta CS}s^{\Delta S}{}_2$ (Supplementary Fig. 2A). These results demonstrate C1rs hetero-dimers exchange readily among the C1 assemblies.

Next, we mixed the $C1r^{\dagger}{}_2s^{\dagger}{}_2$ containing N-terminal His_6-tagged $C1s^{\dagger}$ with the $C1r^{\dagger}{}_2s^{\Delta S}{}_2$ containing C-terminal $StrepII_3$-tagged $C1s^{\Delta S}$ in the presence of 1 mM $CaCl_2$. We used different ratios of $C1r^{\dagger}{}_2s^{\dagger}{}_2(His):C1r^{\dagger}{}_2s^{\Delta S}{}_2(Strep)$ and performed pull-down experiments by Strep-tag affinity chromatography. Strep-tag purification yielded pull down of $C1s^{\dagger}$-His, indicating the formation of the mixed species $C1r^{\dagger}{}_2s^{\dagger}s^{\Delta S}$ (Fig. 3C). Thus, both native MS and pull-down experiments demonstrated that $C1r_2s_2$ hetero-tetramers spontaneously dissociate into transient C1rs hetero-dimers that re-associate into $C1r_2s_2$ hetero-tetramers. We also performed such experiments in the presence of C1q and IgG_6. Mixing preformed C1 complexes ($C1qr^{\dagger}{}_2s^{\dagger}{}_2$-His and $C1qr^{\dagger}{}_2s^{\Delta S}{}_2$-Strep) and performing strep-tag affinity chromatography yielded pull down of $C1s^{\dagger}$-His indicating a hybrid species; $C1qr^{\dagger}{}_2s^{\dagger}s^{\Delta S}$ (Fig. 3C). When we preformed complexes with soluble IgG1 hexamers, we did not observe a band for representing $C1s^{\dagger}$-His, indicating no exchange of the hetero-dimers. We then confirmed the presence of the $C1s^{\dagger}$-His samples with western blot with an anti-His antibody (Supplementary Fig. 2B). Although we see a faint band corresponding to IgG complexes, its intensity is negligible compared to C1 and $C1r_2s_2$ complexes.

Antibody binding reduces C1rs-dimer exchange in C1

Next, we monitored the C1rs-dimer exchange after antibody binding using IgG1 hexamers in solution, i.e. mixing preformed $C1qr^{\dagger}{}_2s^{\Delta S}{}_2$-$IgG_6$ and $C1qr^{\dagger}{}_2s^{\dagger}{}_2$-$IgG_6$ complexes (Fig. 4A). Application of the modified Q-ToF mass analyzer allowed 60-80 kDa differences in assemblies of over 1.5 MDa to be resolved in these native MS analyses (Table 1). Time-course experiments showed that C1rs-dimer exchange in C1-IgG_6 took ~1 hr at RT and ~30 min at 37°C to reach the maximum abundance of hybrid species, instead of ~3 min for C1 complexes in the absence of IgG (Fig 4B). Altogether our data show that C1rs dimers exchange spontaneously in $C1r_2s_2$ tetramers and in C1 ($C1qr_2s_2$) complexes (with full exchange achieved within the measurement time of 2-3 min). When bound to IgG_6, C1 forms more stable complexes, which increases half times of complete exchange to ca. 26 min at RT and 8 min at 37°C.
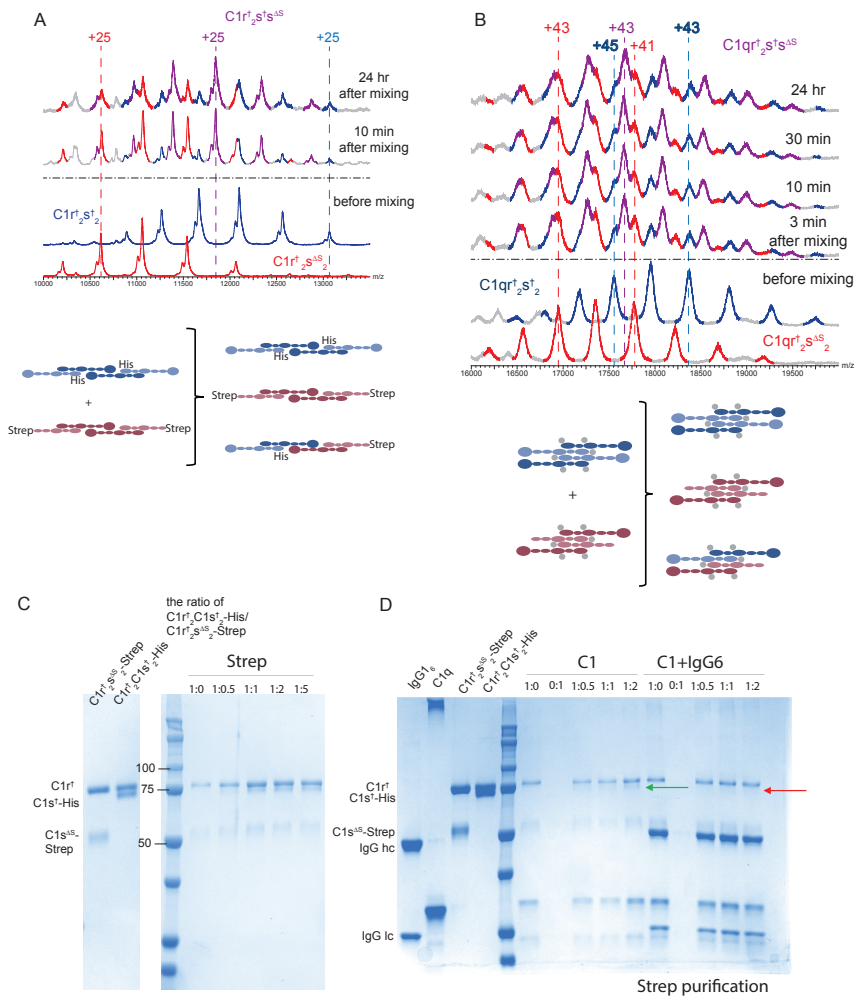
Figure 3. Dimer-exchange analysis of C1 and C1 bound to antibody platforms.

A) Native mass spectra of $C1r^†_2s^†_2$ (blue), $C1r^†_2s^{ΔS}_2$ (red) hetero-tetramers acquired at RT before mixing, 10 min after mixing and 24 hours after mixing. Signals representing $C1r^†_2s^†_2$, $C1r^†_2s^{ΔS}_2$ and the hybrid species $C1r^†_2$-$C1s^†C1s^{ΔS}$ are colored in blue, red and purple respectively. B) Native mass spectra of $C1qr^†_2s^†_2$ (blue) and $C1qr^†_2s^{ΔS}_2$ (red) complexes acquired at RT before mixing and at different points after mixing. The mixing yielded hybrid species $C1qr^†_2s^†s^{ΔS}$ (purple). Cartoon representation of top view $C1qr^†_2s^†_2$, $C1qr^†_2s^{ΔS}_2$ and the species observed in the mixture: $C1qr^†_2s^†_2$, $C1qr^†_2s^{ΔS}_2$ and $C1qr^†_2s^†s^{ΔS}$ (from top to bottom). C) Pull-down experiment of $C1r^†_2s^†_2$ and $C1r^†_2s^{ΔS}_2$ via streptactin-affinity purification. The controls; $C1r^†_2s^{ΔS}_2$ and $C1r^†_2s^†_2$, are shown on the left. The ratios of $C1r^†_2s^†_2$ and $C1r^†_2s^{ΔS}_2$ are shown above the lanes. Strep-tag purification of $C1r^†$-His_6 co-expressed with $C1s^{ΔS}$-Strep are shown in each lane with increasing amount of $C1r^†_2s^†_2$-His from left to right. D) Pull-down experiment of $C1qr^†_2s^†_2$ and $C1qr^†_2s^{ΔS}_2$ and these complexes in complex with IgG_6 (right). The controls; IgG16, C1q, $C1r^†_2s^{ΔS}_2$ and $C1r^†_2s^†_2$ are shown on the left. Strep-tag purification of mixture of C1 complexes are shown in each lane with increasing amount of $C1qr^†_2s^†_2$-His from left to right.

C1-INH releases C1rs dimers and new C1rs is recruited by C1q-antibody complexes

C1-INH regulates complement activity by covalently binding to the catalytic sites of C1r and C1s, which results in the release of the covalently inhibited enzymes from surface-bound C1 complex (*15*). We analyzed the association and dissociation of complexes at RT by native MS using IgG1-RGY antibodies (*28*, *29*). We engineered a C1r variant, denoted $C1r^E$, by changing the cleavage site (^{459}EQRQRI^{464}) to DDDDKI, which is the substrate sequence for the protease enterokinase (EK). Co-expressed and co-purified $C1r^E$ and C1s remain zymogens in the absence of EK. $C1r^E$ and C1s made complexes with C1q and IgG_6 similar to other C1r-C1s tetramers (Supplementary Fig. 4A, C). Addition of EK to $C1r^E_2s_2$ cleaved $C1r^E$, which in turn cleaved C1s. Activated $C1r^E_2s_2$ cleaved C2 (Supplementary Fig. 4B). We reconstituted $C1r^E_2s_2$-C1q-IgG_6 complexes, at a ratio that minimizes free $C1r^E_2s_2$ tetramers observed in the spectra (Fig. 4C). Upon activation of the complex by EK, we added excess C1-INH to $C1r^E_2s_2$-C1q-IgG complexes. Removal of activated $C1r^E_2s_2$ was completed within 10 min of incubation. "Emptied" C1q-IgG_6 complexes emerged in high abundance within 2 min after addition of C1-INH in the absence of free $C1r^E_2s_2$. However, in physiological conditions, there is free $C1r_2s_2$ present in solution. In order to mimic the physiological environment, a tetramer that cannot be dissociated by C1-INH, i.e. $C1r^†_2s^{ΔS}_2$, was added to the solution in the presence of C1-INH. Figure 4D shows that dissociated $C1r^E_2s_2$ in C1-IgG_6 was rapidly replaced by $C1r^†_2s^{ΔS}_2$ that was incorporated into the C1q-IgG_6 complexes. These data indicate that removal of activated complexes from antibody-C1 complexes by C1-INH yields 'emptied' C1q-antibody complexes that are readily refilled by C1rs hetero-dimers enabling a sustained activation.
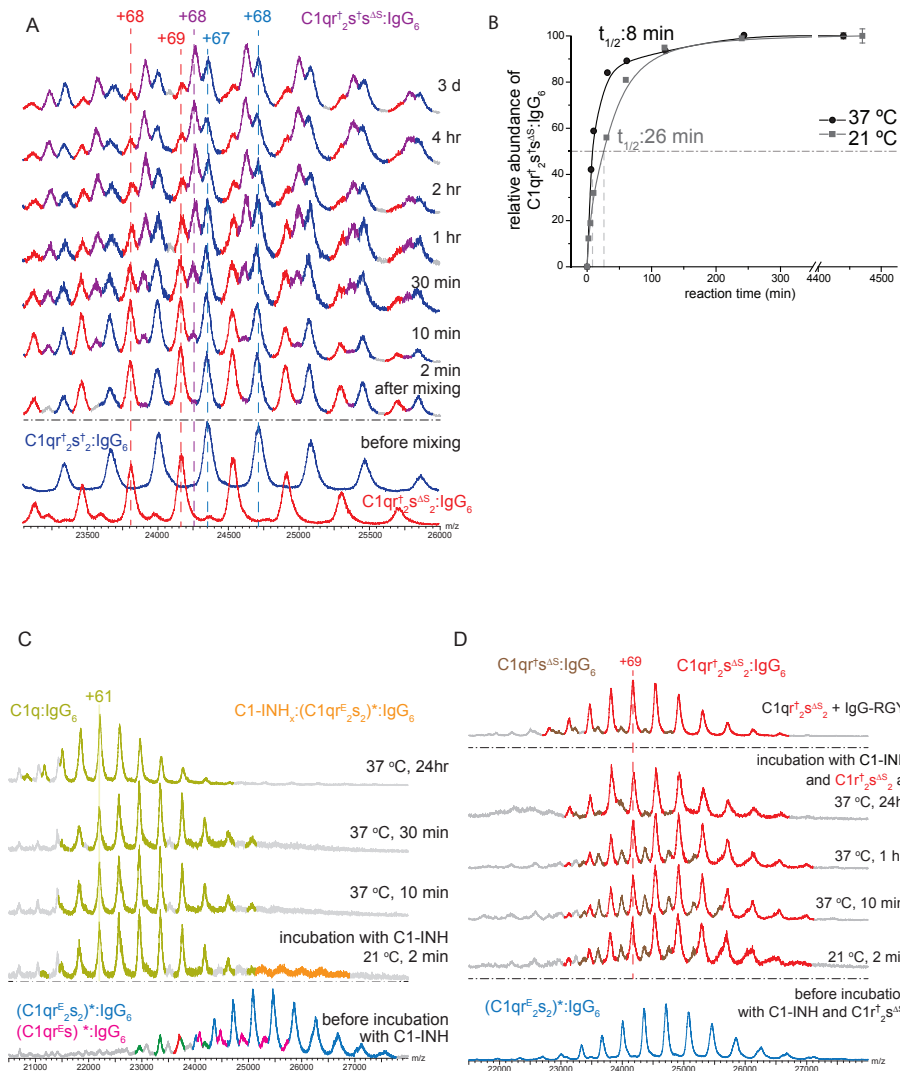
Figure 4. Dimer-exchange analysis of C1 and C1 bound to antibody platforms.

A) Native mass spectra of $C1qr^\dagger_2s^\dagger_2$-IgG$_6$ (blue) and $C1qr^\dagger_2s^{\Delta S}_2$-IgG$_6$ (red) complexes acquired at RT before mixing and at different points after mixing. The resulting hybrid species $C1qr^\dagger_2s^\dagger s^{\Delta S}$-IgG$_6$ is shown in purple. B) Evolvement of the hybrid species $C1qr^\dagger_2s^\dagger s^{\Delta S}$-IgG$_6$ detected by native MS at 37°C (black) and RT (grey). Half times of the association are indicated by dashed lines. C) EK activated $C1r^E_2s_2$, denoted by $(C1r^E_2s_2)^*$, was mixed with C1q and IgG$_6$. $C1q$-$(C1r^E_2s_2)^*$-IgG$_6$ is shown in blue, $C1q$-$(C1r^Es)^*$-IgG$_6$ is shown in pink and C1q-IgG$_6$ is shown in light green. The spectra are acquired before the incubation with C1-INH and at different points after the incubation with C1-INH at 21°C, and 37°C. Excess C1-INH was added to $C1q$-$(C1r^E_2s_2)^*$-IgG$_6$ complexes. D) The system described in (A) was monitored with $C1r^\dagger_2s^{\Delta S}_2$ added together with C1-INH to the solution.

DISCUSSION

Our starting hypothesis originated from structural considerations. Current models for the hetero-tetramer of C1r and C1s proteases in solution and bound to C1q, yielding C1, and its assembly imply major structural rearrangements of C1r and C1s (Bally *et al*, 2009, Gingras *et al*, 2011; Wallis *et al*, 2010). We hypothesized that limited domain rearrangements are needed, when $C1r_2s_2$ hetero-tetramers split in the middle into C1rs hetero-dimers. Our native MS and pull down data confirmed that $C1r_2s_2$ tetramers break into C1rs dimers. Breaking the extended C1s-C1r-C1r-C1s arrangement into two C1rs dimers allows a simple repositioning from the extended C1s-C1r-C1r-C1s into a stacked C1r-C1s-C1s-C1r arrangement bound to C1q (see Fig. 1A for schematic representations).

Calcium ions are critical to stability of the C1 and $C1r_2s_2$ complexes; they are required for C1r-C1s interactions and binding to C1q (*24*). Likewise, Tseng et al. show that C1 dissociates into C1q and $C1r_2s_2$ at lower than 5 μM Ca^{2+} (*36*). High-resolution spectra by native MS necessitate low salt conditions. In our experiments, the proteins were first purified in the presence of 1 mM $CaCl_2$ and the buffer was exchanged to 20 μM Ca-acetate right before starting the native MS experiments. Crystal structure 1GPZ (*19*) is considered to represent the C1r-C1r interactions in the extended C1s-C1r-C1r-C1s arrangement. Notably, the C1-C1r interactions between by CCP1-2 and its partner SP domains do not involve calcium ions. Therefore, the low Ca^{2+} concentration (20 μM) used in native MS experiments do not influence breaking of C1r-C1r interaction in the middle of the elongated tetramer. Additional pull-down experiments performed at 1 mM $CaCl_2$ i.e. at a physiological relevant concentration, support a dynamic assembly and disassembly of $C1r_2s_2$ hetero-tetramers into C1rs hetero-dimers, as observed by native MS. Both experiments support the hypothesis that C1 assembles through C1rs intermediates.

The presented native MS data on C1r and C1s variants with distinct masses show that both $C1r_2s_2$ and $C1qr_2s_2$, i.e. C1, are dynamic complexes that dissociate and re-associate through C1rs hetero-dimer intermediates. C1 is rapidly formed when mixing C1q and $C1r_2s_2$; within the 3-min time period required for native MS-data acquisition. Binding of C1 to complement-inducing antibody hexamers slows down the C1rs-dimer exchange, increasing the half times to reach steady state from <3 min to ca. 26 min. Addition of C1-INH removes the C1r and C1s enzymes rapidly (<3 min) from the C1-IgG complexes, consistent with earlier reports (*15*, *37*). 'Emptied' C1q-IgG complexes are refilled also rapidly forming

C1-IgG complexes, as demonstrated using non-enzymatic C1rs dimers that lack their catalytic SP domains in the presence of C1-INH. Therefore, since the association process is fast, the reduced exchange rate is caused by slow dissociation. This is consistent with ca. a 10-fold increase of the association constant of C1, due to a reduced dissociation rate, while the association rate is diffusion limited (*38*). Given that complement activation on surfaces may be achieved within 2 min (*39*), reduced rate of exchange on surfaces is possibly relevant to C1 activation or C1-INH regulation.

The reduced rate of C1rs dissociation from the surface-bound complexes, causing the observed reduced exchange rate in C1-antibody complexes, may be easily explained structurally. With the globular domains of C1q bound to a surface, the major exit of C1rs is blocked, leaving only the spaces in between the collagen arms and their potential widening through unbinding of individual C1q globular units available for egress. Sufficient blocking is apparently required, because ligands like DNA or heparin cannot activate C1 as effective as surfaces (Ziccardi, 1982). Such a generic surface signal, i.e. sufficient blocking of C1rs egress, and the absence of a specific conformational signal transmitted through the collagen arms is consistent with the large variety of surface targets that may induce C1 activation.

The observations for C1 correlate in part with MBL, ficolins or collectin-11 binding of MASPs. MBL tetramers, trimers and dimers have been shown to bind either MASP1 or MASP2 dimers to form MBL-MASP complexes (*41*). In the spectra of full C1, intact $C1qr_2s_2$ was the most abundant species, next to low amounts of C1qrs. In addition, as reported previously (*29*) we observed incomplete C1q molecules in the mass spectra, i.e. C1q tetramers ($C1q_{2/3}$) and dimers ($C1q_{1/3}$), which resemble MBL tetramers and dimers respectively. These data indicate further homology between C1 and MBL that bind MASP; however, the distinct difference is that MASPs form homo-dimers, whereas C1rs form hetero-dimers. Moreover, our data are compatible with an inter-molecular activation model similar to that of MASPs in MBL complexes (*42*). Our findings on dimer exchange is consistent with the cryo-EM structure of $C1-IgG1_6$ in which catalytic sites of C1r and C1s protrude from C1 complex similar to the structure to MBL-MASP1 complex as shown by SAXS and EM (*25*, *42*). C1 assembly by dimer exchange suggests a similar conformation where C1rs also possibly extends from C1 complex like MASPs, instead of folding under the collagen arms as suggested previously (*43*, *44*). Besides intermolecular activation on cell surface, the enzyme-substrate arrangement (*45*) may be established in the fluid phase. Such

an activation model of C1r and C1s is consistent with uncontrolled fluid-phase activation in the absence of C1-INH. Considering the growing body of data on the involvement of classical pathway complement activation in neurological disorders, such as schizophrenia (*10*) or Alzheimer disease (*11*), our data responds to the pressing need in understanding the precise mechanisms that govern the principle initiation of the proteolytic cascade by C1.

Chapter 3

Supplementary materials

Materials and methods

Expression and Purification of the Proteins

Purified natural human C1q was purchased from Complement Technology, Inc. (TX, USA). IgG1-RGY mutant (E345R/E430G/S440Y), forming hexamers in solution, is provided by Genmab. C1r[†] (S654A) and C1s[†] (S632A) mutants were generated using the Quikchange mutagenesis kit (Stratagene) on TOPO clones inserted in pCR8 vectors (Invitrogen). C1r$^{\Delta CS}$ (residue 18-373), C1s$^{\Delta S}$ (residue 16-423) deletion constructs were generated by PCR. All constructs were sub-cloned into mammalian expression vectors (carrying hexa-histidine tag or StrepII$_3$-tag) provided by U-Protein Express BV (U-PE), Utrecht, The Netherlands. C1r and C1s constructs were co-expressed in N-acetylglucosaminyltransferase I (GnTI) deficient human embryonic kidney 293 cells that stably express Epstein-Bar virus nuclear antigen EBNA1 (HEK293-ES supplied by U-Protein Express BV). The supernatant was harvested on the 5th day of the expression, concentrated and dia-filtered using a Quixstand system. The HIS-tagged proteins were purified by Ni-NTA affinity chromatography (GE Healthcare) followed by a size-exclusion chromatography step on a Superdex 200 column or Superose 6 column (GE Healthcare). Strep-tagged proteins were loaded onto Streptactin columns (GE Healthcare) for affinity purification and the sample was eluted by 5mM D-desthio-biotin. IgG1-RGY was previously described (Diebolder *et al*, 2014). IgG1-RGY was generated by introducing the mutations E345R, E430G and S440Y in the Fc region of human IgG1. IgG1-RGY spontaneously forms ordered hexamers via non-covalent contacts between Fc domains (*28*, *29*).

Size exclusion multi-angle light scattering

Concentrated protein samples (25 µl of each sample) were injected and separated on a Superdex200 Increase PC 2.3/300 GL column (GE Healthcare) with Shimadzu system. In-line multi-angle light scattering analysis was performed with Wyatt miniDAWN TREOS and Shimadzu differential refractive index detectors. Data were analyzed with the ASTRA VI software package (Wyatt Technology Corporation). The molecular weight was determined from the Raleigh ratio calculated by measuring the static light scattering and corresponding protein concentration of a selected peak.

Negative stain electron microscopy

5 µL sample (15 µg/ml) was applied to a glow discharged 200 Mesh Copper EM grid with a continuous carbon film (Electron Microscopy Sciences) and stained with 2% uranyl formate solution. Micrographs were acquired using a Tecnai T12 (FEI) electron microscope, equipped with FEI 4k x 4k Eagle CCD camera at 120 kV. 50,000 x magnification resulting in a pixel size of 4.4 Å at specimen level and a nominal defocus of -2 µm were applied. Micrographs were CTF-corrected and visualized in EMAN2.

Native Mass Spectrometry

All native mass spectrometry measurements were conducted with a hybrid triple-quadrupole/time-of-flight (Waters, UK) mass spectrometer modified for optimal performance in high mass detection (*35*). The original buffers of all proteins analyzed were substituted with aqueous solution containing 150 mM ammonium acetate and 20 µM calcium acetate (pH adjusted to 7.5 with ammonium hydroxide) using centrifugal filters with a MW cut-off of 10 kDa (Merck Millipore, Germany) through at least five sequential cycles at 4°C. Samples were sprayed using a standard static nanospray source at 21°C. When a higher spectra resolution was needed for distinguishing species with similar MW, 20% (mol/mol) triethylammonium acetate (TEAA) was included in the final buffer of samples, reducing the average charge states of protein ions by approximately 30% and resulting in better separated signals.

Except for the kinetic measurements where the duration and temperature of incubations were specified in the corresponding description, all protein complexes were assembled by mixing the natural or recombinant participants at desired ratios followed by incubations at 21°C for at least 10 min in each step. For the measurements of subunit exchange kinetics between C1-containing assemblies, excess C1q or IgG were added into the solution in a titration manner to minimize the free C1r/C1s variants which did not bind by C1q. The endpoints were indicated by the demise of the corresponding signals. To accurately determine the MW and stoichiometry of large protein complexes, we performed supplementary tandem MS measurements by mass-selection of target ions using a quadrupole mass analyzer followed by gas-phase dissociation of the selected ions induced by their collision with xenon gas in the collision cell. Data were analyzed with Mass Lynx (Waters, UK) and Origin Pro (Origin Lab, USA) software.

Pull-down assay

Co-expression of C-terminal Strep-tagged C1s$^{\Delta S}$ and N-terminal His-tagged C1r† and co-expression of both N-terminal His-tagged C1s$^{\Delta S}$ and C1r† were per-

formed in HEK293-ES cells. After the cells were centrifuged, the supernatant of $C1r^{\dagger}\text{-}C1s^{\Delta S}$ complex was mixed with the supernatant of $C1r^{\dagger}\text{-}C1s^{\dagger}$ complex. The samples of $C1r^{\dagger}\text{-}C1s^{\Delta S}$, $C1r^{\dagger}\text{-}C1s^{\dagger}$ and the mixture of $C1r^{\dagger}\text{-}C1s^{\Delta S}$ and $C1r^{\dagger}\text{-}C1s^{\dagger}$ were eluted from Strep-Tactin beads by 5mM D-desthiobiotin. His- tagged $C1r^{\dagger}\text{-}C1s^{\dagger}$ complex was purified with Nickel beads as positive control and purified with Strep-Tactin beads as a negative control. The mixed species $C1r^{\dagger}\text{-}C1s^{\Delta S}\text{-}C1s^{\dagger}$ were pulled down by streptavidin purification.
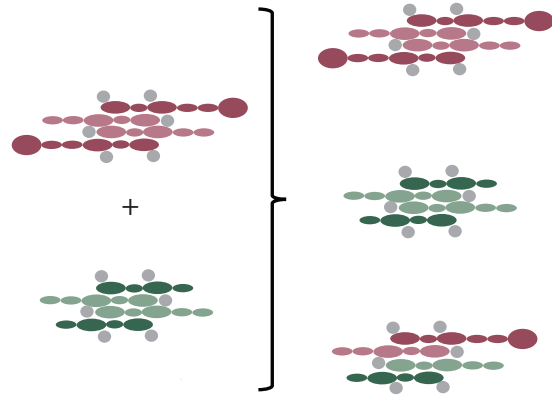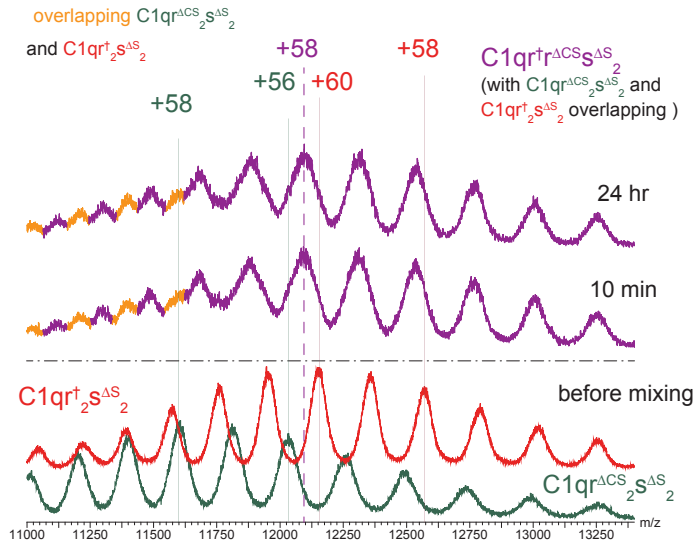
Supplementary figures
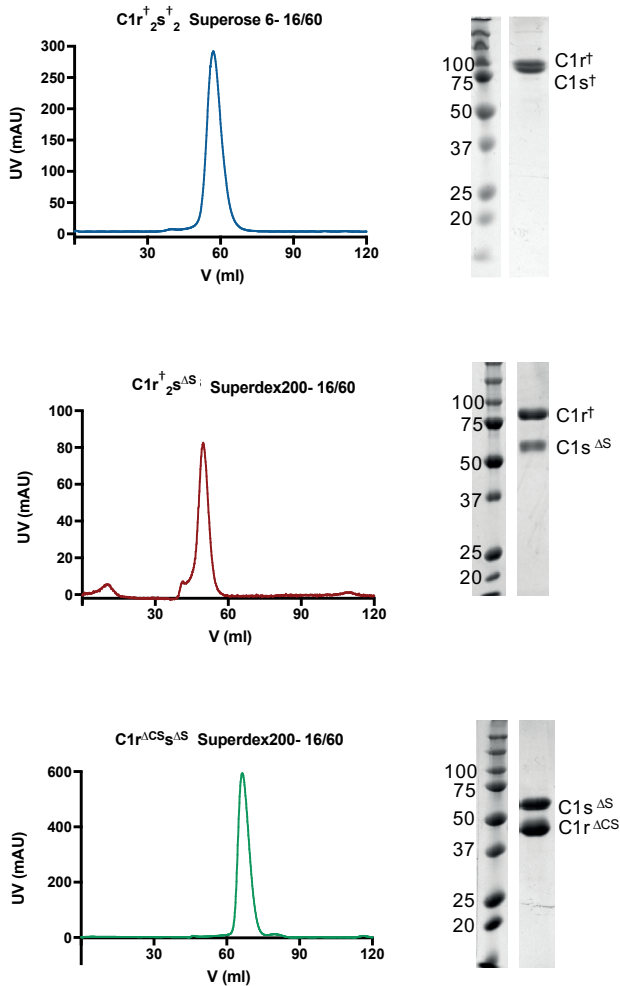
Supplementary Figure 1. Sample quality of C1r-C1s complexes

Representative size-exclusion chromatographs of C1r$^\dagger_2$s$^\dagger_2$, C1r$^\dagger_2$s$^{\Delta S}_2$ and C1r$^{\Delta CS}$s$^{\Delta S}$ from top to bottom using Superdex 200 16/60 or Superose 6 16/60 columns. SDS-PAGE gels of each sample are shown on the right.
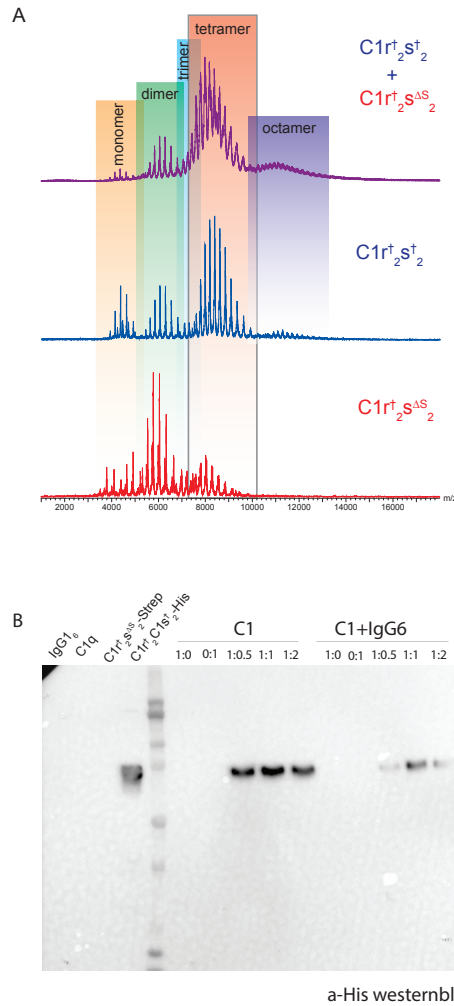
Supplementary Figure 2. Native-mass spectra of the mixtures of C1rs dimers and tetramers

A) Native mass spectra of $C1qr^{\Delta CS}{}_2s^{\Delta S}{}_2$ (red), $C1qr^{\dagger}{}_2s^{\Delta S}{}_2$ (blue) and their mixtures acquired after 10 min and 24 hours at RT. The purple peaks show the formation of hybrid specie $C1qr^{\dagger}r^{\Delta CS}s^{\Delta S}{}_2$, although overlapping with signals of the original species, $C1qr^{\Delta CS}{}_2s^{\Delta S}{}_2$ and $C1qr^{\dagger}{}_2s^{\Delta S}{}_2$. The top spectrum shows the products of mixing C1q with pre-mixed $C1r^{\Delta CS}s^{\Delta S}$ and $C1r^{\dagger}{}_2s^{\Delta S}{}_2$ that went through a 10-min incubation. B) Western blot with an anti-His antibody of pull-down experiment of $C1qr^{\dagger}{}_{2s}{}^{\dagger}{}_2$ and $C1qr^{\dagger}{}_{2s}{}^{\Delta S}{}_2$ and these complexes in complex with IgG6 (right). The controls; IgG6, C1q, $C1r^{\dagger}{}_{2s}{}^{\Delta S}{}_2$ and $C1r^{\dagger}{}_{2s}{}^{\dagger}{}_2$ are shown on the left. Strep-tag purification of mixture of C1 complexes are shown in each lane with increasing amount of $C1qr^{\dagger}{}_{2s}{}^{\dagger}{}_2$-His from left to right."

Supplementary Figure 3. Formation of the mixed C1-IgG$_6$ species at 4°C

Formation of the hybrid species C1qr$^\dagger_2$s†s$^{\Delta S}$ -IgG$_6$ detected by native MS plotted. The data points which were immediately acquired at room temperature (RT) after incubation at 4°C are shown with solid symbols. The data points shown with open triangles were acquired with extended exposure to RT following the immediate acquisitions (the x-coordinates represent the sum of incubation time and acquisition time).

A

B

C
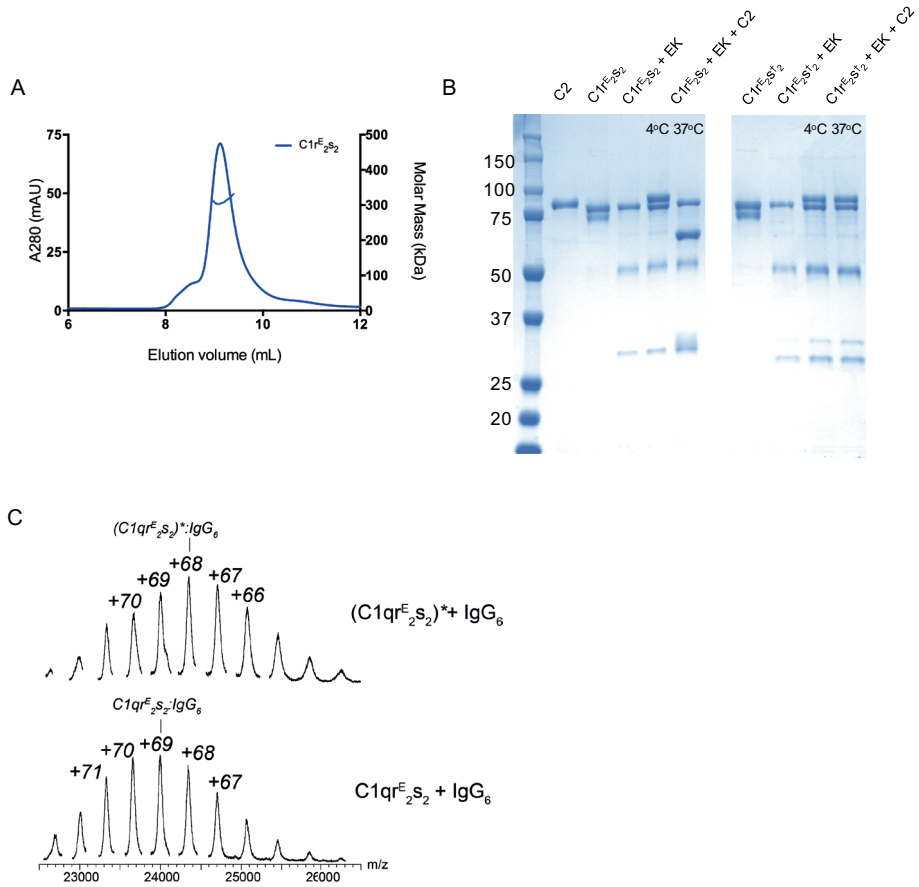
Supplementary Figure 4. Analysis of C1r$^E_2$s$_2$ by SEC-MALS, Native MS and C2 cleavage assay

A) SEC-MALS profile of C1r$^E_2$s$_2$ B) SDS-PAGE of C2 cleavage assay. C2, C1r$^E_2$s$_2$ and C1r$^E_2$s$^†_2$ (first, second and sixth lanes) are shown as controls. EK added C1r$^E_2$s$_2$ and C1r$^E_2$s$^†_2$ are shown at the third and seventh lane. C2 cleavage of activated C1r$^E_2$s$_2$ at 4°C and at 37°C (fourth and fifth lane) and C2 cleavage of activated C1r$^E_2$s$^†_2$ at 4°C and at 37°C are shown (eighth and ninth lane). C) Native mass spectra of C1qr$^E_2$s$_2$-IgG$_6$ before (bottom) and after activation (top).

Supplementary Table 1. Theoretical and measured Mw values of the proteins or protein complexes used or identified in this work.

		Theoretical [a] (kDa)	Measured [b] (kDa)	Number of charge states used for calculation
Building blocks	$C1r^{\Delta CS}$	$41.885 + M(g)$	44.4 ± 0.1	3
	$C1r^{\dagger}$ (co-expressed with $C1s^{\Delta S}$)	$79.377 + M(g)$	83.6 ± 0.1	4
	$C1r^{\dagger}$ (co-expressed with $C1s^{\dagger}$)	$79.377 + M(g)$	84.6 ± 0.1	4
	$C1r^{E}$	$79.284 + M(g)$	84.3 ± 0.1	4
	$C1s^{\Delta S}$ (co-expressed with $C1r^{\dagger}$)	$46.778 + M(g)$	48.1 ± 0.1	5
	$C1s^{\Delta S}$ (co-expressed with $C1r^{\Delta CS}$)	$46.778 + M(g)$	48.9 ± 0.1	3
	$C1s^{\dagger}$	$76.051 + M(g)$	78.5 ± 0.1	5
	$C1s$	$76.067 + M(g)$	78.7 ± 0.1	5
	$C1q$	$421.149 + M(g)$	464.1 ± 0.1	9
	IgG1-RGY (*28*)	$145.432 + M(g)$	148.4 ± 0.1	6
Large complexes	$C1r^{\Delta CS}s^{\Delta S}$	93.3	93.5 ± 0.1	5
	$C1r^{\dagger}_2s^{\Delta S}_2$	265.0	*265.3±0.1*	8
	$C1r^{\dagger}_2s^{\dagger}_2$	326.3	*326.4±0.1*	6
	$C1qr^{\Delta CS}_2s^{\Delta S}_2$	650.7	*650.1±0.3*	8
	$C1qr^{\dagger}_2s^{\Delta S}_2$	729.1	*728.5±0.3*	5
	$C1qr^{\dagger}_2s^{\dagger}_2$	790.4	*790.3±0.1*	6
	$C1qr^{E}_2s^{\dagger}_2$	790.2	*789.8±0.3*	7
	IgG_6	890.3	890.2 ± 0.1	12
	$C1q:(IgG)_6$	1354.4	*1353.2±0.2*	6
	$C1qr^{\Delta CS}_2s^{\Delta S}_2:IgG_6$	1540.3	*1538.7±0.2*	8
	$C1qr^{\dagger}_2s^{\Delta S}_2:IgG_6$	1619.3	*1619.8±0.2*	8
	$C1qr^{\dagger}_2s^{\dagger}_2:IgG_6$	1680.5	*1679.5±0.4*	8
	$C1qr^{E}_2s^{\dagger}_2:IgG_6$	1680.4	*1680.4±0.2*	5

[a] For building blocks, calculated based on amino acid sequence, excluding contribution from glycan chains or other post-translational modification or processing; for large complexes, calculated based on the measured Mw of the building blocks. $M(g)$ denotes Mw of Glycan contents.

[b] Including the contribution from glycan chains (for the glycosylated form only) and other post-translational modification or processing; tabulated are average Mw of the proteoform. Values in Italic style represent results from tandem MS measurements.

REFERENCES

1. M. J. Walport, Complement. Second of two parts. *N. Engl. J. Med.* **344**, 1140–4 (2001).

2. D. Ricklin, E. S. Reis, J. D. Lambris, Complement in disease: a defence system turning offensive. *Nat. Rev. Nephrol.* **12**, 383–401 (2016).

3. J. P. M. Melis *et al.*, Complement in therapy and disease. *Mol. Immunol.*, 1–14 (2015).

4. Y. Cai, B. H. D. Teo, J. G. Yeo, J. Lu, C1q protein binds to the apoptotic nucleolus and causes C1 protease degradation of nucleolar proteins. *J. Biol. Chem.* **290**, 22570–22580 (2015).

5. U. Kishore *et al.*, Structural and functional anatomy of the globular domain of complement protein C1q. *Immunol. Lett.* **95**, 113–28 (2004).

6. F. D. G. McGrath *et al.*, Evidence that complement protein C1q interacts with C-reactive protein through its globular head region. *J. Immunol.* **176**, 2950–2957 (2006).

7. M. Chen, M. R. Daha, C. G. M. Kallenberg, The complement system in systemic autoimmune disease. *J. Autoimmun.* **34**, J276–J286 (2010).

8. S. Ram, L. A. Lewis, P. A. Rice, Infections of people with complement deficiencies and patients who have undergone splenectomy. *Clin. Microbiol. Rev.* **23** (2010), pp. 740–780.

9. M. A. Wu, A. Zanichelli, M. Mansi, M. Cicardi, Current treatment options for hereditary angioedema due to C1 inhibitor deficiency. *Expert Opin. Pharmacother.* **6566**, 1–14 (2015).

10. A. Sekar *et al.*, Schizophrenia risk from complex variation of complement component 4. *Nature.* **530**, 177–183 (2016).

11. S. Hong *et al.*, Complement and microglia mediate early synapse loss in Alzheimer mouse models. *Science.* **352**, 712–6 (2016).

12. M. J. Vasek *et al.*, A complement–microglial axis drives synapse loss during virus-induced memory impairment. *Nature.* **534**, 538–543 (2016).

13. V. N. Schumaker, First component of complement, 21–42 (1987).

14. F. Forneris, J. Wu, P. Gros, The modular serine proteases of the complement cascade. *Curr. Opin. Struct. Biol.* **22** (2012), pp. 333–341.

15. R. B. Sim, G. J. Arlaud, M. G. Colomb, Kinetics of reaction of human C1-inhibitor with the human complement system proteases C1r and C1s. *BBA - Enzymol.* **612**, 433–449 (1980).

16. J. Tschopp, W. Villiger, H. Fuchs, E. Kilchherr, J. Engel, Assembly of subcomponents C1r and C1s of first component of complement: electron microscopic and ultracentrifugal studies. *Proc. Natl. Acad. Sci. U. S. A.* **77**, 7014–7018 (1980).

17. C. J. Strang, R. C. Siegel, M. L. Phillips, P. H. Poon, V. N. Schumaker, Ultrastructure of the first component of human complement: electron microscopy of the crosslinked complex. *Proc. Natl. Acad. Sci. U. S. A.* **79**, 586–590 (1982).

18. P. H. Poon, V. N. Schumaker, M. L. Phillips, C. J. Strang, Conformation and restricted segmental flexibility of C1, the first component of human complement. *J. Mol. Biol.* **168**, 563–577 (1983).

19. M. Budayova-Spano *et al.*, The crystal structure of the zymogen catalytic domain of complement protease C1r reveals that a disruptive mechanical stress is required to trigger activation of the C1 complex. *Eur. Mol. Biol. Organ. J.* **21**, 231–239 (2002).

20. C. L. Villiers, G. J. Arlaud, R. H. Painter, M. G. Colomb, Calcium binding properties of the C1 subcomponents C1a, C1r, and C1s. *FEBS Letts.* **117**, 289–294 (1980).

21. U. V. Girija *et al.*, Structural basis of the C1q/C1s interaction and its central role in assembly of the C1 complex of complement activation. *Proc. Natl. Acad. Sci.*, 201311113 (2013).

22. C. L. Villiers, G. J. Arlaud, M. G. Colomb, Domain structure and associated functions of subcomponents C1r and C1s of the first component of human complement. *Proc. Natl. Acad. Sci. U. S. A.* **82**, 4477–4481 (1985).

23. A. E. Phillips *et al.*, Analogous interactions in initiating complexes of the classical and lectin pathways of complement. *J. Immunol.* **182**, 7708–17 (2009).

24. I. Bally *et al.*, Identification of the C1q-binding Sites of Human C1r and C1s: a refined three-dimensional model of the C1 complex of complement. *J. Biol. Chem.* **284**, 19340–8 (2009).

25. D. Ugurlar *et al.*, Structures of C1-IgG1 provide insights into how danger pattern recognition activates complement. *Science (80-.).* (2018).

26. P. Lössl, M. Van De Waterbeemd, A. J. R. Heck, The diverse and expanding role of mass spectrometry in structural and molecular biology. *EMBO J.*, 1–24 (2016).

27. A. J. R. Heck, Native mass spectrometry: a bridge between interactomics and structural biology. *Nat. Methods.* **5**, 927–933 (2008).

28. C. A. Diebolder *et al.*, Complement is activated by IgG hexamers assembled at the cell surface. *Science.* **343**, 1260–3 (2014).

29. G. Wang *et al.*, Molecular basis of assembly and activation of complement component C1 in complex with immunoglobulin G1 and antigen. *Mol. Cell.* **63**, 135–145 (2016).

30. J. Tschopp, W. Villiger, A. Lustig, J. C. Jaton, J. Engel, Antigen-independent binding of IgG dimers to C 1 q as studied by sedimentation equilibrium, complement fixation and electron microscopy. *Eur. J. Immunol.* **10**, 529–535 (1980).

31. V. N. Schumaker, Component of Complement, 21–42 (1987).

32. S. A. Mortensen *et al.*, Structure and activation of C1, the complex initiating the classical pathway of the complement cascade. *Proc. Natl. Acad. Sci.* **114**, 986–991 (2017).

33. C. Gaboriaud, W. L. Ling, N. M. Thielens, I. Bally, V. Rossi, Deciphering the fine details of C1 assembly and activation mechanisms: "Mission impossible"? *Front. Immunol.* **5**, 565 (2014).

34. J. Snijder, A. J. R. Heck, Analytical approaches for size and mass analysis of large protein assemblies. *Annu. Rev. Anal. Chem. (Palo Alto. Calif).* **7**, 43–64 (2014).

35. R. H. H. Van Den Heuvel *et al.*, Improving the performance of a quadrupole time-of-flight instrument for macromolecular mass spectrometry. *Anal. Chem.* **78**, 7473–7483 (2006).

36. Y. Tseng, P. Zavodszky, V. N. Schumaker, The Human Complement C1 Complex Has a Picomolar Dissociation Constant at Room Temperature'. **4000** (2000).

37. R. J. Ziccardi, N. R. Cooper, Active Disassembly of the First Complement Component, C1, by C1 Inactivator. *J. Immunol.* **123**, 788–792 (1979).

38. R. J. Ziccardi, The role of immune complexes in the activation of the first component of human complement. *J. Immunol.* **132**, 283–288 (1984).

39. M. A. Lindorfer *et al.*, Real-time analysis of the detailed sequence of cellular events in mAb-mediated complement-dependent cytotoxicity of B-cell lines and of chronic lymphocytic leukemia B-cells. *Mol. Immunol.* **70**, 13–23 (2016).

40. R. J. Ziccardi, A new role for C1-inhibitor in homeostasis: Control of Activation of the first component of human complement. **128**, 2–5 (1982).

41. C. B. Chen, R. Wallis, Stoichiometry of complexes between mannose-binding protein and Its associated serine proteases: Defining functional units for complement activation. *J. Biol. Chem.* **276**, 25894–25902 (2001).

42. S. E. Degn *et al.*, Complement activation by ligand-driven juxtaposition of discrete pattern recognition complexes. *Proc. Natl. Acad. Sci.* **111**, 13445–13450 (2014).

Chapter 3

43. A. R. Gingras *et al.*, Structural basis of mannan-binding lectin recognition by its associated serine protease MASP-1: implications for complement activation. *Structure.* **19**, 1635–43 (2011).

44. R. Wallis, D. A. Mitchell, R. Schmid, W. W. Schwaeble, H. Anthony, UKPMC Funders Group Paths reunited : initiation of the classical and lectin pathways of complement activation. *Russell J. Bertrand Russell Arch.* **215**, 1–11 (2010).

45. J. Kardos *et al.*, Revisiting the mechanism of the autoactivation of the complement protease C1r in the C1 complex: structure of the active catalytic region of C1r. *Mol. Immunol.* **45**, 1752–60 (2008).

Chapter 4

Structural mismatch of C1-IgG1 complexes in the presence of proteases

Deniz Ugurlar[1], Laura van Bezouwen[1], Seline A. Zwarthoff[2], Rob N. de Jong[3], Frank J. Beurskens[3], Suzan Rooijakkers[2], Piet Gros[1]

1 Crystal and Structural Chemistry, Bijvoet Center for Biomolecular Research, Department of Chemistry, Faculty of Science, Utrecht University, Padualaan 8, 3584 CH Utrecht, The Netherlands

2 Medical Microbiology, University Medical Center Utrecht, 3584 CX Utrecht, The Netherlands

3 Genmab, Yalelaan 60, 3584 CM Utrecht, The Netherlands

ABSTRACT

The first component C1 of the classical pathway of complement auto-activates upon binding to clusters of antibody-antigen complexes on cell surfaces. In a recent cryo-EM single-particle reconstruction, we have shown that C1 binds IgG1 hexamers through 4, 5 or 6 C1q globular heads making direct contacts with up to 6 binding sites on IgG1-Fc hexamer platforms. Incomplete and heterogeneous binding of the 6 C1q arms to IgG1 hexamers limited the resolution obtained in cryo-EM reconstruction. Here, we tested whether the observed heterogeneity is possibly due to weak C1q-Fc interactions or results from a structural mismatch caused by the presence of $C1r_2s_2$ proteases. Using single-particle cryo-EM, we analyzed a variant of hexamerizing IgG1 with enhanced C1q-binding affinity in complex with either C1q or C1. Our data demonstrate that C1q binds enhanced antibody platforms with 6 C1q globular heads in the absence of the proteases, and with 4 or 5 C1q globular heads in the presence of proteases. These data support the hypothesis that the presence of $C1r_2s_2$ limits C1q conformations resulting in a structural mismatch between C1 and IgG1 hexamers with incomplete binding of the C1q arms to the antibody platform.

INTRODUCTION

The classical pathway of complement contributes to immune responses by recognizing patterns on surfaces (*1*, *2*). C1 is the first component of the classical pathway and recognizes various ligands on surfaces, such as antigen-bound IgG or IgM complexes on foreign cell surfaces, and other ligands like DNA, phosphatidylserine or annexins on injured or apoptotic cells and on damaged tissue (*3*, *4*). Upon recognition, C1 initiates a set of proteolytic activations that lead to inflammatory response, cell lysis and clearance by macrophages and neutrophils. Conditions where the complement system over-activates or activates insufficiently may lead to a variety of diseases. Over-activation of complement is linked to autoimmune diseases, such as systemic lupus erythematosus (*5*) and rheumatoid arthritis (*6*), or ischemia and reperfusion injuries (*7*), whereas insufficient activation may lead to infectious diseases (*8*). Complement has also been used in therapies, where therapeutic antibodies recruit complement for enhanced complement dependent toxicity (CDC) to eliminate pathogenic microorganism or tumor cells (*9*, *10*). These therapeutic antibodies activate complement, such as for the treatment of infectious diseases and cancer. The design of complement-modulating antibodies benefits from understanding the C1 structure and the structural requirements for efficient complement activation.

C1 is a 790 kDa Ca^{2+}-dependent protein complex, assembled from a recognition protein C1q and two serine proteases C1r and C1s (*11*). The recognition protein C1q is composed of 6 C-terminal hetero-trimeric globular heads (gC1q), connected to collagen-like arms that merge into a stalk at the N-terminal ends (*12*). C1r and C1s are homologous serine proteases that form a hetero-tetramer, $C1r_2s_2$. N-terminal domains of $C1r_2s_2$ binds the C1q-collagen arms and form a heterotetrameric platform in between the 6 collagen arms in the presence of calcium. The 6 gC1q-units are responsible for ligand recognition, providing avidity for ligand binding on surfaces. It is considered (*13*), that binding of C1q to multimeric molecular patterns on surfaces induces conformational changes in the associated proteases, which leads to activation of the proteases C1r and C1s and results in the catalytic cleavage of C4 and C2 in the classical pathway.

Antibodies recruit C1 *via* their Fc parts and recognize antigens *via* their variable regions in the Fab arms. A single IgG antibody does not yield efficient complement activation and oligomerization of antibodies is needed for C1 activation (*14*, *15*). Low resolution cryo-electron tomography data by Diebolder *et al* (2014) indicated that C1 binds antibody hexamers on liposomal surfaces. IgG1 molecules

with a single mutation, E345R, promote Fc-Fc interaction and increase CDC significantly, likely through enhancing hexamerization on the targeted cells (*10*). A combination of three mutants, E345R, E430G and S440Y (denoted as RGY) yielded IgG1 hexamers in solution that activate complement in the absence of an antigenic surface. IgG1(RGY) antibodies bind C1q and C1 efficiently, as shown by native mass spectrometry (*17*). The interaction sites of C1q and Fc have been extensively studied (*18–24*). Enhanced C1q affinity and increased CDC can be achieved by mutating residues at the C1q binding site (*23*, *24*). A combination of mutations S267E, H268F and S324T mutants (EFT) enhanced CDC potency 6.9-fold and yielded C1q binding 47 times stronger than wild type IgG1s (*24*). According to the 7 Å cryo-EM map of the gC1q-Fc interface (*25*) residues S267 and H268 of CH2 domain interact with C1qB chain and S324 of CH2' domain interacts with C1q C chain, shown in Figure 1A. In summary, enhanced complement activation can be achieved by introducing mutations that enhance hexamer formation and C1q binding avidity, or by mutations that increase the affinity of the C1q binding site on IgG.

Previously, we applied single-particle cryo-EM reconstruction to determine a 7-10 Å resolution structure of C1 in complex with IgG1(RGY)(*25*). Structural heterogeneity of the particles, due to variable binding of C1 to IgG1 hexamers, limited the resolution of the reconstruction. The data revealed an overall asymmetric structure of C1 with its protease platform bound in between C1q collagen arms and C1q bound through its gC1q units to the hexameric Fc platform. We observed incomplete C1q binding to the Fc hexamer with 4 gC1q domains bound consecutively and the remaining two gC1q units either bound or unbound. What causes the incomplete binding of the 6 C1q arms to the 6 available gC1q binding sites on the IgG1-Fc hexamer platform is unclear.

Here, we tested two possible causes of the observed structural heterogeneity in the C1-IgG1$_6$ complex: limiting IgG-gC1q affinity, and the presence of the proteases, which may limit C1q arms movements and cause mismatch between C1 and the IgG1 hexamer. We combined EFT and RGY mutations in an IgG1 antibody, IgG1(EFTRGY), in order to form Fc hexamers with enhanced affinity and avidity for C1q binding. Cryo-EM single particle analysis of IgG1(EFTRGY) in complex with C1q and C1 yielded 2D projections and 3D reconstructions that show the stoichiometry of gC1q domains bound to Fc regions of the antibody platform.

RESULTS

Solution-phase complement activation by IgG1(EFTRGY)

Like IgG1(RGY), IgG1(EFTRGY) efficiently formed stable hexamers in solution at pH 7.5 (Fig. 1B). Size exclusion chromatography (SEC) enabled separation of hexamers from minor peaks of IgG1 monomers and other oligomers. Figure 1C shows that IgG1(RGY) and IgG1(EFTRGY) have enhanced C4 cleavage by serum C1, compared to the wild type IgG1 controls. However, IgG1(EFTRGY) did not show enhanced C4d production in solution, when compared to IgG1(RGY). None of the IgG1 hexamers were as effective as heat aggregated IgGs, which form a very dense ligand surface. IgG1(EFT) variant, which increased complement activity 6.9-fold on cell surfaces compared to wild type IgG1 (*24*), requires surface binding for activation; and, thus is not suitable for an in-solution C4d production assay. Possibly, high avidity of the RGY variants is sufficient for C1q recruitment and, therefore, combining EFT with RGY may not provide enhanced complement activation in solution, since hexamers were already formed.
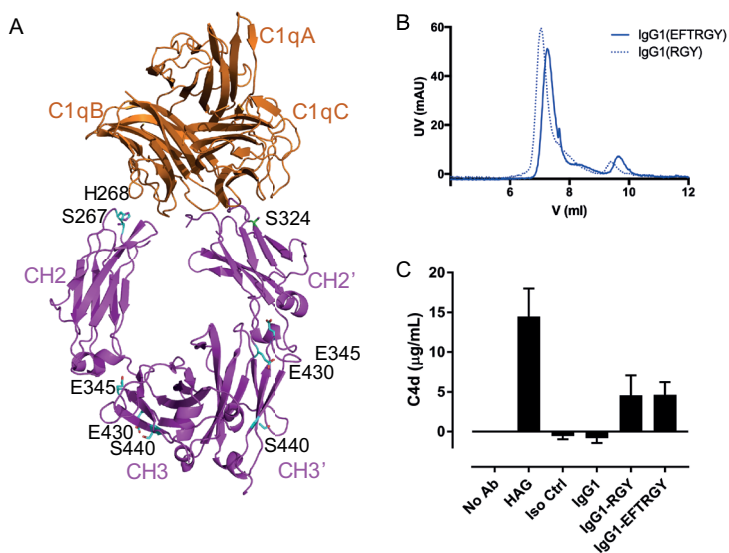
Figure 1. C1-IgG1(EFTRGY) binding and activation in fluid-phase

A) Model of gC1q-Fc based on a 7 Å map of the C1-IgG1(RGY) complex. C1q is shown in orange and Fc region is shown in magenta. EFT and RGY mutations are shown on the structure. B) Size exclusion chromatography of IgG1(RGY) in dotted blue and IgG1(EFTRGY) in blue. C) C4d production assay. The first column (No AB) is negative control and the second column (heat aggregated IgG) is positive control. C4d production levels are presented as average, with standard deviation indicated by error bars.

Stability of C1 and C1q-IgG1(RGY) complexes

We compared analytical SEC of C1-antibody complexes in the presence and absence of calcium (Figure 2A). In the presence of EDTA, $C1r_2s_2$ dissociated from C1-IgG1(RGY) complex resulting in the elution of C1q-IgG1(RGY) complex. The removal of proteases did not cause dissociation of C1q from soluble IgG1(RGY) platforms. Next, we measured the stability of C1q-antibody complexes on antigen-covered magnetic beads, either covered with IgG1, IgG2 and IgG1(RGY), in the absence and presence of the proteases (Figure 2B). Addition of EDTA caused dissociation of both $C1r_2s_2$ and C1q from the surface covered with either wild type IgG1 or IgG2. These data demonstrate that $C1r_2s_2$ proteases increase the stability of C1q-IgG1 and C1q-IgG2 complexes on bead surfaces. However, C1q remained attached to IgG1(RGY) covered surfaces when $C1r_2s_2$ dissociated from C1 complex. Thus, the stability of C1q-IgG complexes on IgG1(RGY) covered beads or IgG1(RGY) complexes in solution was not affected by the absence of $C1r_2s_2$ and C1q remained attached, whereas the presence of $C1r_2s_2$ enhanced the binding of wild-type IgG by C1q.
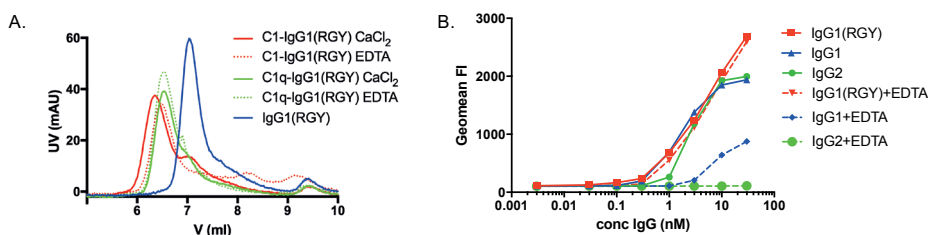

Figure 2. Effects of $C1r_2s_2$ on the stability of C1 and C1q-IgG1(RGY) complexes

A) Size exclusion chromatography of C1-IgG1(RGY) in the presence of $CaCl_2$ (red), and EDTA (dotted red), C1q-IgG1(RGY) in the presence of $CaCl_2$ (green), and EDTA (dotted green); IgG1(RGY) is used as a control (blue). B) C1q deposition assay on DNP-covered magnetic beads. The beads were incubated with human anti-DNP IgG1, IgG2 or IgG1(RGY). C1q on the bead surface was detected when C1 is added to the beads in a buffer with EDTA (dotted line) and no EDTA (continuous line).

Cryo-EM analysis of C1q-IgG1(EFTRGY)

We purified IgG1(EFTRGY) in complex with C1q and C1 for single-particle cryo-EM analysis. Figure 3A shows minor overlap of the peaks of C1q-IgG1(EFTRGY) and IgG1(EFTRGY) in SEC, yielding an efficient separation of the two complexes. We collected fractions between 6 ml and 6.5 ml of the C1q-IgG1(EFTRGY) peak to minimize free IgG1(EFTRGY) in the sample for single-particle cryo-EM analysis. 1,659 micrographs were collected of C1q-IgG1(EFTRGY) complex with an average of 20-30 particles per micrograph. 2D class averaging of 57,290

particles indicated classes of IgG1(EFTRGY) without C1q bound and other classes of C1q bound to IgG1 hexamer (Figure 3B). The side views are mostly from unbound IgG1(EFTRGY) and cover ~20% of all particles limiting the quality of 3D reconstruction. C6 symmetry applied 3D classification from a selection of 14,341 particles from 2D class averages yielded two classes of 45% complexes and 55% unbound IgG1(EFTRGY) particles (Figure 3C).

The major class of unbound IgG1(EFTRGY) displayed a typical hexamer arrangement with a diameter of 18 nm. C6-symmetry imposed 3D refinement of unbound IgG1(EFTRGY) yielded a density map at 9.5-Å resolution, generated from only 7,750 particles (Figure 3D). We also determined cryo-EM reconstructions of IgG1(RGY) in order to compare the two variants. Selecting projections of top views and side views from 2D class averages, 3D refinement yielded a 6.5-Å structure with 6 Fc regions forming a hexamer platform and densities of the Fabs extending from the platform, as shown in Figure 3D. Both antibody complexes show clear density for the Fc-domain platform (Figure 3D). Furthermore, both showed additional densities that may be attributed to Fab domains, located predominantly at one side of the Fc-platform, in contrast to Fab arms positioned on both sides of the Fc platform as observed in the crystal structure of IgG1 b12 (1HZH, (*26*)). Overall, no significant differences in Fc platform were observed between IgG1(RGY) structure and IgG1(EFTRGY); and, in both cases densities suggest that Fab arms are positioned reminiscent of a surface-bound state of the IgG molecules, consistent with their capabilities to activate C1 without surface binding.

3D refinement of intact C1q-IgG1(EFTRGY) complexes in the absence of $C1r_2s_2$ yielded a reconstruction at 22-Å resolution, due to the limited number of particles and the lack of side views. The low-resolution map did not provide enough information to identify the interaction site with Fc regions. According to the top view projections of 'bound' complexes, C1q binds Fc regions of IgG1(EFTRGY) with 6 gC1q units (Figure 3C). The complete binding of C1q to Fc hexamers differs from the previously observed C1-IgG1(RGY) cryo-EM data where C1q binds IgG1(RGY) with 4, 5 or 6 gC1q units. Moreover, no density for C1q-collagen arms and stalk were visible in the averaged classes. Possibly, the flexibility of C1q arms in the absence of $C1r_2s_2$ enables complete binding of 6 gC1q units to Fc platforms.
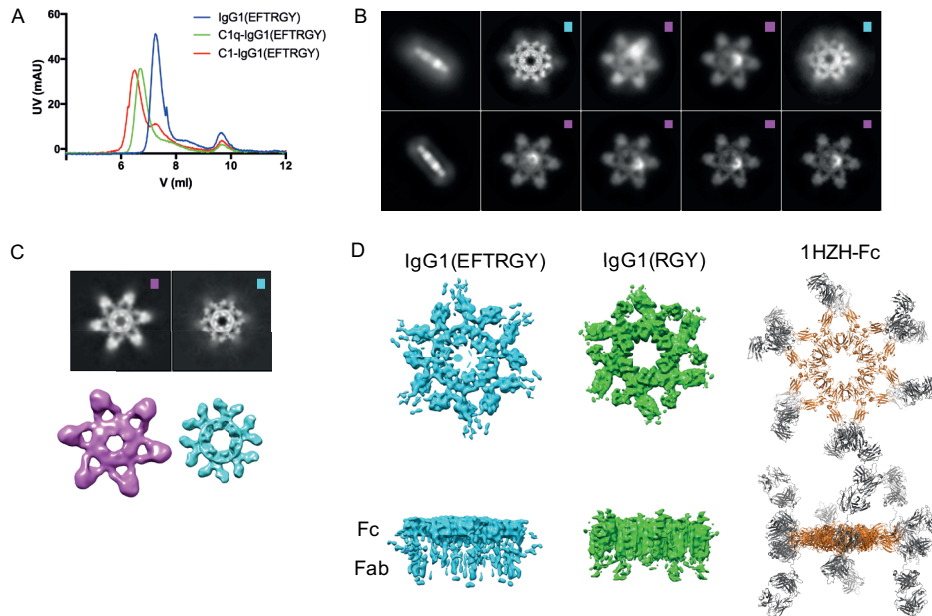
Figure 3. Cryo-EM reconstruction of C1q-IgG1(EFTRGY)

A) Size exclusion chromatography of IgG1(EFTRGY) (blue) and its complexes when bound to C1q (green) and C1(red). B) 2D class averages of C1q- IgG1(EFTRGY) complex. C1q-"Bound" classes are indicated by magenta squares and C1q-"unbound" classes are indicated by cyan squares. C) 3D classification of C1q- IgG1(EFTRGY) complex. The C1q-bound and -unbound classes are shown in magenta and cyan as Fig. 3B. 3D reconstructions of each class are shown below the class averages. D) 3D reconstructions of unbound IgG1(EFTRGY) (cyan) and IgG1(RGY) (green). Crystal structure of IgG1-b12 (pdbID:1HZH) shown in cartoon representation.

Cryo-EM analysis of C1-IgG1(EFTRGY)

We analyzed cryo-EM reconstruction of IgG1(EFTRGY) bound to C1 complex, i.e. containing $C1r_2s_2$, in order to analyze the effects of EFT mutants and $C1r_2s_2$ on the structure of the complex. 60,760 particles from 809 micrographs yielded 2D class averages which showed intact complexes of C1-IgG1(EFTRGY). The top middle class in Figure 4A indicated only 4 gC1q bound antibody hexamers and other classes did not indicate any complete C1q binding with 6 gC1q units (Figure 4A). Figure 4B shows the reconstruction of the gC1q-Fc platform, where 4 consecutive gC1q domains are bound and two gC1q units are not visible in the density. We aligned a (unsharpened) density map of C1-IgG1(EFTRGY) obtained at 14.5-Å resolution onto the previously obtained 10-Å resolution density map of C1-IgG1(RGY) (*25*) using the Chimera volume fitting tool. The two missing gC1q units in C1-IgG1(EFTRGY) coincide with the location where heteroge-

neous binding was observed in C1-IgG1(RGY). Possibly, the high affinity binding site in IgG1(EFTRGY) caused a change in the orientation of the gC1q domains concomitant with a straightening in the C1q arms, shown by the arrows in Figure 4C, which may result in binding of only 4 gC1q units to the six available binding sites on the Fc platforms.
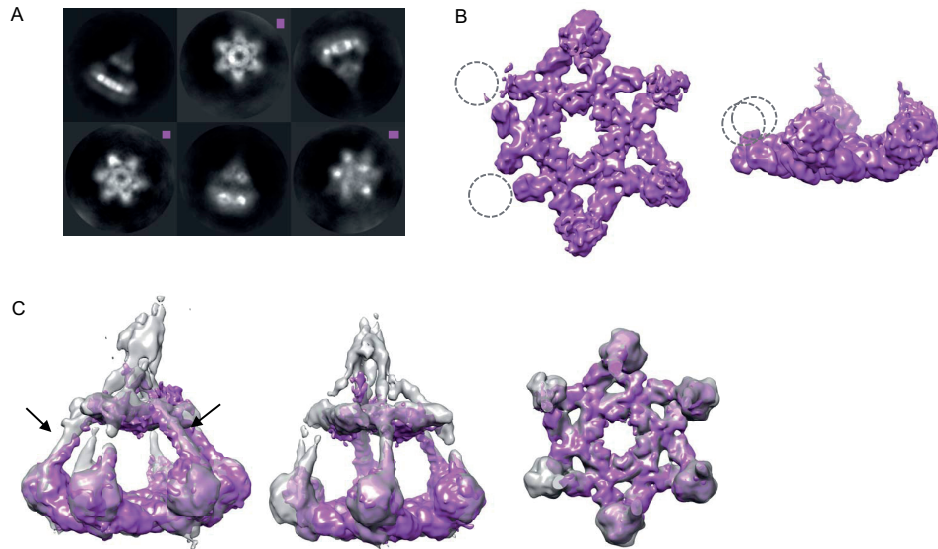

Figure 4. Cryo-EM reconstruction of C1-IgG1(EFTRGY)

A) 2D class averages of C1- IgG1(EFTRGY) complex. Top views of the C1-bound classes are shown with a magenta box. B) 3D reconstruction of C1-IgG1(EFTRGY) complex from top (left) and side (right) views. The missing gC1q domains are indicated as dashed circles. C) C1- IgG1(EFTRGY) aligned to C1- IgG1(RGY) (*25*) presented as side views (left) and top view(right).

DISCUSSION

The classical pathway initiation complex C1 binds a variety of ligands, such as surface-bound antibodies and pentraxins, DNA and amyloids. Recognition by and activation of C1 requires avidity through binding ligands with its 6 gC1q units. IgG antibodies activate C1 efficiently, when they oligomerize on surfaces (*10*). IgG(RGY) variants form hexamers in solution and generate sufficient avidity for recognition by and activation of C1. Considering the variety of ligands presenting different patterns, understanding the modes of C1 recognition of such patterns is important. Here, we analyzed the potential sources of stability and structural heterogeneity of C1-IgG1 using *in vitro* binding assays and cryo-EM reconstructions.

Our data show that $C1r_2s_2$ affects the stability of C1q-IgG complexes on strepta-vidin bead surfaces. C1 bind IgG1 and IgG2 efficiently on antigen (biotinylated DNP) covered bead surfaces; however, C1q alone, after $C1r_2s_2$ dissociation, forms complexes with IgG1 much less efficiently than C1 and does not bind IgG2 at all. In contrast, C1q-IgG1(RGY) complexes were stable and complexes remained intact after dissociating $C1r_2s_2$ proteases. We hypothesize that hexamerization of antigen-bound IgG molecules on a surface and high-avidity C1 binding are thermodynamically coupled events. While surface-bound monomeric and oligo-meric IgGs are in dynamic equilibrium, binding of C1 may favor formation and stabilization of IgG hexamers. Possibly, binding of the $C1r_2s_2$ proteases to C1q pre-arranges the gC1q units in a way that promotes recognition and stabiliza-tion of transiently formed hexamers of surface-bound IgG molecules. In the absence of the $C1r_2s_2$ proteases, the C1q arms may spread further apart and bind, more distant, surface-bound IgG molecules that are not in direct contact to each other, and thereby challenge the high-avidity binding mode that depends on IgG hexamerization. Stable IgG1(RGY) hexamers, however, exhibit 6 binding sites constitutively and provide a high-avidity binding site for both C1q and C1. This model explains that increased C1q-Fc affinity through e.g. EFT mutations (*24*) and increased Fc-Fc interaction by RGY mutations (*16*) enhance C1 high-avidity binding to cells yielding enhanced CDC. Moreover, it explains that these effects are not additive, once IgG hexamerization is established.

The presented limited cryo-EM data showed that C1q binds IgG1(RGY) with all 6 gC1q units bound at the 6 C1q-Fc interaction sites in IgG1(RGY). Thus, in the absence of $C1r_2s_2$ proteases, homogeneous and symmetric binding of C1q to IgG1(RGY) hexamers is achieved. The absence of density for the collagen arms and stalk of C1q in the density map of C1q-IgG1(RGY)$_6$ support the notion that flexible collagen arms allow unobstructed binding of the 6 gC1q units to the hexameric Fc platform. Binding of C1 to IgG hexamers with increased C1q-Fc affinity (EFTRGY) enhanced the prevalence of asymmetric C1-IgG1$_6$ complexes with only 4 or 5 gC1q units bound to the hexameric Fc platforms. Overall, the tighter binding of gC1q causes straightening of the collagen arms. We conclude that the increased C1q-Fc affinity mutations aggravate the observed apparent mismatch in C1-IgG1(RGY)$_6$, where the diagonal 18-nm distance between C1q-binding sites the IgG1-Fc platform is too narrow for C1 to bind symmetrically with all its 6 gC1q units. Apparently, binding of 4 consecutive gC1q units and, therefore, C1q collagen arms suffice for C1 high-avidity binding and activation. It will be interesting to analyze C1 binding to IgM and IgG3 hexamers, which

have been predicted to form wider C1q-binding platforms (*27*, *28*). Moreover, we predict that density maps at higher resolution may be obtained more readily for such C1 complexes, because of minimizing the structural heterogeneity observed for C1-IgG1$_6$ complexes.

In conclusion, the low-resolution density reconstructions of C1q-IgG(RGY), C1q-IgG(EFTRGY) and C1-IgG1(EFTRGY) complexes provided unprecedented insights that allow us to answer mechanistic questions and further optimize experimental conditions for high resolution reconstructions. With the aid of Cryosparc, cryo-EM analysis was performed very quickly. However, the modest number of particles and orientations limited the resolution of the reconstructed density maps and as a consequence, limits the interpretations of the structures. Better sample preparation and collecting a larger dataset will be the next step for determining high resolution structures that will uncover complement triggering mechanisms.

Chapter 4

Supplementary materials

Materials and methods

Expression and purification of the proteins

Pooled Normal Human Serum (NHS) serotype AB was obtained from Sanquin, Amsterdam, The Netherlands. IgG1(EFTRGY) and IgG1(RGY) mutant, were provided by Genmab (Utrecht, The Netherlands). The production of these antibodies was performed as previously described (Diebolder *et al*, 2014). Plasma-purified human C1q was purchased from Complement Technology, Inc. (Tyler, TX, USA). IgG1-RGY variants (E345R, E430G, and S440Y), were described previously (*16*). C1r (S654A) and C1s (S632A) mutants were generated using the Quikchange mutagenesis kit (Agilent Genomics, Santa Clara, CA) on TOPO clones inserted in pCR8 vectors (Thermo Fisher Scientific, Waltham, MA). C1s (S632A) constructs were fused with an N-terminal hexa-histidine tag. Both constructs were sub-cloned into mammalian expression vectors provided by U-Protein Express BV (U-PE), Utrecht, The Netherlands. C1r and C1s constructs were transiently co-expressed in human embryonic kidney 293 (HEK293) cells (supplied by U-Protein Express BV). After 5 days of transfection, the medium containing secreted $C1_2s_2$ was collected, concentrated into a QuixStand benchtop system (GE Healthcare) and dia-filtrated by a buffer containing 25mM Tris, 500mM NaCl, 2mM $CaCl_2$ at pH 8.5. $C1r_2s_2$ was purified with immobilized-metal affinity chromatography (IMAC) using pre-packed HisTrap FF columns (GE Healthcare). After sample application, the column was initially washed with 25mM imidazole, then the proteins of interest were eluted by increasing the concentration of imidazole up to 250 mM. The sample was concentrated up to 5 mg/ml for size exclusion chromatography which was performed on a gel filtration column (Superdex 200, GE Healthcare) using a buffer containg 25 mM Tris pH 8.5, 250 mM NaCl 2mM $CaCl_2$.

Sample preparation for Cryo-EM

$C1q$-$IgG1_6$ complex was prepared by mixing 1:6 molar ratio of C1q and IgG1(EFTRGY). $C1$-$IgG1_6$ complex was prepared by mixing $C1r_2s_2$, C1q and IgG1(RGY) or IgG1(EFTRGY). The complexes were purified with a Sephadex 4000 SEC column with a gel filtration buffer containing 25 mM Tris pH 7.5, 150 mM NaCl 0.5 mM $CaCl_2$ (Figure 2.a, b). After gel filtration of C1q-IgG1(EFTRGY), IgG1(RGY) and C1-IgG1(EFTRGY), the fractions were immediately used without concentration. 3 µl of the sample at a concentration of ~0.15-0.2 mg/ml was applied to freshly glow discharged Quantifoil R1.2/1.3

holey carbon grids (Quantifoil Micro Tools, Germany). The grids were blotted for 2 s at 100% humidity and at room temperature in an Vitrobot plunge-freezer using liquid ethane (Thermo Fisher Scientific).

Single-particle Cryo-EM data collection and processing

Cryo-EM images were collected on a Talos Arctica operating at 200 kV equipped with a Gatan energy filter and a K2 Summit camera. The energy slit was operating at 20 eV. Movies were recorded by the EPU software (Thermo Fisher Scientific), at a nominal magnification of 130,000× yielding a pixel size at the specimen of 1.025 Å in super-resolution counting mode. Movies were collected for 8 s with a total of 40 frames with a calibrated dose of about 2.4 e⁻/Å2 per frame, at defocus values between −1.6 and −3 μm. All the movie stacks from C1q-IgG1(EFTRGY), IgG1(RGY) and C1-IgG1(EFTRGY) datasets were aligned using MotionCorr_v2.1 (*29*) and CTF parameters were defined using gCtf (*30*). Particles from C1q-IgG1(EFTRGY) data were picked by Relion particle picking software (*31*) and particles from IgG1(RGY) and C1-IgG1(EFTRGY) data were picked by Gautomatch. The particles were aligned and classified by 2D Classification by Relion according to their 2D projection views. Bad particles were removed and the rest was used for 3D classification in Cryosparc (*32*), followed by 3D refinement and sharpening in Cryosparc.

Solution-phase C4d production assay

Complement activation was determined by measuring C4d concentrations, a marker for classical complement pathway activation, after incubating 100 μg/mL antibody in 90% normal human serum for 1 hour at 37 ºC. C4d concentrations were measured in an ELISA (MicroVue C4d EIA kit, Quidel Corporation, San Diego, US) generally according to the manufacturer's instructions, with the exception that all C4d levels were determined using 1:100 diluted samples in order to circumvent non-linearity deviations introduced by comparing different dilutions. C4d concentration in serum was measured twice each, in two independent experimental replicates. The amount of C4d produced during the incubation was determined by subtracting the C4d level in serum measured in the no antibody control reaction. Data was processed using GraphPad Prism v7.02 and is presented as mean and standard deviation.

C1q binding assay on magnetic beads

Streptavidin-coated beads (Dynabeads® M-270 Streptavidin, Invitrogen, 2.8 μm diameter) were washed once in PBS-TH (phosphate buffered saline with 0.05% Tween and 0.5% human serum albumin) and loaded with biotinylated 2,4-dini-

trophenol (DNP-PEG2-GSGSGSGK(Biotin)-NH2, Pepscan Therapeutics B.V., Lelystad, The Netherlands) by incubating ~6-7 x 10^6 beads/ml with 1 μg/ml DNP-biotin in PBS-TH for 30 minutes at 4°C under shaking conditions. After washing with PBS-TH, ~12-14 x 10^6 beads/ml were incubated in PBS-TH with a 3-fold dilution range of human anti-DNP IgG1, IgG2 or IgG1(RGY) (kindly provided by Suzan Rooijakkers (IgG1, IgG2) and Genmab (IgG1(RGY))) starting from 30 nM and shaken for 30 min at 4°C. After washing with PBS-TH, ~24-28 x 10^6 beads/ml were incubated in VBS-TH^{++} (Veronal buffered saline: 2 mM Veronal, 145 mM NaCl, pH 7.4 containing 0.5 mM $CaCl_2$, 0.25 mM $MgCl_2$, 0.05%Tween and 0.5% human serum albumin) with 1 nM C1 (Complement Technology, Inc., Tyler, TX, USA) with or without 10 mM EDTA, under shaking conditions for 30 min at 37°C. Subsequently, beads were washed in VBS-TH^{++} and C1q on the bead surface was detected using 2 μg/ml FITC-conjugated rabbit anti-C1q (Dako, Agilent) and flow cytometry (BD FACSVerse, BD Biosciences). Geomean fluorescence intensity of single beads was determined using FlowJo analysis software.
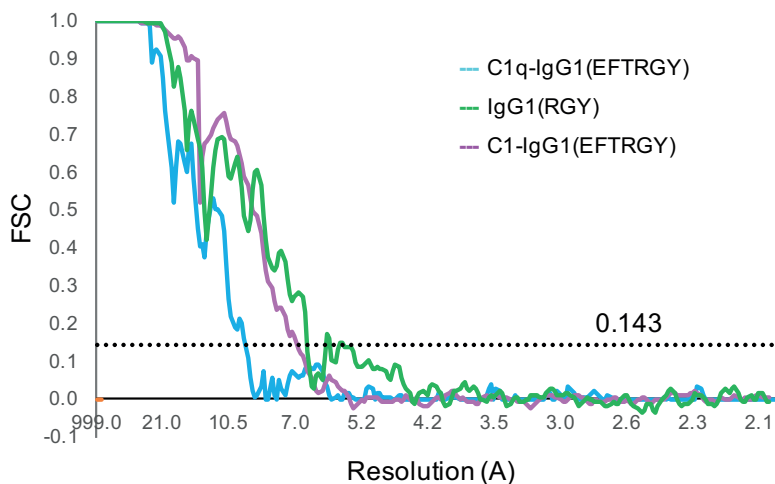
Supplementary Figure 1. Fourier shell correlation curves of C1q-IgG1(EFTRGY) (cyan), IgG1(RGY) (green) and C1-IgG1(EFTRGY) (magenta) as a function of resolution between two independent half-maps reconstructed from the data. The gold standard 0.143 is plotted as horizontal dashed line in grey.

References

1. G. Bajic, S. E. Degn, S. Thiel, G. R. Andersen, Complement activation, regulation, and molecular basis for complement-related diseases. *EMBO J.* **34**, 1–23 (2015).

2. M. Martin, J. Leffler, A. M. Blom, Annexin A2 and A5 serve as new ligands for C1q on apoptotic cells. *J. Biol. Chem.* **287**, 33733–33744 (2012).

3. A. Nayak, L. Pednekar, K. B. M. Reid, U. Kishore, Complement and non-complement activating functions of C1q: A prototypical innate immune molecule. *Innate Immun.* **18** (2012), pp. 350–363.

4. C. Gaboriaud, P. Frachet, N. M. Thielens, G. J. Arlaud, The human C1q globular domain: Structure and recognition of non-immune self ligands. *Front. Immunol.* **2**, 1–8 (2012).

5. M. Chen, M. R. Daha, C. G. M. Kallenberg, The complement system in systemic autoimmune disease. *J. Autoimmun.* **34**, J276–J286 (2010).

6. M. Okroj, D. Heinegård, R. Holmdahl, A. M. Blom, Rheumatoid arthritis and the complement system. *Ann. Med.* **39** (2007), pp. 517–530.

7. W. B. Gorsuch, E. Chrysanthou, W. J. Schwaeble, G. L. Stahl, The complement system in ischemia-reperfusion injuries. *Immunobiology.* **217** (2012), pp. 1026–1033.

8. L. Skattum, M. Van Deuren, T. Van Der Poll, L. Truedsson, Complement deficiency states and associated infections. *Mol. Immunol.* **48** (2011), pp. 1643–1655.

9. J. P. M. Melis *et al.*, Complement in therapy and disease. *Mol. Immunol.*, 1–14 (2015).

10. R. N. de Jong *et al.*, A novel platform for the potentiation of therapeutic antibodies based on antigen-dependent formation of IgG hexamers at the cell surface. *PLoS Biol.* **14** (2016), doi:10.1371/journal.pbio.1002344.

11. G. J. Arlaud, N. M. Thielens, C. Illy, Assembly of the C1 complex. *Behring Inst. Mitt.*, 189–195 (1993).

12. G. J. Arlaud *et al.*, Structural biology of C1: dissection of a complex molecular machinery. *Immunol. Rev.* **180**, 136–145 (2001).

13. M. Budayova-Spano *et al.*, The crystal structure of the zymogen catalytic domain of complement protease C1r reveals that a disruptive mechanical stress is required to trigger activation of the C1 complex. *Eur. Mol. Biol. Organ. J.* **21**, 231–239 (2002).

14. N. C. Hughes-Jones, B. Gardner, Reaction between the isolated globular sub-units of the complement component C1q and IgG-complexes. *Mol. Immunol.* **16**, 697–701 (1979).

15. D. R. Burton, Antibody: the flexible adaptor molecule. *Trends Biochem. Sci.* **15**, 64–69 (1990).

16. C. A. Diebolder *et al.*, Complement is activated by IgG hexamers assembled at the cell surface. *Science (80-.).* **343**, 1260–3 (2014).

17. G. Wang *et al.*, Molecular basis of assembly and activation of complement component C1 in complex with immunoglobulin G1 and antigen. *Mol. Cell.* **63**, 135–145 (2016).

18. M. S. Kojouharova, I. G. Tsacheva, M. I. Tchorbadjieva, K. B. M. Reid, U. Kishore, Localization of ligand-binding sites on human C1q globular head region using recombinant globular head fragments and single-chain antibodies. *Biochim. Biophys. Acta.* **1652**, 64–74 (2003).

19. M. S. Kojouharova *et al.*, Mutational analyses of the recombinant globular regions of human C1q A, B, and C chains suggest an essential role for arginine and histidine residues in the C1q-IgG interaction. *J. Immunol.* **172**, 4351–4358 (2004).

20. U. Kishore, M. S. Kojouharova, K. B. M. Reid, Recent progress in the understanding of the structure-function relationships of the globular head regions of C1q. *Immunobiology.* **205**, 355–364 (2002).

21. U. Kishore *et al.*, C1q and tumor necrosis factor superfamily: modularity and versatility. *Trends Immunol.* **25**, 551–561 (2004).

Chapter 4

22. J. E. Thommesen, T. E. Michaelsen, G. Å. Loset, I. Sandlie, O. H. Brekke, Lysine 322 in the human IgG3 CH2 domain is crucial for antibody dependent complement activation. *Mol. Immunol.* **37**, 995–1004 (2001).

23. E. E. Idusogie *et al.*, Engineered antibodies with increased activity to recruit complement. *J. Immunol.* **166**, 2571–2575 (2001).

24. G. L. Moore, H. Chen, S. Karki, G. A. Lazar, Engineered Fc variant antibodies with enhanced ability to recruit complement and mediate effector functions. *MAbs.* **2**, 181–189 (2010).

25. D. Ugurlar *et al.*, Structures of C1-IgG1 provide insights into how danger pattern recognition activates complement. *Science (80-.).* (2018).

26. E. O. Saphire, Crystal Structure of a Neutralizing Human IgG Against HIV-1: A Template for Vaccine Design. *Science (80-.).* **293**, 1155–1159 (2001).

27. D. M. Czajkowsky, Z. Shao, The human IgM pentamer is a mushroom-shaped molecule with a flexural bias. *Proc. Natl. Acad. Sci. U. S. A.* **106**, 14960–5 (2009).

28. G. Vidarsson, G. Dekkers, T. Rispens, IgG subclasses and allotypes: From structure to effector functions. *Front. Immunol.* **5**, 1–17 (2014).

29. S. Zheng, E. Palovcak, J.-P. Armache, Y. Cheng, D. Agard, Anisotropic Correction of Beam-induced Motion for Improved Single-particle Electron Cryo-microscopy. *bioRxiv*, 1–30 (2016).

30. K. Zhang, Gctf: Real-time CTF determination and correction. *J. Struct. Biol.* **193**, 1–12 (2016).

31. S. H. W. Scheres, Semi-automated selection of cryo-EM particles in RELION-1.3. *J. Struct. Biol.* **189**, 114–22 (2015).

32. A. Punjani, J. L. Rubinstein, D. J. Fleet, M. A. Brubaker, cryoSPARC: algorithms for rapid unsupervised cryo-EM structure determination. *Nat. Methods.* **14**, 290–296 (2017).

Chapter 5

Discussion

Research in the 20th and 21st century has provided structural and functional insights into the complement system and revealed complement involvement in a wide range of inflammatory and neurodegenerative disorders and cancer. Broad functions of complement involve: the clearance of immune complexes, cellular debris and apoptotic cells, integration of the innate and adaptive immunity, tissue and organ development and tissue repair. The discovery of such a variety of roles paved the way for bringing the attention that complement system deserved, ever since it was discovered in the 19th century as an agent that "complements" antibodies in blood. The complement system is no longer overlooked by immunologists and clinical doctors as *only* a blood-based antimicrobial system, but is now regarded as a key player in overall immunity and tissue homeostasis.

C1, as the name suggests, is the first component of the complement system and recognizes a large variety of targets for complement activation. Although extensive research has been done on C1, it has remained one of the biggest mysteries of the complement system. Research into C1 is vital because:

i) C1 is responsible for the elimination of antibody-coated targets; therefore, developing better antibody therapeutics requires understanding of the C1-mediated effector mechanism (*1, 2*)

ii) deficiency of C1 causes autoimmune diseases such as systemic lupus erythematosus, the mechanism of which is not fully understood (*3, 4*)

iii) C1 is activated by foreign substances such as carbon nanomaterial which are used in gene and cancer therapy (*5, 6*). Regulation of non-physiological C1 activation is therefore critical for biomedical use of such materials.

iv) C1q is accumulated in tissues with accelerated ageing (*7*). C1 involvement in age-related Wnt receptor signaling and declined tissue regeneration and repair during ageing remains to be understood (*8, 9*).

v) C1q is localized to synapses and contributes to synapse elimination (*10*). The roles of C1q in synaptic pruning and neurological disorders (*11–13*) need to be discovered.

Due to the broad functional impact of C1, C1 research is far more urgent than ever. New strategies to specifically activate or inhibit the complement pathway (CP) are crucial for developing therapies for all diseases mentioned above.

Previous structures of the complement classical pathway

C1 is assembled from Ca^{2+}-dependent interaction of recognition protein C1q and two proteases of C1r and C1s (*14*). In the 1960-1980s, scientists performed groundbreaking investigations to understand the structure of C1 and its activa-

Chapter 5

101

tion mechanism (*15–19*). C1 (C1q-C1r$_2$s$_2$) structure has been studied by small angle X-ray, neutron scattering and negative-stain electron microscopy (*20–23*). According to these studies, free C1r$_2$s$_2$ is arranged as a string of C1s-C1r-C1r-C1s and forms a 50-nm elongated structure. Two C1s molecules interact with C1r with their N-terminal CUB-EGF-CUB domains, and two C1r molecules interact with each other in the middle of the elongated structure by their CCP1-CCP2-SP domains. High-resolution structures of fragments of C1r$_2$s$_2$ have been solved by X-ray crystallography and NMR spectroscopy (*24–28*). A C1r CCP1-2-SP dimer structure in zymogen and active states demonstrated how the C1r dimer sits in the middle of the tetramer in a locked conformation and then rearranges to enable C1r-C1r enzyme-substrate conformation to activate (*25*). Homo-dimer structures of C1s CUB-EGF-CUB showed how hetero-dimers of C1r and C1s interact with each other (*29*). Very recently, a heterodimer structure of C1r-C1s showed how CUB-EGF-CUB domains of C1r and C1s interact with each other to form a stable complex (*30*).

C1r$_2$s$_2$, when it is bound to C1q, has a more compact structure, compared to the free C1r$_2$C1s$_2$ tetramer (*21*). Ca^{2+} binding sites, located in each CUB domain of C1r and CUB1 of C1s, enabled the building of models of the stacked C1r-C1s-C1s-C1r arrangement (*31, 32*). These models indicated that C1r proteases sit outside with 4 binding sites and C1s proteases sit inside with 2 binding sites giving a total of 6 collagen binding sites. The tetrameric arrangement of the C1s CUB-EGF-CUB structure showed how C1r and C1s CUB-EGF-EUB domains are stacked in between collagen arms. The structures of collagen peptide-bound CUB1 of C1s (4LOR) (*33*), and CUB2 of the C1r/C1s homolog MASP-1 (3POB) (*34*), revealed how Ca^{2+} binding residues of CUB domains interact with a lysine residue of each collagen arm. These data and proposed models suggest a substantial conformational change of the tetramer upon association with C1q. How the protease tetramer changes its conformation from elongated C1s-C1r-C1r-C1s to stacked C1r-C1s-C1s-C1r has been unclear.

Previous models of C1 suggested that C1r and C1s CCP1-2 SP domains folded inside the C1q cone under the protease platform (*29, 31, 35, 36*). C1 binding to surfaces yield a conformational change that triggers unfolding of the arms and therefore intramolecular activation. Conversely, low resolution cryo-ET reconstruction of C1 bound to antibody-antigen complexes on liposomes (*37*) and SAXS structure of free C1 (*38*) did not demonstrate such folding inside the collagen arms. Furthermore, studies on the homologs, MASP-MBL complexes, suggest intermolecular activation where activation only occurs between two adja-

cent complexes on activating surfaces (*39*). Despite the differences of the lectin and classical pathway of complement, such as MASPs forming homo-dimers and C1r-C1s forming hetero-tetramers, these complexes resemble each other and they might activate in a similar fashion on cell surface. However, we lack the experimental data to determine either inter- or intra-molecular activation model or elaborate on the mechanistic details of activation.

This thesis addresses 3 remaining research questions:
1) How is C1 assembled?
2) What are the surface-induced conformational changes?
3) How is C1 activated by binding surfaces?

1) How is C1 assembled?

New technological advances in native mass spectrometry (native MS) not only facilitated the study of the assembly of large macromolecular complexes, but also the dynamics of the complex components (*40*). Native MS provides characterization of a wide range of proteins; from 10 kDa histones to large virus assemblies (20,000 kDa) (*41*). Wang *et al.* studied C1 bound to antigen-saturated IgG hexamer by native MS and detected complexes of ~2 MDa (*42*). Wang *et al.* obtained molecular insights such as the stoichiometry of the C1-IgG complex, the assembly of subcomplexes of C1q, $C1r_2s_2$ and IgG and the antigen-dependent binding state of IgG platform. However, like every other technique, native MS has its limitations, such as: experiments are performed only in room temperature; high concentrations of protein complexes are needed; proteins may undergo dissociation artifacts in gas-phase; and low ionic strength is required for high resolution spectra. Considering these limitations, native MS is much more powerful when complemented with other functional/structural experiments.

We studied the dynamics of C1 complex assembly by native MS. Previously, all of the models relied on fixed static $C1r_2s_2$ complexes that require large conformational changes in order to form C1 complex with C1q. Our native MS data show that $C1r_2s_2$ hetero-tetramers dissociate into transient C1r-C1s hetero-dimers (C1rs) and re-associate into tetramers spontaneously. Our finding provided an explanation for the rearrangement of elongated $C1r_2s_2$ hetero-tetramer C1s-C1r-C1r-C1s into an antiparallel stacked C1r-C1s-C1s-C1r conformation upon binding C1q. Instead of folding and rotating of the hetero-tetramer, two dimers slide and shift alongside each other to bind C1q collagen arms. Such a rearrangement of C1rs dimers for C1 assembly is energetically favorable compared to previous models that require very large and complicated movements. Moreover, assembly

of C1 is dynamic with C1rs dimers continuously exchanging in between C1. The flexibility of C1q arms in free state might allow C1rs dimers to shift in-and-out. C1 binding to complement-inducing IgG hexamers reduces C1rs-dimer exchange markedly, confirmed by the magnetic bead assay. Antibody platforms on cell surface stabilize C1 complexes as proposed by Ziccardi (*16*).

Our 10 Å single particle cryo-EM structure of C1 bound to IgG1 hexamers (*43*) provided insights into how C1r and C1s are stacked in C1. The density for $C1r_2s_2$ shows two intact densities with a gap in the middle, suggesting that C1rs dimers separate from each other. This observation is in agreement with our native MS data that C1 is assembled from two C1rs dimers. Based on the density map, we modeled C1r and C1s using previously known structures of the C1r and C1s fragments and their homologs (*24*, *29*, *34*, *44*, *45*). In our model, N-terminal domains of C1r and C1s are located in between the collagen arms, as predicted previously. The $C1r_2s_2$ tetramer stack was more compact than that of the C1s tetramer arrangement in the crystal structure (*29*). The sliding of the tetramer by 20 Å between two C1rs dimers is possibly induced by the compaction of C1q collagen arms upon binding to antibody platforms. We also observed a ~45° rotation of C1s CUB2 compared to previous homo-dimer crystal structures (4LMF, 3DEM). The recent structure of C1r-C1s hetero-dimer confirms the CUB2 rotation and therefore supports our model based on our mid-resolution density map (*30*). Although we modeled the protease structure based on 10 Å density map and known x-ray structures, we could not distinguish which density belongs to C1r or C1s. Hence, the possibility of a stack conformation as C1s-C1r-C1r-C1s instead of C1r-C1s-C1s-C1r should not be omitted.

2) What are the surface-induced conformational changes?

Our cryo-EM structure of C1 bound to IgG platforms demonstrates a non-symmetric C1 with a tilted stalk and a tilted protease platform (*43*). C1 binds Fc regions of the 18-nm IgG platform with 6 gC1q domains. Considering that free C1 has a much wider (30-35 nm) opening of the arms, as previously shown by SAXS structure (*38*), our data suggest a compaction of the C1 arms from 35 nm to 18 nm opening, when binding IgG platform. The compaction of the arms yields bending of the collagen arms due to the protease platform in between the arms. Two collagen arms, located at the furthest diagonal of the protease platform, possibly cause a shift of two C1rs dimers by sliding two C1rs dimers close to each other. These collagen arms bend the most since they are the furthest from each other. Moreover, C1q is observed to fold around like a helix from C-terminal gC1q domains following each collagen-like arm and merging at the stalk.

The bending of the collagen arms breaks the helical structure and possibly cause a tilt in the stalk. Similarly, cryo-electron tomograms show tilted C1 complexes on antibody-covered liposomes. To summarize, binding antibody platforms cause compaction of the collagen arms, inducing a shift between dimers of the proteases and bending of the arms, which, as a consequence, tilt the stalk and yield a non-symmetric C1 complex.

A structural mismatch between C1q and $IgG1_6$ is observed in our cryo-EM structures. C1 binds IgG1 hexamer platforms with 4, 5 or 6 globular heads, with two legs being either bound or not bound, while C1q binds all Fc regions of the IgG platform with 6 gC1q heads. Free C1q has flexible arms which enable all gC1q to reach their binding partner Fcs. IgG1 platform, which is probably too small for C1 docking, is an imperfect platform for a complete binding. The structural mismatch of C1 and $IgG1_6$ is either a regulation mechanism or an imperfect feature of nature. On the other hand, IgG3 or IgM hexamers form wider platforms (*46, 47*) which might be a better match for C1 binding. Since we do not know the effects of mismatch in activation, research in either larger or smaller platforms is necessary to understand the effect of the danger patterns. Moreover, other ligands, such as C-reactive protein, serum amyloid protein or pentraxin3 (*48, 49*) create different oligomeric states and distances of patterns on surfaces. How these patterns will affect the conformational change, and thus activation, is unknown.

Cryo-EM reconstruction of $C1-IgG1_6$ provided C1q-Fc binding interface, which has been previously studied extensively (*50*); however, no high-resolution structure of C1q-Fc complex was available. The key residues involved in binding are Pro329 and Pro331, (*51*) and enhanced binding of C1q to Fc are achieved by mutations of S267E/H268F/S324T (*52*). However, the interacting partners of these residues in C1q and Fc and how these residues contribute to binding were not yet determined. The 7 Å density map allowed positioning of the known structures of gC1q (1PK6) and Fc (1HZH) into their densities. The density for C1q had lower resolution than Fc regions due to imposed symmetry on asymmetric C1q. In our model, there are two interaction sites: the first one located between chain B and CH2 domain; the second one between chain C and CH2' domain. These binding sites suggest a two-step C1q binding mechanism where C1q first recognizes IgG with the first binding site and stabilizes the interface with the second binding site.

We hypothesize that C1 induces the organization of the assembly of 6 IgGs forming a hexamer platform. Considering that each gC1q head has two binding

sites, gC1q might first bind Fc before the platform is made and then bind with the second binding site after the hexamerization of IgGs. Hypothetically, C1q binds Fc platform in a rotating manner, one gC1q head at a time, enabling the organization of IgG hexamers on a cell surface during binding event. We have shown that C1q molecules alone do not form such hexamerization on surfaces. Possibly the flexibility of C1q arms does not induce IgG molecules to come together. Preformed platforms easily accommodate C1q because a prior organization is not needed. Therefore, first C1 organizes IgGs, then C1-induced IgG hexamers stimulate conformational changes in C1.

3) How is C1 activated by danger patterns on cell surfaces?

Proposed models of C1 activation consider that i) C1r and C1s are inactive zymogens that are present as $C1r_2s_2$ in plasma; ii) inactive $C1r_2s_2$ zymogens bind to C1q to form $C1qr_2s_2$; iii) C1 binds to surfaces through C1q, inducing autoactivation of the zymogens C1r into active C1r proteases; which in turn iv) leads to conversion of the C1s proenzymes into proteases (*36*, *53*, *54*). C1s of the activated C1 cleaves C4 and C2, starting the subsequent steps of the complement cascade. C1-INH regulates surface-induced activation by promoting dissociation of C1 complex and releasing C1r and C1s from C1 (*55*). Alternatively, at 37°C and in the absence of C1-INH, C1 activates spontaneously in the fluid phase, whereas C1 remains inactive at 4°C (*56*). In vivo, C1-INH is considered to inhibit fluid-phase C1 activation by instantaneously blocking activated proteases (*57*).

We propose a new mechanism of C1 assembly that also provides insights into the activation mechanism of C1 both in fluid-phase and induced by activating surfaces. Dynamic exchange of C1rs dimers provides an explanation of how C1 might activate spontaneously in fluid-phase. Dissociation of C1r-C1r dimers of $C1r_2s_2$ tetramers might enable the enzyme substrate conformation needed for C1r to activate the neighboring C1r. The spontaneous activation is immediately inhibited by C1-INH so that the activation is only surface-specific. Surface-induced activation is more efficient than spontaneous activation in fluid-phase because C1-INH might not reach proteases as efficiently as in solution-phase. Moreover, C1 binding to its target on activating surfaces stops C1rs-dimer exchange, therefore stabilizes C1 complex, which, enables complement activation on cell surfaces.

Previous models extensively discussed possible activation steps considering an intra or inter molecular activation; see the section "Previous structures of the complement classical pathway". However, these models did not distinguish C1r-C1r, C1r-C1s, C1s-C4/C2 activation steps and did not give an explanation for

each step. In order to understand which protein cleaves when, we need to look at the structure of C1 complex. Although we did not observe densities for C1r and C1s CCP2-SP domains, CCP1 domains of C1r and C1s extend from CUB2 domains linearly outwards, proposing an extended conformation for CCP2 and SP domains. C1r CCP1 is folded around the collagen arm and extends slightly downwards, projecting C1r CCP2-SP towards C1s. Our structure shows that both C1r and C1s have extended conformations in C1 and contradict folding back of CCP1-CCP2-SP domains in between the collagen arms. The extended conformation suggests an intermolecular activation where C1r can cleave C1s from a neighboring C1 complex. It is also possible that C1r cleaves C1s from the same C1 complex (intramolecular activation) since CCP1 is bent towards C1s. We propose that both intra- and inter-molecular activation is possible for C1r cleaving C1s. Although the CUB2-CCP1 junction is very flexible (*58*) C1r folding completely is not likely. C1r might be cleaved either in fluid-phase during dynamic exchange (intramolecular) or by the neighboring complexes on the surface (intermolecular). When and how C1r is autoactivated remains to be solved.

After activation of C1r and C1s, the next step of C1 is to cleave C4 and C2. The model of the C4bC2 structure based on its homolog C3bB (2XWB) (*59*) shows that the C4 cleavage site and the C2 cleavage site are ~70 Å apart from each other. In order to be cleaved by the same C1s, the structure needs to undergo a large rotation movement while still bound to surface. Alternatively, C2 might be either cleaved by a neighboring C1s (intermolecular) or possibly by C1r. Preliminary results (data not shown) show cleavage of C4 by C1r; however, this needs to be studied further. Besides C4 and C2, C1s has other non-complement ligands including MHC class I molecule, insulin-like growth factor binding protein 5 (IGFBP5), Wnt receptor, and nuclear autoantigens, reviewed by Kouser *et al.* (*8*). These ligands play a role in C1 broad functions; e.g., in tissue homeostasis and immune tolerance. However, the activation mechanism of classical pathway in non-classical roles is not defined yet. Understanding C1 mechanism will provide insights into other roles of C1 in different tissues and interstitial fluids.
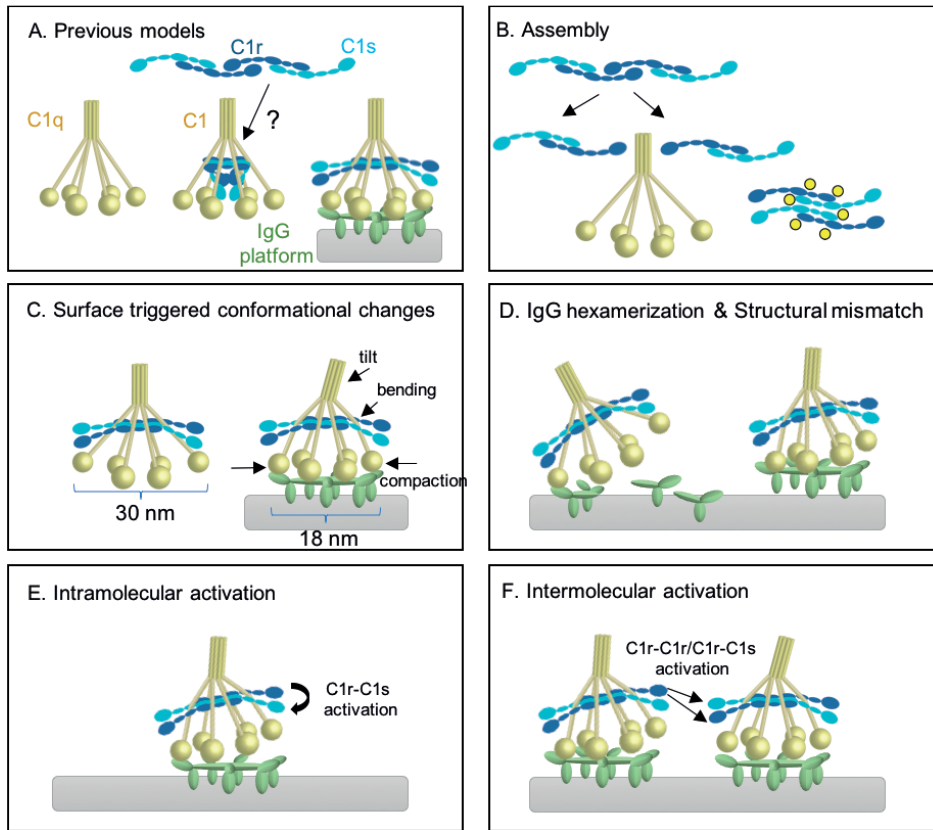
Chapter 5

Figure 1. Schematic representation of the proposed C1 assembly and activation models

A) Cartoon representation of previous models of $C1r_2s_2$ (top), free C1q (left), C1 (middle) and C1 bound to IgG platform on a cell surface. $C1r_2s_2$ changes its conformation from elongated to compact when associating with C1q. $C1r_2s_2$ folds inside the C1q arms below the protease platform and gets activated by movements of C1q arms upon binding to antibodies on cell surface. B) Cartoon representation of our assembly model where $C1r_2s_2$ dissociates into two transient dimers, which associate with C1q by sliding in between collagen arms. C) Free C1 model (left) with 30 nm opening of the arms. Cartoon model of Cryo-EM structure of $C1$-$IgG1_6$ (right) shows compaction and bending of C1q arms and a tilted stalk upon binding 18 nm IgG1 platforms. D) Hypothetical model shows that C1 induces hexamerization of IgG1 on the surface. 18 nm IgG1 platform creates a structural mismatch between C1 and $IgG1_6$. E) Possible C1r-C1s intramolecular activation and F) C1r-C1s intermolecular activation between neighboring C1-IgG16 complexes.

FUTURE PERSPECTIVES

This thesis provides novel insights into C1 assembly and activation, by combining native MS and cryo-EM. Our mid- to low-resolution structures combined with 50 years of research in the complement field have answered several questions and

created new questions to be answered. The remaining critical questions are: What are the kinetics of dynamic association and dissociation of C1 complexes? How are CCP2-SP domains located in C1 complex? How and when is C1r activated? How do the C1r SP domains reach the cleavage site in C1s? Which protein cleaves C4 and C2? How does C1-INH regulate complement activation in fluid-phase and on activating surfaces? What happens to C1-INH after blocking the spontaneous activation in solution? How is C1 activated by different ligands on surfaces such as DNA, amyloid, pentraxins? How can we observe the details of the conformational changes involved during C1 activation? What are the mechanism of C1 activation in other physiological processes, such as Wnt signaling pathway and synaptic pruning in central nervous system?

Fast developing technology and better knowledge of protein behavior will allow higher resolution Cryo-EM structures that will allow understanding the mechanism of C1 activation. In order to achieve high resolution, one could think of stabilizing the complex either by designing better ligand platforms with different Ig types or by fixing C1rs protease by introducing covalent interactions. C1-INH is the key protein that remained a mystery. All proposed models should include C1-INH in their pictures. Once we understand the complete picture of complement activation mechanism, we will be able to develop better antibody-based therapeutics and identify drug targets for a large variety of complement-related diseases.

Chapter 5

REFERENCES

1. R. N. de Jong *et al.*, A novel platform for the potentiation of therapeutic antibodies based on antigen-dependent formation of IgG hexamers at the cell surface. *PLoS Biol.* **14** (2016), doi:10.1371/journal.pbio.1002344.

2. G. L. Moore, H. Chen, S. Karki, G. A. Lazar, Engineered Fc variant antibodies with enhanced ability to recruit complement and mediate effector functions. *MAbs.* **2**, 181–189 (2010).

3. M. Chen, M. R. Daha, C. G. M. Kallenberg, The complement system in systemic autoimmune disease. *J. Autoimmun.* **34**, J276–J286 (2010).

4. M. J. Walport, K. A. Davies, M. Botto, C1q and systemic lupus erythematosus. *Immunobiology.* **199**, 265–285 (1998).

5. W. L. Ling *et al.*, Proteins of the innate immune system crystallize on carbon nanotubes but are not activated. *ACS Nano.* **5**, 730–7 (2011).

6. K. M. Pondman *et al.*, Complement activation by carbon nanotubes and its influence on the phagocytosis and cytokine response by macrophages. *Nanomedicine Nanotechnology, Biol. Med.* **10**, 1287–1299 (2014).

7. A. T. Naito *et al.*, Complement C1q activates canonical Wnt signaling and promotes aging-related phenotypes. *Cell.* **149**, 1298–1313 (2012).

8. L. Kouser *et al.*, Emerging and novel functions of complement protein C1q. *Front. Immunol.* **6** (2015), doi:10.3389/fimmu.2015.00317.

9. J. Lu, U. Kishore, C1 complex: An adaptable proteolytic module for complement and non-complement functions. *Front. Immunol.* **8** (2017), doi:10.3389/fimmu.2017.00592.

10. B. Stevens *et al.*, The Classical Complement Cascade Mediates CNS Synapse Elimination. *Cell.* **131**, 1164–1178 (2007).

11. S. Hong *et al.*, Complement and microglia mediate early synapse loss in Alzheimer mouse models. *Science.* **352**, 712–6 (2016).

12. A. Sekar *et al.*, Schizophrenia risk from complex variation of complement component 4. *Nature.* **530**, 177–183 (2016).

13. D. M. Bonifati, U. Kishore, Role of complement in neurodegeneration and neuroinflammation. *Mol. Immunol.* **44**, 999–1010 (2007).

14. G. J. Arlaud, N. M. Thielens, C. Illy, Assembly of the C1 complex. *Behring Inst. Mitt.*, 189–195 (1993).

15. N. R. Cooper, R. J. Ziccardi, Reconstitution of C1 in native proenzyme form and its use in a quantitative C1 activation test. *J. Immunol.* **119**, 1664–1667 (1977).

16. R. J. Ziccardi, Spontaneous activation of the first component of human complement (C1) by an intramolecular autocatalytic mechanism. *J. Immunol.* **128**, 2500–2504 (1982).

17. P. Gál, S. Cseh, V. N. Schumaker, P. Závodszky, The structure and function of the first component of complement: genetic engineering approach (a review). *Acta Microbiol. Immunol. Hung.* **41**, 361–380 (1994).

18. G. J. Arlaud, R. B. Sim, A. M. Duplaa, M. G. Colomb, Differential elution of Clq, Clr and Cls from human Cl bound to immune aggregates. Use in the rapid purification of Cl subcomponents. *Mol. Immunol.* **16**, 445–450 (1979).

19. H. J. Muller-Eberhard, H. G. Kunkel, Isolation of a thermolabile serum protein which precipitates gamma-globulin aggregates and participates in immune hemolysis. *Proc. Soc. Exp. Biol. Med. Soc. Exp. Biol. Med. New York NY.* **106**, 291–295 (1961).

20. J. Tschopp, W. Villiger, H. Fuchs, E. Kilchherr, J. Engel, Assembly of subcomponents C1r and C1s of first component of complement: electron microscopic and ultracentrifugal studies. *Proc. Natl. Acad. Sci. U. S. A.* **77**, 7014–7018 (1980).

21. C. J. Strang, R. C. Siegel, M. L. Phillips, P. H. Poon, V. N. Schumaker, Ultrastructure of the first component of human complement: electron microscopy of the crosslinked complex. *Proc. Natl. Acad. Sci. U. S. A.* **79**, 586–90 (1982).

22. S. J. Perkins *et al.*, Neutron scattering studies of subcomponent C1q of first component C1 of human complement and its association with subunit C1r2C1s2 within C1. *J. Mol. Biol.* **179**, 547–557 (1984).

23. C. L. Villiers, G. J. Arlaud, M. G. Colomb, Domain structure and associated functions of subcomponents C1r and C1s of the first component of human complement. *Proc. Natl. Acad. Sci. U. S. A.* **82**, 4477–4481 (1985).

24. M. Budayova-Spano *et al.*, Monomeric structures of the zymogen and active catalytic domain of complement protease c1r: further insights into the c1 activation mechanism. *Struct. London Engl. 1993.* **10**, 1509–1519 (2002).

25. J. Kardos *et al.*, Revisiting the mechanism of the autoactivation of the complement protease C1r in the C1 complex: structure of the active catalytic region of C1r. *Mol. Immunol.* **45**, 1752–60 (2008).

26. C. Gaboriaud, V. Rossi, I. Bally, G. J. Arlaud, J. C. Fontecilla-Camps, Crystal structure of the catalytic domain of human complement c1s: a serine protease with a handle. *EMBO J.* **19**, 1755–65 (2000).

27. B. Bersch, J. F. Hernandez, D. Marion, G. J. Arlaud, *Solution structure of the epidermal growth factor (EGF)-like module of human complement protease C1r, an atypical member of the EGF family.* (1998), vol. 37.

28. L. a Gregory, N. M. Thielens, G. J. Arlaud, J. C. Fontecilla-Camps, C. Gaboriaud, X-ray structure of the Ca2+-binding interaction domain of C1s. Insights into the assembly of the C1 complex of complement. *J. Biol. Chem.* **278**, 32157–64 (2003).

29. U. V. Girija *et al.*, Structural basis of the C1q/C1s interaction and its central role in assembly of the C1 complex of complement activation. *Proc. Natl. Acad. Sci.*, 201311113 (2013).

30. J. O. M. Almitairi *et al.*, Structure of the C1r–C1s interaction of the C1 complex of complement activation. *Proc. Natl. Acad. Sci.*, 201718709 (2018).

31. I. Bally *et al.*, Identification of the C1q-binding Sites of Human C1r and C1s: a refined three-dimensional model of the C1 complex of complement. *J. Biol. Chem.* **284**, 19340–8 (2009).

32. A. E. Phillips *et al.*, Analogous interactions in initiating complexes of the classical and lectin pathways of complement. *J. Immunol.* **182**, 7708–17 (2009).

33. V. U. Girija, A. R. Gingras, J. E. Marshall, R. Panchal, A. Sheikh, Structural basis of the C1q/C1s interaction and its central role in assembly of the C1 complex of complement activation. *Proc. Natl. Acad. Sci.* **110**, 13916–20 (2013).

34. A. R. Gingras *et al.*, Structural basis of mannan-binding lectin recognition by its associated serine protease MASP-1: implications for complement activation. *Structure*. **19**, 1635–43 (2011).

35. A. E. Phillips *et al.*, Analogous interactions in initiating complexes of the classical and lectin pathways of complement. *J. Immunol.* **182**, 7708–17 (2009).

36. R. Wallis, D. A. Mitchell, R. Schmid, W. W. Schwaeble, H. Anthony, UKPMC Funders Group Paths reunited : initiation of the classical and lectin pathways of complement activation. *Russell J. Bertrand Russell Arch.* **215**, 1–11 (2010).

37. C. A. Diebolder *et al.*, Complement is activated by IgG hexamers assembled at the cell surface. *Science (80-.).* **343**, 1260–3 (2014).

38. S. A. Mortensen *et al.*, Structure and activation of C1, the complex initiating the classical pathway of the complement cascade. *Proc. Natl. Acad. Sci.* **114**, 986–991 (2017).

Chapter 5

39. S. E. Degn *et al.*, Complement activation by ligand-driven juxtaposition of discrete pattern recognition complexes. *Proc. Natl. Acad. Sci.* **111**, 13445–13450 (2014).

40. A. J. R. Heck, Native mass spectrometry: a bridge between interactomics and structural biology. *Nat. Methods.* **5**, 927–933 (2008).

41. J. Snijder, A. J. R. Heck, Analytical approaches for size and mass analysis of large protein assemblies. *Annu. Rev. Anal. Chem. (Palo Alto. Calif).* **7**, 43–64 (2014).

42. G. Wang *et al.*, Molecular basis of assembly and activation of complement component C1 in complex with immunoglobulin G1 and antigen. *Mol. Cell.* **63**, 135–145 (2016).

43. D. Ugurlar *et al.*, Structures of C1-IgG1 provide insights into how danger pattern recognition activates complement. *Science (80-.).* (2018).

44. A. J. Perry *et al.*, A molecular switch governs the interaction between the human complement protease C1s and its substrate, complement C4. *J. Biol. Chem.* **288**, 15821–15829 (2013).

45. H. Feinberg *et al.*, Crystal structure of the CUB1-EGF-CUB2 region of mannose-binding protein associated serine protease-2. *EMBO J.* **22**, 2348–59 (2003).

46. D. M. Czajkowsky, Z. Shao, The human IgM pentamer is a mushroom-shaped molecule with a flexural bias. *Proc. Natl. Acad. Sci. U. S. A.* **106**, 14960–5 (2009).

47. G. Vidarsson, G. Dekkers, T. Rispens, IgG subclasses and allotypes: From structure to effector functions. *Front. Immunol.* **5**, 1–17 (2014).

48. T. W. Du Clos, C. Mold, Pentraxins (CRP, SAP) in the process of complement activation and clearance of apoptotic bodies through Fcγ receptors. *Curr. Opin. Organ Transplant.* **16**, 15–20 (2011).

49. A. Inforzato *et al.*, PTX3 as a paradigm for the interaction of pentraxins with the Complement system. *Semin. Immunol.* **25** (2013), pp. 79–85.

50. S. Schneider, M. Zacharias, Atomic resolution model of the antibody Fc interaction with the complement C1q component. *Mol. Immunol.* **51**, 66–72 (2012).

51. U. Kishore *et al.*, C1q and tumor necrosis factor superfamily: modularity and versatility. *Trends Immunol.* **25**, 551–561 (2004).

52. G. L. Moore, H. Chen, S. Karki, G. a Lazar, Engineered Fc variant antibodies with enhanced\nability to recruit complement and mediate\neffector functions. *MAbs.* **2**, 181–189 (2010).

53. C. Gaboriaud *et al.*, Structure and activation of the C1 complex of complement: unraveling the puzzle. *Trends Immunol.* **25**, 368–73 (2004).

54. P. Gál, J. Dobó, P. Závodszky, R. B. M. Sim, Early complement proteases: C1r, C1s and MASPs. A structural insight into activation and functions. *Mol. Immunol.* **46**, 2745–52 (2009).

55. R. B. Sim, G. J. Arlaud, M. G. Colomb, Kinetics of reaction of human C1-inhibitor with the human complement system proteases C1r and C1s. *BBA - Enzymol.* **612**, 433–449 (1980).

56. J. P. Windfuhr, J. Alsenz, M. Loos, The critical concentration of C1-esterase inhibitor (C1-INH) in human serum preventing auto-activation of the first component of complement (C1). *Mol. Immunol.* **42**, 657–63 (2005).

57. R. J. Ziccardi, A new role for C1-inhibitor in homeostasis: Control of Activation of the first component of human complement. **128**, 2–5 (1982).

58. B. Major *et al.*, Calcium-dependent conformational flexibility of a CUB domain controls activation of the complement serine protease C1r. *J. Biol. Chem.* **285**, 11863–11869 (2010).

59. F. Forneris *et al.*, Structures of C3b in complex with factors B and D give insight into complement convertase formation. *Science.* **330**, 1816–20 (2010).

APPENDIX

SUMMARY

Proteins are the key components of all biological processes in a living organism. Every protein has a unique structure which influences its function. Therefore, solving structures of proteins has advanced our understanding of biological processes and greatly facilitated development of drugs. Structural biology techniques like X-ray crystallography, nuclear magnetic resonance and cryo-electron microscopy allowed determination of thousands of protein structures until now, which only covers the tip of the iceberg. The integration of different structural biology techniques and combining the structural information with cell biology, protein engineering, and bioinformatics will allow us to solve the remaining mysteries of macromolecular assemblies and related diseases.

This thesis focuses on the proteins of the complement system, which is an important part of our innate immune defense in blood and interstitial fluids. The complement system is responsible for the clearance of the infectious microorganisms and injured host cells. The recognition of danger patterns on these cell surfaces activates a network of plasma and membrane-associated proteins and induces the complement response. An imbalance in complement components, either by unregulated or inadequate activation causes a wide range of diseases, including autoimmune diseases, age-related diseases and neurodegenerative diseases. On the other hand, complement system is recruited by therapeutic antibodies for eliminating tumour cells. Considering the broad involvement in diseases and a great potential in therapeutic applications, structural and mechanistic insights into complement activation are essential.

The central protein of this thesis is a large macromolecular complex called C1, which is the initiation complex of the classical pathway of complement. C1 is a 790-kDa complex, which consists of a recognition protein, C1q, and a heterotetramer of proteases, $C1r_2s_2$, which is bound in between C1q collagen arms. When C1q binds multivalent surface signals such as antibody-antigen complexes, the associated serine proteases C1r and C1s get activated and initiate the proteolytic cascade. Although the complement system has been studied extensively since more than 50 years, the previous C1 models were insufficient to understand how the components of the C1 complex associate and how they initiate the first step of the proteolytic cascade upon recognition of C1 ligands. This thesis covers the key questions related to the assembly and activation of C1.

Appendix

Chapter 1 provides a thorough introduction about the complement system. First, biological functions of the complement system are described, with an overview of a large variety of complement-related diseases. Then, how 30 different cell surface and soluble proteins form a proteolytic cascade to induce complement is portrayed in detail. Furthermore, this chapter provides a detailed explanation of antibodies. A historical perspective of C1 and the structural knowledge about this complex molecule is reviewed. Finally, Chapter 1 provides an overall picture of consensus (structural) models of C1 assembly and activation and describes the current open questions regarding C1 activation.

Chapter 2 sheds light on the activation mechanism of C1 by antibody recognition on cell surfaces. Two cryo-electron microscopy techniques were used in order to visualize the C1 complex bound to antibody platforms. First, C1-IgG1 complexes on di-nitrophenyl coated liposomes were captured by cryo-electron tomography. The data show crowding of C1-IgG1 complexes on liposome surfaces and suggest inter-molecular activation between neighboring C1 complexes on crowded surfaces. Secondly, single particle analysis of soluble C1-IgG1$_6$ complexes revealed binding of a single, isolated C1 complex bound to hexameric IgG platforms through 4, 5 or 6 C1q globular heads (gC1q) making contacts with the corresponding Fc regions of the hexamer platforms. Imposing 6-fold symmetry to gC1q-Fc$_6$ platform yielded a 7-Å electron density map that allowed identification of two gC1q-Fc interaction sites. The interaction sites were confirmed by mutagenesis and complement-dependent-cytotoxicity analysis. Asymmetric and heterogeneous binding of gC1q-Fc$_6$ platforms results in compaction of C1q arms between the recognition units on Fc$_6$-platforms. The compaction of C1 causes a rearrangement of C1r$_2$s$_2$ proteases that allows C1r to reach and activate C1s within the same C1 complex, thereby initiating the proteolytic cascade. Based on the experimental results, two C1 activation mechanisms were proposed: intra-molecular activation within single C1 complexes and inter-molecular activation between neighboring C1 complexes on crowded surfaces.

Like pieces of a puzzle, pieces of C1 complex, i.e. C1q, C1r, C1s have to assemble in a perfect way to form a functioning C1 complex. **Chapter 3** focuses on dynamic assembly of C1 (i.e. C1r$_2$s$_2$ binding to C1q) and the effects of antibody binding on the assembly. Using the latest advances in native mass spectrometry, C1 complex formation and dissociation can be detected. The results show that C1r$_2$s$_2$ is a dynamic complex. C1r$_2$s$_2$ spontaneously dissociates into C1rs hetero-dimers, which then associate with C1q into C1 (C1r$_2$s$_2$). Binding of C1 to antibody complexes stabilizes C1 complex and reduces the rate of dissociation of C1rs hetero-dimers from C1. These data suggest that C1 assembly does not require

major protease rearrangements of C1r and C1s as previously proposed for C1 assembly. Moreover, the dynamic assembly model proposed in chapter 3 explains the difference of surface induced activation and fluid phase activation. Reduced complex dynamics on surfaces results in efficient danger-pattern specific complement activation.

Chapter 4 studies the heterogeneity of C1-IgG1$_6$ binding, which was observed in chapter 2. Incomplete and heterogeneous binding of the six C1q arms to IgG1 hexamers limited the structural resolution obtained using cryo-EM reconstruction. The experiments were designed considering two possible causes of the heterogeneity, i.e. weak C1q-Fc interactions and structural mismatch caused by the presence of C1r$_2$s$_2$ proteases. A variant of IgG1 hexamer with enhanced C1q-binding affinity was studied in complex with either C1q or C1. Preliminary data from low-resolution density reconstructions provided insights that allow answering mechanistic questions and further optimize experimental conditions for high resolution reconstructions. In the absence of proteases, C1q binds enhanced antibody platforms with 6 C1q globular heads, and in the presence of proteases, C1q binds with 4 or 5 C1q globular heads. These data support the hypothesis that the presence of C1r$_2$s$_2$ restricts C1q conformations resulting in a structural mismatch between C1 and IgG1 hexamers with incomplete binding of the C1q arms to the antibody platform. Low-resolution data of C1-IgG complexes allowed understanding the causes of heterogeneity and showed the path to the next experiments for obtaining high resolution data.

Finally, **Chapter 5** provides an overview of the conclusions from the previous chapters. This chapter discusses the proposed activation and assembly mechanism and points out the remaining challenges of the complement research. It reflects future perspectives to complete the pieces of the complement puzzle.

Overall, the research presented in this thesis contributes to the current knowledge of the complement system and leads the next steps of future studies.

Appendix

NEDERLANDSE SAMENVATTING

Eiwitten spelen een belangrijke rol in de biologische processen van levenden organismes. Elk eiwit heeft een unieke structuur en dit beïnvloedt zijn functie. Het oplossen van de structuren van eiwitten vergroot ons begrip van biologische processen en draagt bij aan de ontwikkeling van medicijnen. Structurele biologie-technieken zoals eiwitkristallografie, kern magnetische resonantie en cryo-elektro-nenmicroscopie maakten tot nu toe het oplossen van duizenden eiwitstructuren mogelijk. De integratie van verschillende structurele biologietechnieken en het combineren van de structurele informatie met celbiologie, eiwittechnologie en bio-informatica zal ons in staat stellen om de resterende onderzoeksvragen van macromoleculaire formaties en gerelateerde ziekten op te lossen.

Dit proefschrift richt zich op de eiwitten van het complementsysteem. Deze eiwit-ten vormen een belangrijk onderdeel van ons aangeboren immuunafweer in bloed en extracelulaire vloeistoffen. Het complementsysteem is verantwoordelijk voor de klaring van infectieuze micro-organismen en beschadigde gastheercellen. De herkenning van gevaar-patronen op deze celoppervlakken activeert een netwerk van plasma- en membraan-geassocieerde eiwitten en leidt tot de complementre-actie. Een onbalans in complement door ongereguleerde of inadequate activering veroorzaakt een breed scala aan ziekten, waaronder auto-immuunziekten, leeftijd gerelateerde ziekten en neurodegeneratieve ziekten. Aan de andere kant wordt het complementsysteem benut door therapeutische antilichamen voor het elimineren van tumorcellen. Gezien de brede betrokkenheid van het complementsysteem bij ziekten en het grote potentieel in therapeutische toepassingen zijn inzichten in structuur en mechanisme in complement activering cruciaal.

Het eiwit dat centraal staat in dit proefschrift is een groot macromoleculair complex met de naam C1, welk het initiatiecomplex van de klassieke route van complement is. C1 is een 790-kDa-complex, dat bestaat uit een herkenningseiwit (C1q), en een hetero-tetrameer (C1r$_2$s$_2$) van proteasen die gebonden is tussen C1q collageenarmen. Wanneer C1q oppervlakte signalen zoals antilichaam-antigeencomplexen bindt, worden de bijbehorende serineproteasen C1r en C1s geactiveerd, welke vervolgens de proteolytische complement cascade initiëren. Hoewel het complementsysteem uitgebreid is bestudeerd sinds meer dan 50 jaar, waren de eerdere C1-modellen onvoldoende om te begrijpen hoe de componen-ten van het Cl-complex associëren en hoe ze de eerste stap van de proteolytische cascade initiëren na herkenning van C1-liganden. Dit proefschrift behandelt de open vragen met betrekking tot de formatie en activatie van C1.

Hoofdstuk 1 biedt een grondige introductie over het complementsysteem. Eerst worden de biologische functies van het complementsysteem met een overzicht van verschillende complement gerelateerde ziekten beschreven. Vervolgens wordt in detail weergegeven hoe 30 verschillende membraan- en oplosbare eiwitten de proteolytische cascade vormen om complement te activeren. Ook worden het historische perspectief van de structurele kennis van C1 besproken. Ten slotte geeft hoofdstuk 1 een algemeen beeld van de huidige hypotheses van C1 formatie en activatie en beschrijft de huidige open vragen met betrekking tot C1-activering.

Hoofdstuk 2 richt zich op het activeringsmechanisme van C1 door herkenning van antilichamen op celoppervlakken. Twee cryo-elektronenmicroscopietechnieken werden gebruikt om het C1-complex gebonden aan antilichaamplatforms te visualiseren. Ten eerste werden C1-IgG1-complexen op liposomen bedekt met dinitrophenyl gevisualiseerd met behulp van cryo-elektronentomografie. De data toont veel C1-IgG1-complexen bij elkaar op liposoomoppervlakken en suggereert intermoleculaire activering tussen aangrenzende C1-complexen op drukke oppervlakken. Ten tweede onthulde een single particle analyse van oplosbaar C1-IgG1$_6$-complex de binding van een enkelvoudig, geïsoleerd C1-complex gebonden aan hexamere IgG-platforms. De analyse laat zien dat 4, 5 of 6 C1q-bolvormige koppen (gC1q) contact maken met de bijbehorende Fc gebieden van de hexameer platforms. Het toepassen van 6-voudige symmetrie aan gC1q-Fc$_6$-platform leverde een 7-Å resolutie structuur op. Hierin konden twee interactieplaatsen tussen gC1q en Fc geïdentificeerd worden. Deze interactie plaatsen zijn vervolgens gevalideerd door mutagenese en complement-afhankelijke cytotoxiciteitsanalyse. Asymmetrische en heterogene binding van C1 aan het IgG1$_6$-platform resulteert in vervorming van de C1q-armen tussen de herkenningseenheden op Fc$_6$ platforms. De vervorming van C1 veroorzaakt een herschikking van C1r$_2$s$_2$-proteasen, waardoor het voor C1r mogelijk is om C1s binnen hetzelfde C1-complex te bereiken en activeren. Hierdoor wordt de proteolytische complement cascade geïnitieerd. Aan de hand van de data worden twee mogelijke C1 activeringsmechanismen voorgesteld: intramoleculaire activatie binnen een enkel C1-complex en intermoleculaire activatie tussen aangrenzende C1-complexen op oppervlaktes met veel C1-complexen.

Net als de stukjes van een puzzel moeten stukken C1-complex, namelijk C1q, C1r, C1s, op een perfecte manier samenkomen om het functioneren van het complex mogelijk te maken. **Hoofdstuk 3** richt zich op de dynamische formatie van C1 (d.w.z. C1r$_2$s$_2$ binding aan C1q) en op de binding van de volledig C1 aan antilicha-men. Met behulp van de nieuwste ontwikkelingen in native massaspectrometrie

kunnen de complexvorming en dissociatie worden gedetecteerd. De resultaten tonen aan dat $C1r_2s_2$ een dynamisch complex. $C1r_2s_2$ dissocieert spontaan in C1rs-hetero-dimeren, die vervolgens met C1q associëren tot C1 ($C1r_2s_2$). Binding van C1 aan antilichaamcomplexen stabiliseert het C1-complex en vermindert de snelheid van dissociatie van C1r-heterodimeren van C1. Deze gegevens suggereren dat C1-formatie geen opmerkelijke herschikkingen van proteasen van C1r en C1s vereist zoals voorgesteld was in eerdere hypotheses. Bovendien verklaart het dynamische formatiemodel het verschil tussen oppervlakte-geïnduceerde activering en vloeistoffase-activering. De verminderde dynamiek van de complexen op oppervlaktes resulteert in efficiënte gevaar-patroon-specifieke complementactivering.

Hoofdstuk 4 bestudeert de waargenomen heterogeniteit van $C1\text{-}IgG1_6$-binding, die eerder werd beschreven in Hoofdstuk 2. Onvolledige en heterogene binding van de zes C1q-armen aan IgG1-hexameren beperkte de resolutie van de verkregen cryo-EM reconstructie. Experimenten werden ontworpen waarin rekening gehouden werd met twee mogelijke oorzaken van de heterogeniteit, namelijk de zwakke C1q-Fc-interacties en een structurele onbalans veroorzaakt door de aanwezigheid van $C1r_2s_2$-proteasen. Een variant van IgG1-hexameer met verhoogde C1q-bindingsaffiniteit werd bestudeerd in complex met C1q of C1. De preliminaire gegevens van reconstructies met een lage resolutie bieden inzichten die ons in staat stellen om mechanische vragen te beantwoorden en de experimentele omstandigheden voor reconstructies met hoge resolutie te optimaliseren. C1q bindt versterkte antilichaamplatforms met 6 C1q-bolvormige koppen in afwezigheid van de proteasen, en met 4 of 5 C1q-bolvormige koppen in de aanwezigheid van proteasen. Deze gegevens ondersteunen de hypothese dat de aanwezigheid van $C1r_2s_2$ de vorming van C1q-conformaties beperkt, wat resulteert in een structurele disbalans tussen C1- en IgG1-hexameren met onvolledige binding van de C1q-armen aan het antilichaamplatform. De lage resolutie data van C1-IgG-complexen geven inzicht in de oorzaken van de waargenomen heterogeniteit en suggereren opties voor het behalen van hoge resolutie data.

Tot slot geeft **hoofdstuk 5** een samenvatting van de conclusies uit de vorige hoofdstukken. Dit hoofdstuk bespreekt het voorgestelde activerings- en formatiemechanisme en wijst op de resterende uitdagingen van het complementonderzoek. Het bespreekt toekomstige plannen om de puzzel van het complementsysteem te voltooien.

Het onderzoek dat in dit proefschrift wordt gepresenteerd draagt bij aan de huidige kennis van het complementsysteem en bepaalt de volgende stappen in toekomstige studies.

Appendix

CURRICULUM VITAE

Deniz Ugurlar was born on June 7th, 1986 in Istanbul, Turkey. After graduating from high school in 2004, she started her undergraduate studies of Chemical Engineering in Bogazici University in Istanbul. She obtained her BSc degree in Chemical Engineering in 2009. She moved to the Netherlands to continue her MSc studies in Molecular and Cellular Life Sciences at Utrecht University. During her master studies, she performed two research projects. Her first research project entitled "Advances in the Structural Characterization of Complement Convertase Formation and Dissociation: C2, Bb and Ba" was performed in Crystal and Structural Chemistry group in Piet Gros' lab. Then, she moved to Hamburg to perform a 6-months research project entitled "Structural determination of M3, and Ig domain of M-band Titin" in EMBL Hamburg in Matthias Wilman's lab. She obtained her MSc degree in 2011 in Utrecht University. Same year, she started her PhD project in Piet Gros' lab with the focus of the classical pathway of complement. She has been selected as top PhD candidate of 2017 on the occasion of the 2018 Symposium of the Bijvoet Center of Utrecht University. The results of her PhD project are presented in this thesis. Since October 2017, she has been working as an Application Scientist at Thermo Fisher Scientific.

LIST OF PUBLICATIONS

Diebolder CA, Beurskens FJ, de Jong RN, Koning RI, Strumane K, Lindorfer M a, Voorhorst M, **Ugurlar D,** Rosati S, Heck AJR, van de Winkel JGJ, Wilson IA, Koster AJ, Taylor RP, Saphire EO, Burton DR, Schuurman J, Gros P & Parren PWHI (2014) Complement is activated by IgG hexamers assembled at the cell surface. *Science* 343: 1260–3

Wang G, de Jong RN, van den Bremer ETJ, Beurskens FJ, Labrijn AF, **Ugurlar D**, Gros P, Schuurman J, Parren PWHI & Heck AJR (2016) Molecular Basis of Assembly and Activation of Complement Component C1 in Complex with Immunoglobulin G1 and Antigen. *Mol. Cell* 63: 135–145

Ugurlar D, Howes SC, de Kreuk BJ, Koning RI, de Jong RN, Beurskens FJ, Schuurman J, Koster AJ, Sharp TH, Parren PWHI, Gros P (2018) Structures of C1-IgG1 provide insights into how danger pattern recognition activates complement. *Science*, 359: 794-797

Appendix

ACKNOWLEDGEMENTS

"Nobody said it was easy, no one ever said it would be this hard" I never understood why Coldplay named this song "The Scientist". Now I know why. My PhD journey was a long, difficult process, similar to all the other PhD candidates. However, I was extremely lucky to be surrounded by some of the smartest and kindest people I have ever met, who made this period a wonderful one.

My journey started in Bogazici University in Istanbul where I was doing my bachelor in Chemical Engineering. I took a couple of courses from Associate Prof. Elif Ozkirimli Olmez, who introduced me to structural biology. After learning more about proteins and reading crystallography papers for one of the courses, I already knew what I wanted to do next. Elif Hocam, I can't thank you enough for opening my eyes and letting me discover my passion in research.

Piet, in the beginning of my PhD journey, you showed me the happiness curve of an average PhD candidate. Although my curve did not quite develop as you suggested, I must say that I am extremely happy at the moment. I think your motivating nature and long discussions about "how things work" kept me working hard to seek answers to our questions. Thank you for sharing both failures and successes with me and supporting me during my PhD at all times.

I am grateful to my amazing collaborators. Rob, Frank and Paul; thank you for supporting me and providing me with valuable data that made me successful in the end. You gave me enough freedom to use your samples and work independently until I got good results. Above all, I appreciate the generous offer from Genmab for sponsoring the printing of the thesis. Guanbo and Albert, thank you for the collaboration that gave me amazing native MS results which were essential for complement research. Seline and Suzan, apart from the great results you have provided, I appreciate the long discussions we had in order to understand the complement system and your support to accomplish my projects. I must say that I was very fortunate to collaborate with such inspiring people that extended my horizon.

I would like to thank to the other group leaders of the K&S family. Bert, Eric, Loes, Martin, and finally Friedrich for the cryo-EM support. It was such a privilege to be surrounded by so many amazing scientists. It was great to have you around for urgent questions and in-depth scientific discussions.

Appendix

cakes and healthy living :) I am still sorry for when I left the tent open during our Black forest trip. Viviana, you brought some kindness and positive vibes to N808. I always enjoyed spending time with you, especially those Zumba classes :) Joke thank for all the help of cloning, but also being positive and amazingly helpful. The lab without you is like a bird without wings. Lucas and Matthieu, keep up the good spirit you brought to the lab and thank you for the fun times. Gonzalo, good luck with C1 and keep the hopes high up! Bianca, thank you for all the help for the graduation process! Cryo-EM guys: Robbert, Manuel, Amuda, Max, Juliette, I am glad that your group joined us on the 8th floor. Thank you for bringing some cryo-EM wisdom to the lab but most importantly thank you for all your good vibes!

Dear "community" of Utrecht, thanks for being my family here. We have been growing in number and I hope we keep growing :) Evrim bebisim, heel erg bedankt voor je aanhoudende onderstenuning en je onwijs grote hart. (turkcem yetmedi sana olan hislerimi ifade etmeye :)) Cici, the baby elephant of our family. Your loving nature and positive energy always kept me happy. Odan hazir biliyorsun, bekliyoruz :). Tugcecim knowing that you are always there for me makes me very happy. I wish to celebrate your defense very soon! Pinartom, finally here we are. You were my continuous support throughout the PhD. It felt like we continued our studies together after collage. I feel like there is no one else that understands me as well as you do, from both scientific and social perspective.

I have a big, joyful and supportive family. Dedecim ananecim, siz kizlarinizi boyle yetistirmeseydiniz, biz torunlar bu gunlere gelemezdik. Ileri goruslulugunuz icin size tesekkur ediyorum. Teyzelerim halalarim ve kuzenlerim, hepiniz tek tek biliyorsunuz bendeki yerinizi! Destekleriniz icin cok tesekkur ediyorum. Fatos teyzem, yemek masalarinda cozulen geometri sorulari, ellerle havada cizilen acilar, bana oyle bir boyut kazandirdi ki, tum yaptiklarimda senin emegin var. O yuzden bu tezimi sana ithaf ediyorum... My brother Doga, I have always followed your steps in a way. I learned to read and write so early just because you were there as an example; I went to the same high school just to be as cool as you are. Now I am becoming a doctor just because you are the smartest doctor I have ever known (and you are a real one :)) You also bring two amazing people to our life: Muge and Meliskuzu. I hope to follow your steps in having such a beautiful family.

I am so happy that my family got even bigger last year. My brothers, Aydin and Metin, my Elti-power team, Bahar and Serpil, aslan Umut and my inlaws Melek and Faik Celik who were as supportive as my own parents. Thank you for the love you have given me during these years.

Annecim ve Babacim bana her zaman inandiginiz, guvendiginiz ve beni sonsuz desteklediginiz icin size cok tesekkur ediyorum. Bu uzun yolculuga korkusuzca ciktiysam, sizden binlerce kilometre uzakta bir kac basariya imza attiysam, bu sizin bana sagladiginiz cesaret sayesindedir.

Finally, Murat, the one who is by my side no matter what. I mean, literally. If we count all the times you came to the lab (in the evenings and the weekends) just to cheer me up, you would almost get a PhD degree. Thank you for experiencing every bit of the pain and the happiness together with me. If there was some kind of an award in the category of being the best partner of PhD candidates, you would win the Nobel prize... or an Oscar :) You deserve both.

Appendix